WL-TR-94-3094

UNSTEADY TRANSONIC WIND TUNNEL TEST ON A SEMISPAN STRAKED DELTA WING MODEL OSCILLATING IN PITCH

Part 1: Description of Model, Test Setup, Data Acquisition and Data Processing

Atlee M. Cunningham, Jr.
Lockheed Fort Worth Company
Forth Worth TX

and

Ruud G. den Boer
C. S. G. Dogger
E. G. M. Geurts
A. P. Retél
R. J. Zwaan
National Aerospace Laboratory (NLR)
Amsterdam, The Netherlands

December 1994

Final Report for Period March 1989 - December 1993.

Flight Dynamics Directorate
Wright Laboratory
Air Force Materiel Command
Wright-Patterson Air Force Base, Ohio 45433-7542

NOTICE

When Government drawings, specification, or other data are used for any purpose other than in connection with a definitely Government-related procurement, the United States Government incurs no responsibility or any obligation whatsoever. The fact that the Government may have formulated or in any way supplied the said drawings, specifications, or other data, is not to be regarded by implication, or otherwise in any manner construed, as licensing the holder, or any other person or corporation, or as conveying any rights or permission to manufacture, use, or sell any patented invention that may in any way be related thereto.

This report is releasable to the National Technical Information Service (NTIS). At NTIS, it will be available to the general public, including foreign nations.

This technical report has been reviewed and is approved for publication.

L J Huttsell

LAWRENCE J. HUTTSELL
Aerospace Engineer
Aeroelasticity Section
Structural Dynamics Branch

Max Blair

for: TERRY M. HARRIS
Technical Manager
Aeroelasticity Section
Structural Dynamics Branch

Joseph W. Moschler

JOSEPH W. MOSCHLER
Chief, Structural Dynamics Branch
Structures Division

If your address has changed, if you wish to be removed from our mailing list, or if the addressee is no longer employed by your organization, please notify, WL/FIBG, WPAFB, OH, 45433-7542 to help us maintain a current mailing list.

Copies of this report should not be returned unless return is required by security considerations, contractual obligations, or notice on a specific document.

REPORT DOCUMENTATION PAGE

Form Approved
OMB No. 0704-0188

1. AGENCY USE ONLY (Leave blank)	2. REPORT DATE	3. REPORT TYPE AND DATES COVERED
	December 1994	Final Report March 1989 - December 1993

4. TITLE AND SUBTITLE

Unsteady Transonic Wind Tunnel Test on a Semispan Straked Delta Wing, Oscillating in Pitch Part 1: Description of the Model, Test Setup, Data Acquisition, and Data Processing

5. FUNDING NUMBERS

PR: 2401
TA: 02
WU: 92

6. AUTHOR(S)

A. M. Cunningham, Jr., R. G. den Boer, C. S. G. Dogger, E. G. M. Geurts, A.P. Retél and R. J. Zwaan

7. PERFORMING ORGANIZATION NAME(S) AND ADDRESS(ES)

Lockheed Fort Worth Company
Fort Worth Texas
and
National Aerospace Laboratory (NLR)
Amsterdam, The Netherlands

8. PERFORMING ORGANIZATION REPORT NUMBER

NLR CR 93570 L

9. SPONSORING / MONITORING AGENCY NAME(S) AND ADDRESS(ES)

Flight Dynamics Directorate
Wright Laboratory
Air Force Materiel Command
Wright Patterson AFB OH 45433-7542

10. SPONSORING / MONITORING AGENCY REPORT NUMBER

WL-TR-94-3094

11. SUPPLEMENTARY NOTES

12a. DISTRIBUTION / AVAILABILITY STATEMENT

Approved for public release; distribution unlimited.

12b. DISTRIBUTION CODE

13. ABSTRACT *(Maximum 200 words)*

A wind tunnel investigation was conducted in 1992 to investigate the unsteady aerodynamic aspects of transonic high incidence flows over a simple straked wing model. This test was designed to show how low speed vortex type flows evolve into complicated shock vortex interacting flows at transonic speeds. Requirements for this test were based on a low speed test conducted in 1986 on a full span model in the NLR Low Speed Tunnel. The transonic model was a semispan version of the low speed model with some modifications. It was equipped with a three-component semispan balance to measure total wing loads, seven rows of high response pressure transducers to measure unsteady pressures and 15 vertical accelerometers to measure model motion and vibrations. The model was oscillated sinusoidally in pitch at various amplitudes and frequencies for mean model incidences varying from 4° to 48°. In addition, maneuver type transient motions of the model were tested with amplitudes of 16° and 30° total rotation at various starting angles. The test was conducted in the NLR HST in the Mach range of 0.225 to 0.90 with some preliminary vapor screen flow visualization data taken at M=0.6 and 0.9. This part of the report presents a description of the model, test setup, data acquisition, and data processing.

14. SUBJECT TERMS

unsteady aerodynamics, aeroelasticity, pressure data, transonic, high incidence flow, shock vortex interaction

15. NUMBER OF PAGES

92

16. PRICE CODE

17. SECURITY CLASSIFICATION OF REPORT	18. SECURITY CLASSIFICATION OF THIS PAGE	19. SECURITY CLASSIFICATION OF ABSTRACT	20. LIMITATION OF ABSTRACT
UNCLASSIFIED	UNCLASSIFIED	UNCLASSIFIED	UNCLASSIFIED

FOREWORD

This report summarizes the results of an investigation into transonic high incidence unsteady aerodynamics. Transonic wind tunnel tests were conducted for a semispan straked delta wing model oscillating in pitch at high incidences.

This test was conducted under a cooperative program of research between the Lockheed Fort Worth Company (LFWC), Fort Worth, Texas, USA (Formerly the Fort Worth Division of General Dynamics until 28 February 1993) and the National Aerospace Laboratory (NLR), Amsterdam, The Netherlands. The test was conducted in April/May 1992. The models and corresponding support system were designed at NLR under an earlier separate program with funding from the Fort Worth Division of General Dynamics (now LFWC) and NLR. The fabrication of models, test preparation, wind tunnel test and reporting were performed at NLR under a subcontract from LFWC. This work was funded under Air Force contract F33657-84-C-0247 (CCP 4551) for the Aeronautical Systems Center, Wright-Patterson Air Force Base, Ohio. The work was administered by Mr. F. Zapata of the F-16 SPO (ASC/YPEF) and Mr. L. J. Huttsell of the Flight Dynamics Directorate of Wright Laboratory (WL/FIBG) Wright-Patterson Air Force Base, Ohio under work unit 24010292.

The program manager was Dr. A. M. Cunningham, Jr. at LFWC. The principal investigators were Dr. Cunningham at LFWC, Mr. R. G. den Boer for the wind tunnel test programs at NLR. Mr. den Boer was assisted by the following NLR specialists: C. D. G. Dogger, E. G. M. Geurts, A. P. Retel and R. J. Zwaan. The authors would like to acknowledge the following person who contributed substantially in the project:

Mr. E. W. M. Slijkerman for the design of the wind tunnel model and support; Messrs. T. Horsman and F. Hofman for the fabrication and instrumentaion of the model; and Messrs. O. van Teunenbroek and A. van der Kamp for their contribution in the software development.

The test program for the straked delta wing is documented in three separate reports. This report (Part 1) contains a description of the model, test setup, data acquisition, and data processing. Part 2 contains selected test points for harmonic oscillation and Part 3 contains selected data for simulated maneuvers. Parts 2 and 3 are published as WL-TR-94-3095 and WL-TR-94-3096, respectively. An overview of this test program is also published as WL-TR-94-3017.

TABLE OF CONTENTS

LIST OF FIGURES

LIST OF TABLES

NONDIMENSIONALIZATION, SYMBOLS AND DEFINITIONS

For a description of the axis system and sign conventions, the reader is referred to Appendix A. Pressures and loads have been made dimensionless according to the following conventions:

Nondimensionalization

Mean (steady; the postscript 0 indicates the 0-th harmonic component)

Pressure : $Cp\ 0 = (p\ 0 - ps) / q$

Balance loads : $CN\ 0$ = Normal Force /q*Sref
$Cm\ 0$ = Pitching Moment/q*Sref*cref
$Cl\ 0$ = Rolling Moment/q*Sref*bref

Sectional loads:

$$CN\_u\ 0 = -\int_0^1 Cp^+\ 0 \qquad d(x/c) \text{ chordwise}$$

$$CN\_l\ 0 = \int_0^1 Cp^-\ 0 \qquad d(x/c)$$

$$CN\_t\ 0 = \int_0^1 (Cp^-\ 0 - Cp^+\ 0) \qquad d(x/c)$$

$$Cm\_u\ 0 = -\int_0^1 Cp^+\ 0 \qquad (x/c-0.25) \quad d(x/c)$$

$$Cm\_l\ 0 = \int_0^1 Cp^-\ 0 \qquad (x/c-0.25) \quad d(x/c)$$

$$Cm\_t\ 0 = \int_0^1 (Cp^-\ 0 - Cp^+\ 0) \qquad (x/c-0.25) \quad d(x/c)$$

$$CN\_u\ 0 = -\int_0^1 Cp^+\ 0 \qquad d(y/b) \text{ spanwise}$$

$$Cl\_u\ 0 = -\int_0^1 Cp^+\ 0 \qquad (y/b\ \ ) \quad d(y/b)$$

Unsteady (all unsteady signals have been decomposed into harmonic components;
the harmonic component is indicated by the postscript h;
each harmonic component has been decomposed into a real (in phase)
and an imaginary (out of phase) part; e.g.)

$$Cp\ h = Re(Cp\ h) + i*Im(Cp\ h)$$

Pressure : $Cp\ h = (p\ h\ \ ) / q*dalpha$

Balance loads : $CN\ h$ = Normal Force /q*Sref*dalpha
$Cm\ h$ = Pitching Moment/q*Sref*cref*dalpha
$Cl\ h$ = Rolling Moment/q*Sref*bref*dalpha

Sectional loads:

$$CN\_u\ h = -\int_0^1 Cp^+ h \quad d(x/c) \text{ chordwise}$$

$$CN\_1\ h = \int_0^1 Cp^- h \quad d(x/c)$$

$$CN\_t\ h = \int_0^1 (Cp^- h - Cp^+ h) \quad d(x/c)$$

$$Cm\_u\ h = -\int_0^1 Cp^+ h \quad (x/c-0.25)\ d(x/c)$$

$$Cm\_1\ h = \int_0^1 Cp^- h \quad (x/c-0.25)\ d(x/c)$$

$$Cm\_t\ h = \int_0^1 (Cp^- h - Cp^+ h) \quad (x/c-0.25)\ d(x/c)$$

$$CN\_u\ h = -\int_0^1 Cp^+ h \quad d(y/b) \text{ spanwise}$$

$$Cl\_u\ h = -\int_0^1 Cp^+ h \quad (y/b\ \ )\ d(y/b)$$

Notes: 1 All harmonic (h>0) components have been nondimensionalized by the first harmonic of dalpha (in radians).

2 For layout reasons, the 0 indicating the 0-th harmonic component (mean value) is sometimes omitted in tables and plots.

3 Reference lengths are summarized below:
Sref = 0.144406 (m^2)
cref = 0.820700 (m)
bref = 0.417900 (m).

4 Pitching moments:
- Wing : about the rotation axis.
- Sections: about 25 % local chord.

6 Coefficients of spanwise sections:
Integration from y=0 to tip; rolling moment about y=0.

7 The section number of the section coefficients is either indicated at the left hand side of the presented values (e.g. see Table 6) or by an additional subscript (e.g. CN_u_1).

Symbols and definitions

acc	(m/s^2)	Acceleration (acc_11 is the acceleration measured by accelerometer 11; see Table 1)
ADC		Analog Digital Converter
alpha, α	(deg)	Incidence relative to the x-axis as determined from the LVDT signal harmonic oscillations: zeroth harmonic component of the signal maneuvers: half the sum of the maximum of the (1-cos) input and the minimum of the cosine input of one sequence (Note that the incidence relative to the root chord is alpha + 0.0803; see Appendix A).
b	(m)	(local) span; measured from root chord of SiS model (y=0)

bref	(m)	reference span used in nondimensionalizing the rolling moment: 0.4179 (distance between y=0 and tip section, excluding the wing tip fairing (see Sections 2.2.2 and 2.2.3)
c	(m,mm)	chord
Cd		drag coefficient
Cl		rolling moment coefficient
Cm		pitching moment coefficient
CN		normal force coefficient
COP		Computer of Pharao measurement system
Cp		pressure coefficient
cr,cref	(m)	length of reference chord SiS: root chord (at y=0) (0.820700)
DAC		Digital Analog Converter
dalpha,dα	(deg,rad)	model amplitude as determined from the LVDT transducer signal harmonic oscillations: first harmonic component of the signal maneuvers: half the difference between the maximum of the (1-cos) input and the minimum of the cosine input of one sequence (see also Figure 12)
DAT		Data Acquisition computer of Tunnel
dpn, DPN		data point number
DPT		Data Processing computer of Tunnel
f,freq	(Hz)	frequency, frequency of model oscillation
harm,h		harmonic component; harm = 1 refers to the model frequency
i		$\sqrt{-1}$
Im		Imaginary part e.g. CN h= Re (CN h) + i*Im(CN h)
k	(-)	reduced frequency, π*f*cref/V
LCO		Limit Cycle Oscillation
LE		Leading Edge
LVDT		Linear Variable Differential Transducer, refers to the displacement transducer mounted between a fixture on the turntable and a crank on the main axis
M,Mach	(-)	freestream Mach number
MCCU		Multi Channel Conditioning Unit (see Section 2.3)
MCFE		Multi Channel Front End (see Section 2.3)
p	(Pa)	pressure
p.a.		pitching axis
p_d	(deg)	pitch deflection of balance (>0 nose up)
PHARAO		Processor for Harmonic And Random Oscillations
PLTDA		Phase Locked Time Domain Averaging

ps	(Pa)	freestream static pressure
q,Q	(Pa)	freestream dynamic pressure
R		radius (see Figure 6)
r_d	(deg)	roll deflection of balance (>0 portside down)
Re	(-)	Reynolds number Re=V*cref/υ
Re		Real part, e.g. CN h= Re (CN h) + i*Im(CN h)
SiS		Simple Strake
SITES		Shock Induced Trailing Edge Separation
Sref	(m^2)	wing reference area: total wing area,including strake, excluding the area for y>0, see Figure 6 and Appendix A (0.144406)
T	(s)	Duration of a full (1-cos) input (see Figure 12), T=1/3.8
TE		Trailing Edge
V		freestream velocity
WRP		Wing Reference Plane
x	(mm)	ordinate (see Appendix A; see also x/c)
x/c	(-,%)	relative chordwise position
y	(mm)	spanwise ordinate (see Appendix A; see also y/b)
y/b	(-,%)	relative spanwise position
z	(mm)	ordinate (see Appendix A)

Greek

α	(deg)	incidence relative to the x-axis harmonic oscillations: zeroth harmonic component of the signal maneuvers: half the sum of the maximum of the (1-cos) input and the minimum of the cosine input of one sequence (Note that the incidence relative to the root chord of the SiS configuration is alpha + 0.0803; see Appendix A)
υ	(m^2/s)	(freestream) kinematic viscosity

Subscripts

ELL	Elliptic (see Section 4.1 and Table 3)
ETD	Equal Time Delay (see Section 4.1 and Table 3)
m	model (f_m = model frequency)
c	cut-off (f_c = cut-off frequency)
s	sample (f_s = sample frequency)

Superscripts

+	upper
-	lower

Postcripts

following order postscripts for section coefficients:

C1_2_3 h
- 1: N Normal force
  - m pitching moment
  - l rolling moment
- 2: u upper
  - l lower
  - t total
- 3: section number
  - h harmonic

h	harmonic; when no harmonic is indicated the mean value is presented
i	instationary
_in	inertia part
_j	section number
_l	lower
_m	mean (0-th harmonic)
_u	upper
_t	total
Zero	(0-th harmonic) mean; when no harmonic is indicated the mean value is presented
0	(0-th harmonic) mean; when no harmonic is indicated the mean value is presented

1 INTRODUCTION

1.1 Motive

The unsteady transonic flow during maneuvers of fighters is not very well understood. For instance, large time delays and severe dynamic overshoots in normal force may occur, which cannot be predicted accurately by numerical methods. As a consequence to be conservative, structures must be overdesigned or flight envelopes must be unnecessarily restricted. Therefore, a better understanding of the unsteady transonic vortex flows which occur during maneuvers, is of interest for development and operation of fighters.

In response to the above needs an unsteady transonic wind tunnel test simulating maneuver aerodynamics was conducted under a cooperative program of the Lockheed Forth Worth Company (LFWC, formerly the Forth Worth Division of General Dynamics) and the National Aerospace Laboratory (NLR).
This program was funded by the U.S. Air Force, LFWC and NLR.

1.2 Objectives

The objectives of the unsteady wind tunnel test devoted to maneuver aerodynamics are:

1 Development of a better understanding of the physics of the unsteady transonic vortex flow about a simple straked delta wing.
2 Generation of a steady and unsteady airloads data base for use in the validation of fluid dynamics computer codes.

To meet these objectives, a wind tunnel experiment on a highly instrumented semispan simple straked wing model was defined. Both pitch oscillation and maneuver simulation were included. In a way the test was considered as a continuation of the test with a full-span model at low speeds performed by NLR in 1986 (Ref. 1). Accordingly, the planform of the SiS model was chosen indentical to the planform of the full-span model.

1.3 Outline of this report

This report deals with the unsteady transonic wind tunnel test on the semispan model of the simple straked delta wing. Often it is referred to as SiS configuration. The outline of the report, which is also indicated in the foreword, is repeated below.

This report consists of three parts. Because presentation of all the measured data on paper would require more than 30,000 pages, only a limited number of data points is presented.

Part 1 presents the objectives of the program, a description of the model and test setup, the data acquisition and data processing techniques and also the test program for the experiment.

Part 2 presents five harmonics of five selected data points of the test on the straked delta wing, as measured during harmonic oscillation of the model, in plotted and tabulated form. These data are also made available on a floppy disk. As a reference, plots of overall quantities, deduced from a large number of data points, are presented.

Part 3 presents selected data obtained during simulation of maneuvers with the semispan straked delta wing. These data are also made available on floppy disk.

Readers who are interested to obtain part or all of the measured data and/or the geometric data of the model (e.g., in the CATIA or VDAFS format) should contact Lockheed or NLR.

2 TEST SETUP

2.1 Wind tunnel

The test was performed in the 1.60*2.00 m^2 High Speed Tunnel (HST) at NLR in Amsterdam. This wind tunnel has a closed circuit with a test section length of about 2.5 m. Top and bottom of the test section are slotted walls with an open ratio of 12 percent. The velocity range of this tunnel is $0<M<1.35$ and by changing the stagnation pressure from 12 kPa to 390 kPa a wide range of Reynolds numbers can be covered. The diplacement thickness of the wind tunnel sidewall boundary layer is 7 mm. For further details the reader is referred to Reference 2. Data in this section refer to the state of the wind tunnel during the test. After the test, in the summer of 1992, the tunnel was modified. One of the modifications concerned the enlargement of the test section to 1.80*2.00 m^2, although adjustment of the upper and lower walls still enable operation in the "old" configuration.

2.2 Model

2.2.1 General arrangement

For the test on the SiS model, the same highly instrumented outboard wing panel and support system were used as for a test devoted to Limit Cycle Oscillations (LCO). Figure 1 shows the relation between the SiS configuration and the LCO configuration.
Figure 2 shows the basic wing panel and corresponding support system. Main geometry information of the wing panel is collected in Appendix B. Support was provided through a semispan balance beam, mounted on a shaft, which in turn was supported by bearings mounted on the sidewall turntable.
Oscillatory motion of the balance beam and consequently of the outboard wing panel was provided by an electro-hydraulic shaker system mounted on the sidewall turntable of the tunnel. Adjustment of the mean angle of attack was done by rotating the turntable.

The SiS configuration included a strake which was attached to the outboard wing (Figure 3). In the LCO configuration a fighter type fuselage was fixed to the turntable.

All model and support parts were designed and fabricated by NLR. Also instrumentation and calibration were accomplished at NLR. For details of the design of the two wind tunnel models the reader is referred to Reference 3.

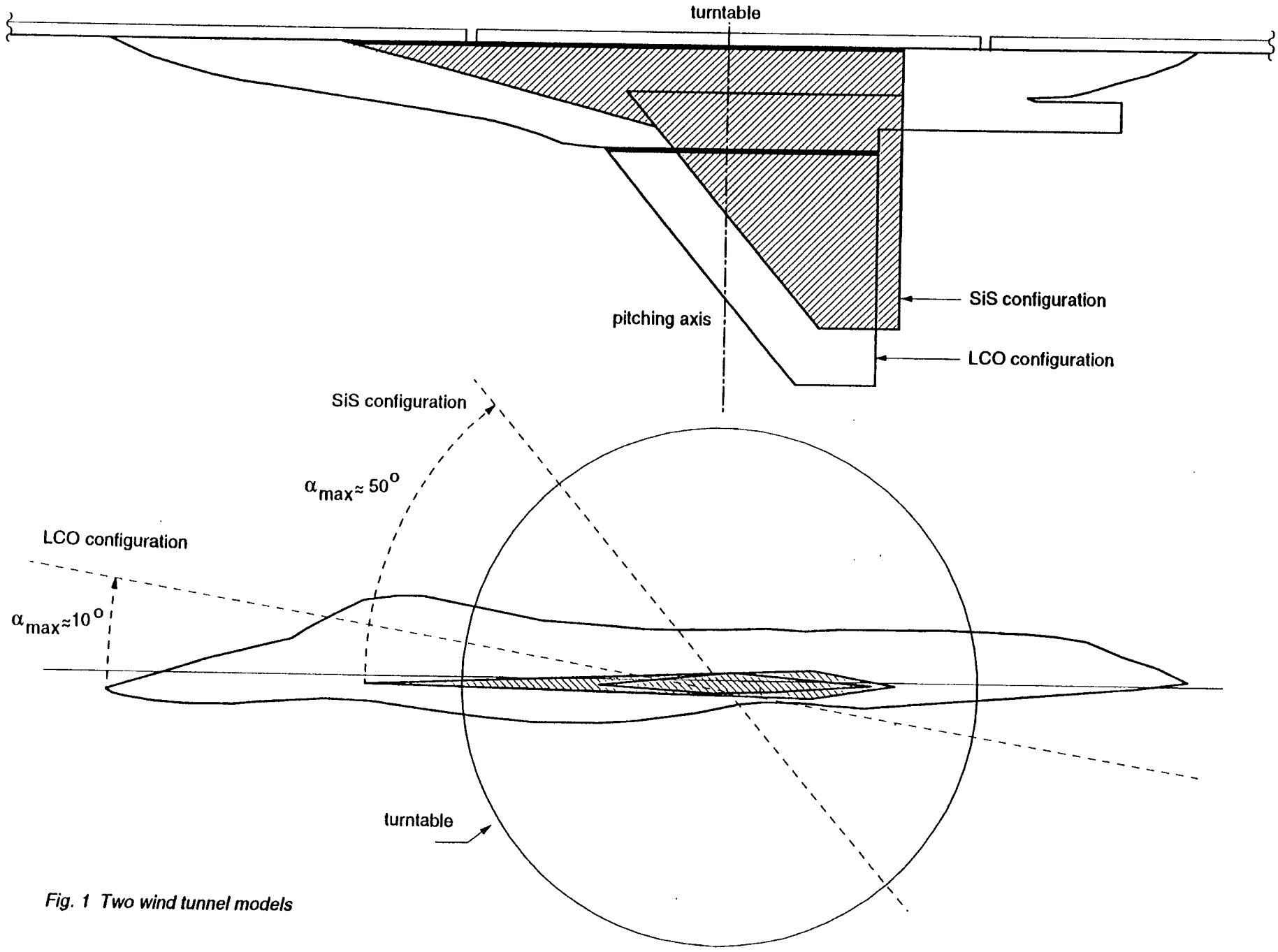

Fig. 1 Two wind tunnel models

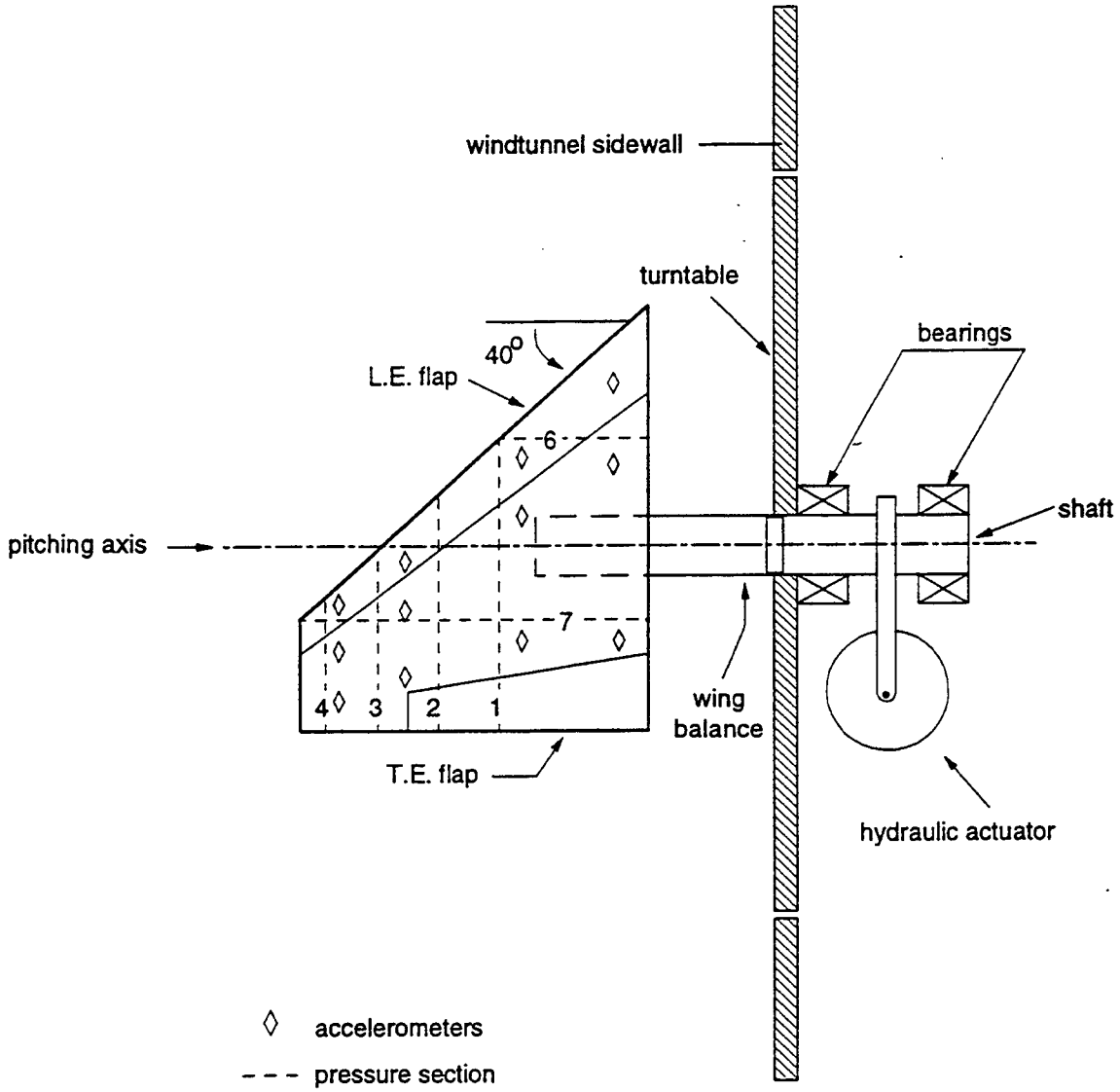

Fig. 2 Outboard wing panel and support system

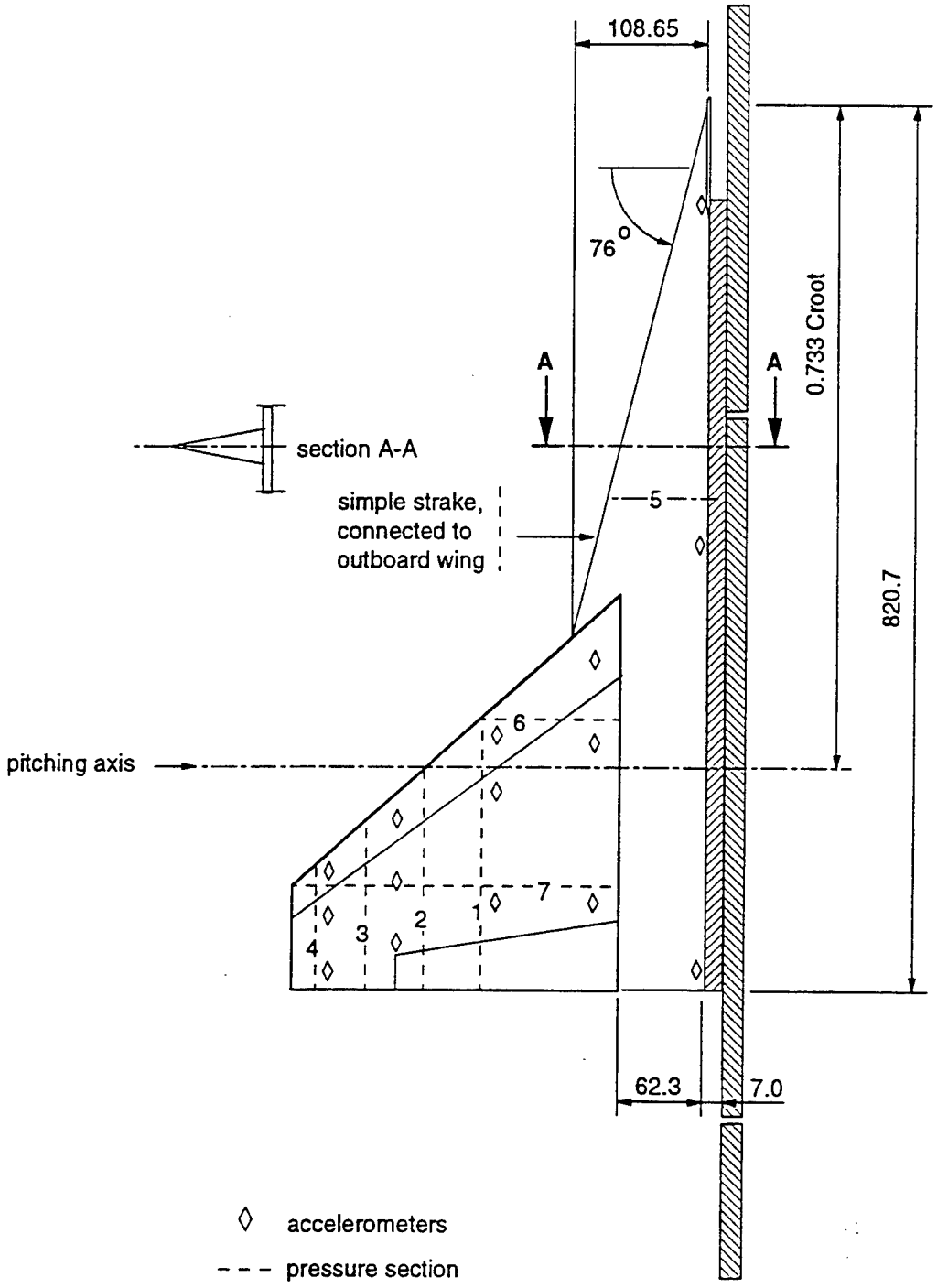

Fig. 3 SiS configuration (dimensions in mm)

2.2.2 Outboard wing panel, support and excitation

The panel was linearly lofted between root and tip and had a constant NACA 64A204 (mod.) section. The wing twist was -3.0 deg. Support was provided through a semispan balance beam, mounted on a shaft, which in turn was supported by bearings mounted at the sidewall turntable (Figure 2). To reduce inertia loads, the wing panel was made of high strength aluminum alloy. For strength reasons the attachment of the wing panel to the balance beam was not at the root chord, but at about 40 per cent of its span. The lower side of the wing panel was thickened over the first part of the span to accommodate, but not make contact with, the balance beam. Main geometry information of the wing panel is collected in Appendix B.

During the design of the model, the thickness of the balance beam and consequently the thickening of the wing were varied to investigate the influence on both the natural frequencies of the model-balance combination and the aerodynamics. The goal during this design process was to find an optimum between conflicting design objectives:

- A first natural frequency of the wing panel and balance combination above the highest test frequency.
- Minimization of the balance beam dimensions in order to have the beam stored within the available interior space of the wing panel.
- Minimization of the static deformations of the balance beam in order to avoid changes in the aerodynamics.
- Meeting the specified strength requirements.

By modifying only the lower part of the wing in the region between y = -62.3 mm and y = -209.9 mm, a high first natural frequency was obtained, while the aerodynamics in the outboard region were almost unchanged. The modification started downstream of the leading edge flap and extended to the trailing edge. The additional thickness varied from zero at y = -209.9 mm to 2.5 per cent local chord of the outboard wing panel at y = -62.3 mm.

The chordwise position of the balance beam relative to the model was chosen in such a way that the location of the pitching axis was the same as in the corresponding low-speed model (Ref. 1): 73.3 % of the root chord of the semispan model.

Oscillatory motion of the balance beam and consequently of the outboard wing panel was provided by an electro-hydraulic shaker system which consisted of a hydraulic power supply, linear actuator and servovalve and a feedback control unit (Ref. 4). The hydraulic actuator could deliver a maximum static force of 13000 N and a dynamic force of 8000 N at a total piston stroke of 35 mm at low

frequencies to 1.1 mm at 90 Hz. The hydraulic actuator was suspended in a box which was bolted rigidly to the turntable. The piston was connected to a crank which converted the linear motion into a rotational motion. Because of different amplitude-frequency requirements for the LCO test and the SiS test, the distance between the working line of the piston and rotation axis was chosen 80 mm and 60 mm, respectively. The mean position and dynamic motion of the balance beam with respect to the turntable were measured by an LVDT mounted between a crank on the shaft and a fixture on the turntable.

The wing panel was of a "clamshell" design so that all instrumentation inside the wing was accessible. Figure 4 shows the outboard wing panel with and without the balance beam. It had instrumented leading and trailing edge flaps. At the tip, a fairing with a tip radius of 0.5 * the local wing thickness was mounted.

2.2.3 SiS configuration

The SiS configuration is shown in Figures 1,3,5,6 and 7. Since the test on this configuration was the transonic counterpart to the low-speed test of Reference 1, the strake had to move with the wing and was, therefore, attached to the basic wing panel. In this way a semispan model was obtained with the same planform as (half of the) full-span model used in the test reported in Reference 1. Loads from both the wing and strake were carried through the semispan balance beam. The rotation axis was located at the same position as in the low-speed test: 73.3 per cent root chord. The spanwise cross-section of the strake has (half) a diamond shape with half a top angle of 11.4 deg. At the tunnel wall the cross-section was rounded with a radius which varied linearly from 0 mm at the apex to 100 mm at a position 417.2 mm downstream of the apex. The sharp leading edge was in the wing reference plane. The y=0 plane, which corresponded to the plane of symmetry of the (full-span) low-speed model, was located on a distance from the sidewall which corresponded to the local displacement thickness of the tunnel sidewall boundary layer (7.0 mm). To impose the start of the vortex on the apex, a little flat plate of 1.5 mm thickness was attached to the model (Figures 5 and 6). Downstream of this plate the model was extended from the symmetry plane in starboard direction to y=1.5 mm, leaving a gap of 5.5 mm between sidewall and model. Downstream of x=-96.4 mm, the model was extended another 5 mm to y=6.5 mm, providing passage of the balance beam (Figure 7). Between x=-96.4 mm and -520.6 mm a filler plate of 5.0 mm thickness could be mounted, reducing the gap between model and tunnel wall to 0.5 mm. Close to the kink in the leading edge, the strake leading edge was thickened to provide a smooth connection with the outboard wing panel. Also the region where the outboard wing panel

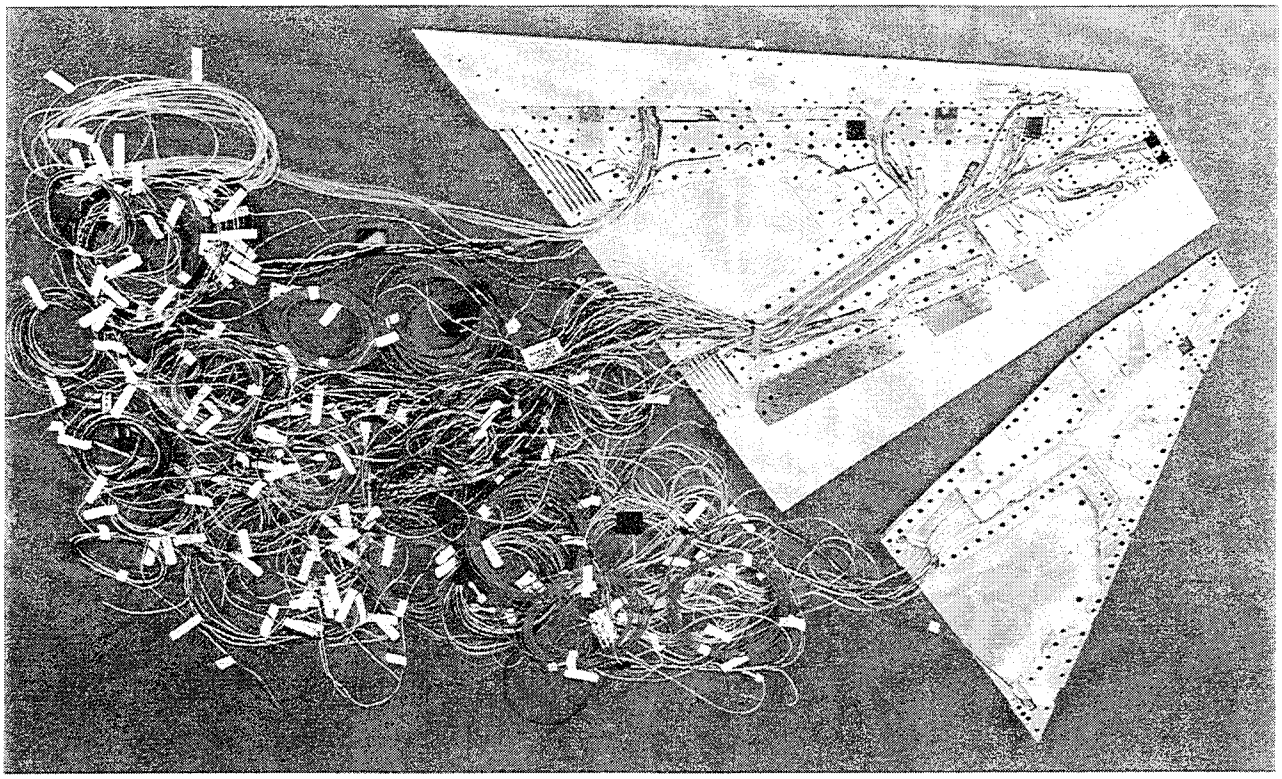

Fig. 4a The outboard wing panel without balance beam

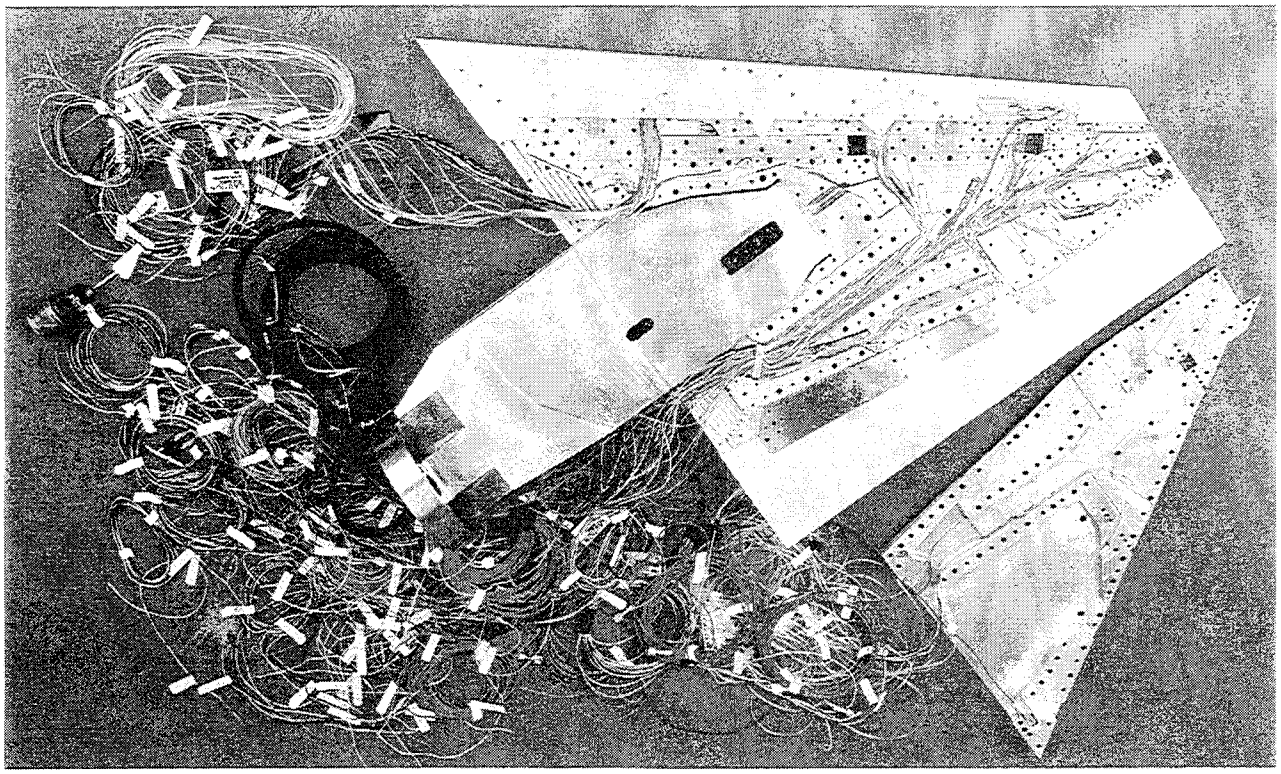

Fig. 4b The outboard wing panel with balance beam

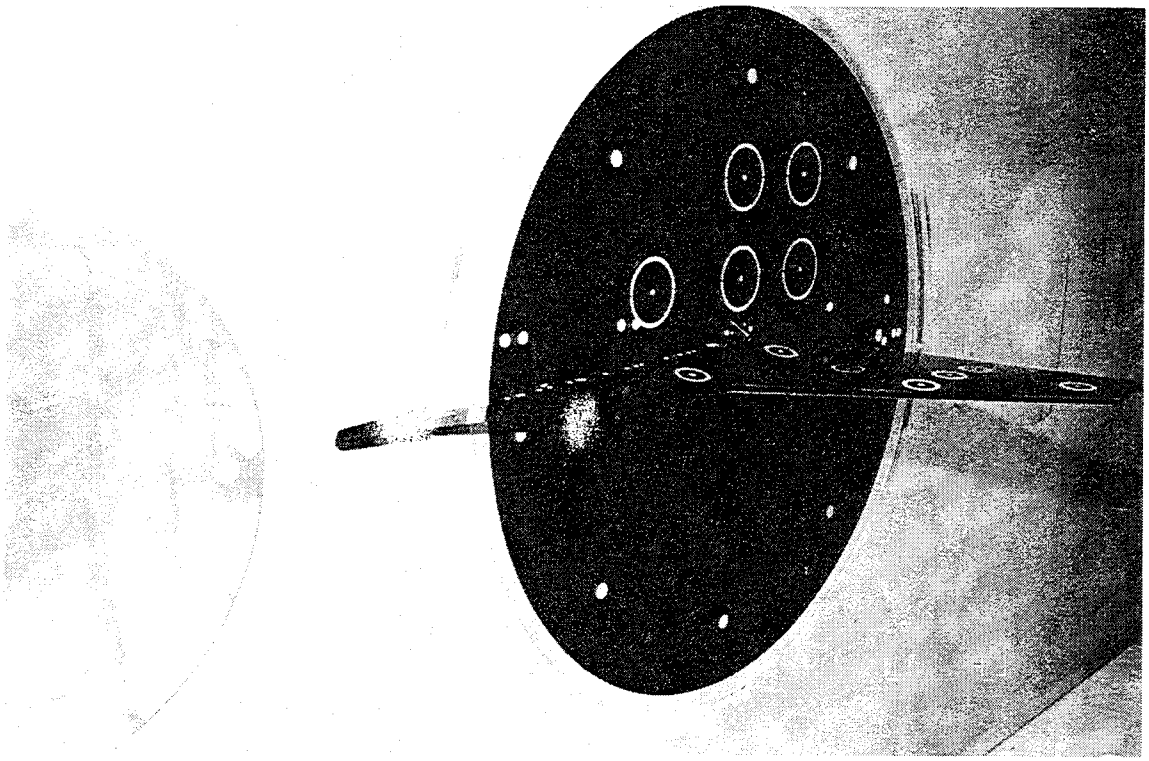

Fig. 5a The SiS configuration in the wind tunnel; overall view

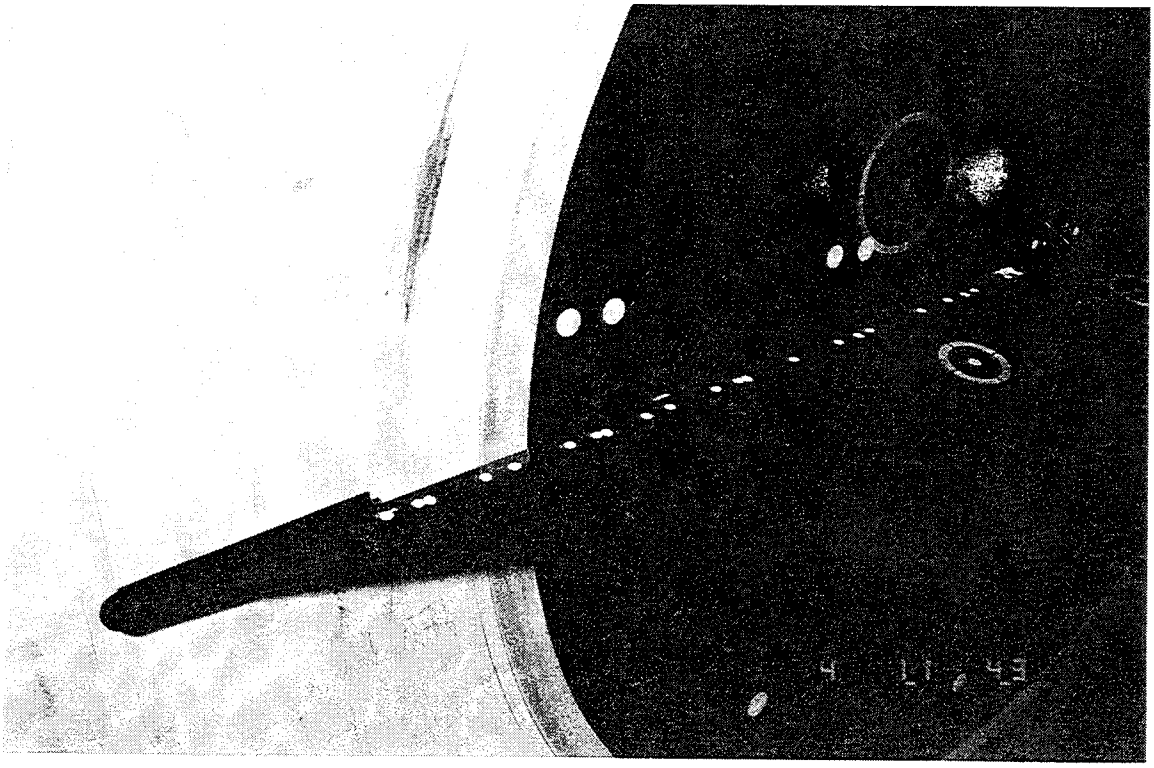

Fig. 5b The SiS configuration in the wind tunnel; detail of apex with "little flat plate"

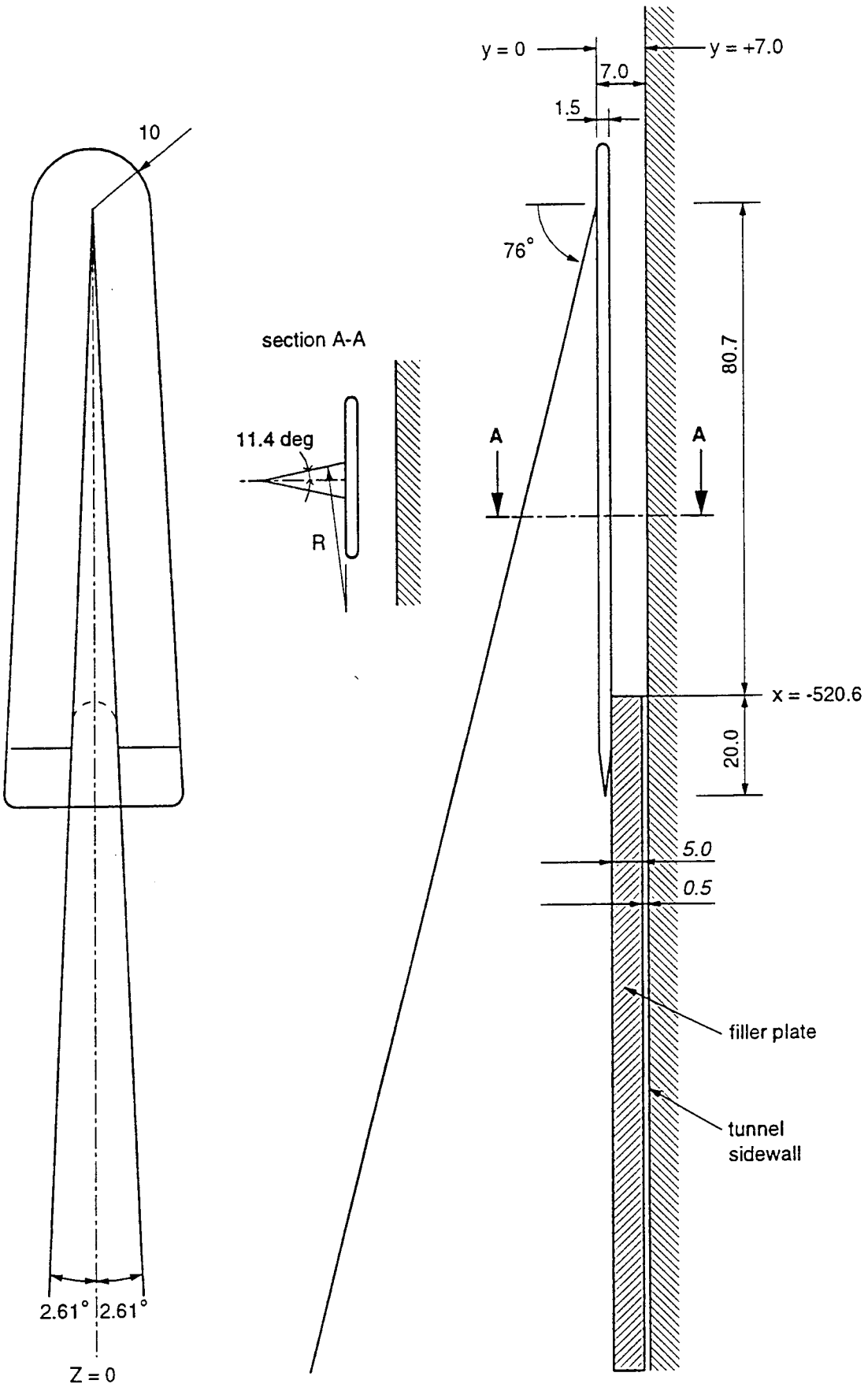

Fig. 6 Little flat plate at apex and filler plate of SiS configuration (dimensions in mm)

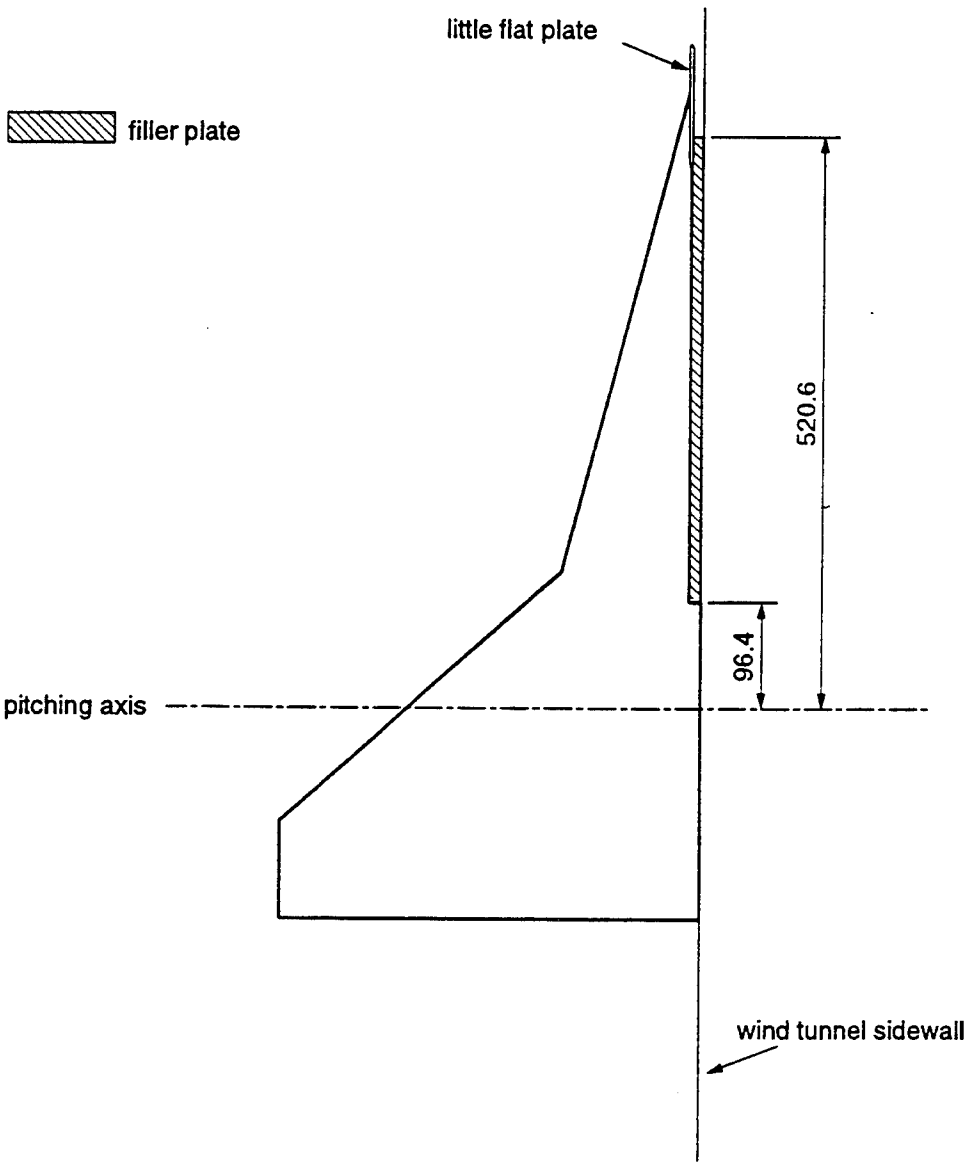

Fig. 7 Positioning of little flat plat and filter plate (SiS configuration; dimensions in mm)

was attached to the inboard part of the model was smoothed. The leading and trailing edge flaps were fixed at zero deg. The strake was provided with three accelerometers and an additional spanwise pressure section at 40.42 per cent of the root chord; for details of the instrumentation the reader is referred to Section 2.2.4. The model was provided with transition strips of 2 mm width on the upper and lower side of the outboard wing (y <-108.65 mm), starting 14.5 mm downstream of the leading edge (measured perpendicular to the leading edge). The grit size was 88 µm (Carborundum 150).

Directly after the pressure and loads measurements on the SiS model, a preparatory visualization test was done during half a day using the vapor screen technique and a high speed video camera. For this test the large markers, shown in Figure 5, were painted on the model. The results of this visualization test are not included in this report; additional flow visualization test are planned for 1995.

2.2.4 Instrumentation

The main wing balance measured normal force, pitching moment and rolling moment.

A linear variable differential transducer (LVDT) was mounted between a crank on the shaft of the excitation mechanism and a fixture on the sidewall turntable to measure both the mean and unsteady component of the relative position of the balance beam with respect to the sidewall turntable. Mean incidence of the turntable was measured by a very sensitive accelerometer attached to the turntable, measuring a component of the gravitational acceleration.

The basic wing panel was provided with four chordwise rows (Sections 1 to 4) and two spanwise rows (Sections 6 and 7) of miniature pressure transducers as shown in Figure 2. A third spanwise row (Section 5) was provided in the strake (Figure 3). The pressure points of the chordwise rows were located toward the wing tip in order to concentrate instrumentation in the region where phenomena like shock-induced separation and leading edge separation, take place. The three spanwise rows were intended to observe shock-vortex interactions at higher incidences. Sections 5 and 6 (40.42 and 65.88 per cent root chord) correspond to spanwise sections in the model of Reference 1. All pressure transducers were mounted such that they were electrically isolated, free of local model deformations, and not influenced by model accelerations. The sensitivity of the pressure transducers showed a small variation with temperature. By measuring the model temperature with two temperature sensors,

the correct sensitivity of the pressure transducers could be selected for processing recorded electrical signals into pressure data (see also Section 4.2.2).

Accelerometers, measuring accelerations in z-direction, were located at 12 positions on the basic wing as shown in Figure 2 and at 3 positions on the strake as shown in Figure 3.

The location of the instrumentation was included in the printout of each data point. As a reference this information is summarized in Figure 8 and Table 1. In total, 95 pressure transducers, 1 displacement transducer, 2 temperature sensors, 15 accelerometers and 3 balance components were measured during the SiS test.

During the test some sensors were not working properly. Table 2 gives an overview.

2.3 Measurement system

The wind tunnel test was performed using the fully digital computer controlled measurement system PHARAO (Processor for Harmonic And Random Oscillations). The system acquired 128 signals simultaneously.

The measurement system as used during the test is outlined in Figure 9. Three main parts can be distinguished:

1 Multichannel Conditioning Units (MCCU's).
2 Multichannel Front Ends (MCFE's).
3 Computers to control the MCCU's and MCFE's.

In the MCCU's the filters for splitting the signal into an ac and a dc part, as well as the preamplifier and the ac and dc postamplifiers are integrated in one module for each two channels, together with a shared excitation source. Eight of these modules are integrated in one Multichannel Conditioning Unit (MCCU), which is suitable for 16 input signals. Each MCCU has its own ADC and computer interface. The dc measurement is done in the MCCU's. As a special feature the dc component of all channels can be stored in a track/hold circuit and the high-pass filter can be bypassed. In this way, a fixed voltage can be subtracted from the preamplified ac+dc signal. The aim of this mode is the possibility to measure and amplify slowly varying input signals with a large dc component. This mode is called the subtract mode of the MCCU's; it was used in the SiS test during the simulation of maneuvers. The MCCU's were

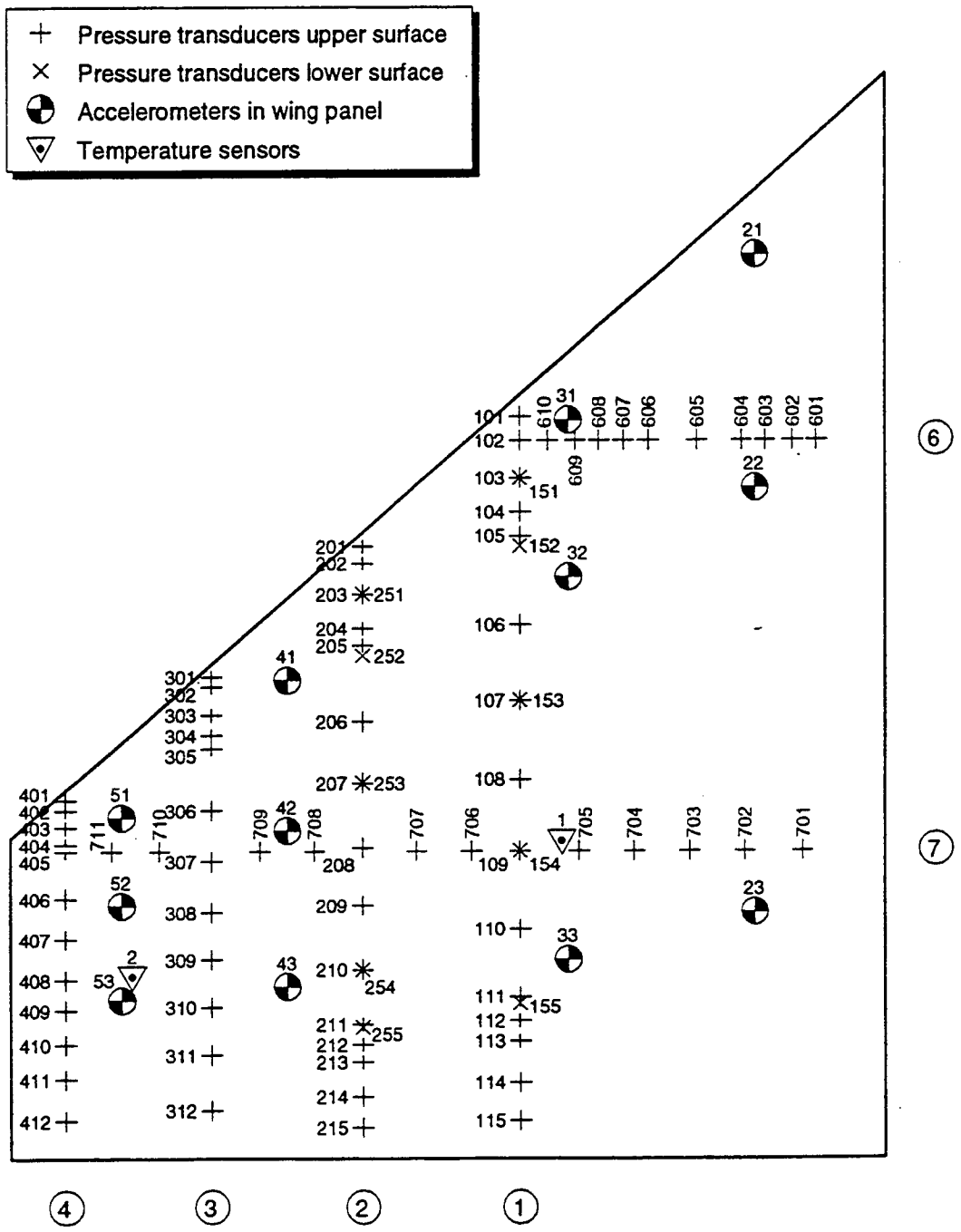

Fig. 8 Location of instrumentation in outboard wing panel (see also table 1)

Table 1a Coordinates of accelerometers in wing and strake
(measures in mm; see also Figure 8)

NR.	x	y
11	-425.6	- 12.0
12	-215.6	- 12.0
13	167.4	- 12.0
21	-138.6	-116.9
22	- 46.6	-116.9
23	121.4	-116.9
31	- 74.6	-189.9
32	- 10.6	-189.9
33	141.4	-189.9
41	29.4	-304.9
42	89.4	-304.9
43	152.4	-304.9
51	85.0	-374.9
52	121.4	-374.9
53	157.4	-374.9

Table 1b Coordinates of temperature sensors
(measures in mm; see also Figure 8)

NR.	x	y
1	96.4	-194.9
2	147.4	-371.9

Table 1c Coordinates of pressure points of Sections 1 and 2
(measures in mm; see also Figure 8)

			PRESSURE SECTION 1 chord = 300.65	PRESSURE SECTION 2 chord = 246.21
			y = -209.06 y/b = 0.500	y = -273.97 y/b = 0.656
nr. up	 low	% chord	x	x
101		2.00	-75.31	-21.93
102		5.00	-66.29	-14.55
103	151	10.00	-51.25	-2.24
104		15.00	-36.22	10.07
105		18.00	-27.20	17.46
	152	20.00	-21.19	22.38
106		30.00	8.88	47.00
107	153	40.00	38.95	71.62
108		50.00	69.01	96.24
109	154	60.00	99.08	120.86
110		70.00	129.15	145.47
111		79.00	156.21	167.63
	155	80.00	159.22	170.09
112		82.50	166.73	176.25
113		85.00	174.25	182.40
114		90.00	189.28	194.71
115		95.00	204.32	207.02

Table 1d Coordinates of pressure points of Sections 3 and 4
(measures in mm; see also Figure 8)

		PRESSURE SECTION 3 chord = 194.13	PRESSURE SECTION 4 chord = 144.42
		y = -336.06 y/b = 0.804	y = -395.32 y/b = 0.946
nr. up low	% chord	x	x
301	2.0	29.13	77.86
302	5.0	34.95	82.19
303	10.0	44.65	89.40
304	15.0	54.35	96.92
305	18.0	60.18	100.95
306	30.0	83.46	118.27
307	40.0	102.87	132.70
308	50.0	122.28	147.13
309	60.0	141.68	161.56
310	70.0	161.09	175.99
311	79.0	178.55	188.98
312	90.0	199.90	204.86

Table 1e Coordinates of pressure points of Section 5
(measures in mm; see also Figure 8)

	PRESSURE SECTION 5 b = 82.7
	x = -269.6 (40.42 % cr)
nr. up	% span	y
501	6.62	5.47
502	20.43	16.90
503	34.05	28.16
504	47.67	39.42
505	54.49	45.06
506	61.29	50.69
507	68.10	56.32
508	74.91	61.95
509	81.72	67.59
510	88.53	73.21

Table 1f Coordinates of pressure points of Section 6
(measures in mm; see also Figure 8)

	PRESSURE SECTION 6 b = 233.73
	x = - 60.62 (65.88 % cr)
nr. up	**% span**	**y**
601	38.90	90.91
602	42.93	100.35
603	46.93	109.70
604	50.99	119.17
605	59.03	137.96
606	67.07	156.77
607	71.11	166.21
608	75.56	176.21
609	80.00	186.99
610	84.44	197.37
102	89.45	209.06

Table 1g Coordinates of pressure points of Section 7
(measures in mm; see also Figure 8)

	PRESSURE SECTION 7 b = 417.90
	x = 100.71 (85.54 % cr)
nr. up	**% span**	**y**
701	22.71	94.90
702	28.21	117.90
703	33.72	140.90
704	39.26	164.07
705	44.69	186.74
109	50.03	209.06
706	55.28	231.03
707	60.46	252.67
208	65.56	273.97
708	70.59	294.99
709	75.54	315.69
307	80.42	336.06
710	85.22	356.12
711	90.19	376.90
405	94.60	395.32

Table 2 Overview of sensors which did not work properly

PRESSURE TRANSDUCERS		ACCELEROMETERS	DATA POINT NUMBER (dpn)
st.	**unst.**		
105	105		all dpn's
	210		all dpn's
		22	all dpn's
		32	all dpn's

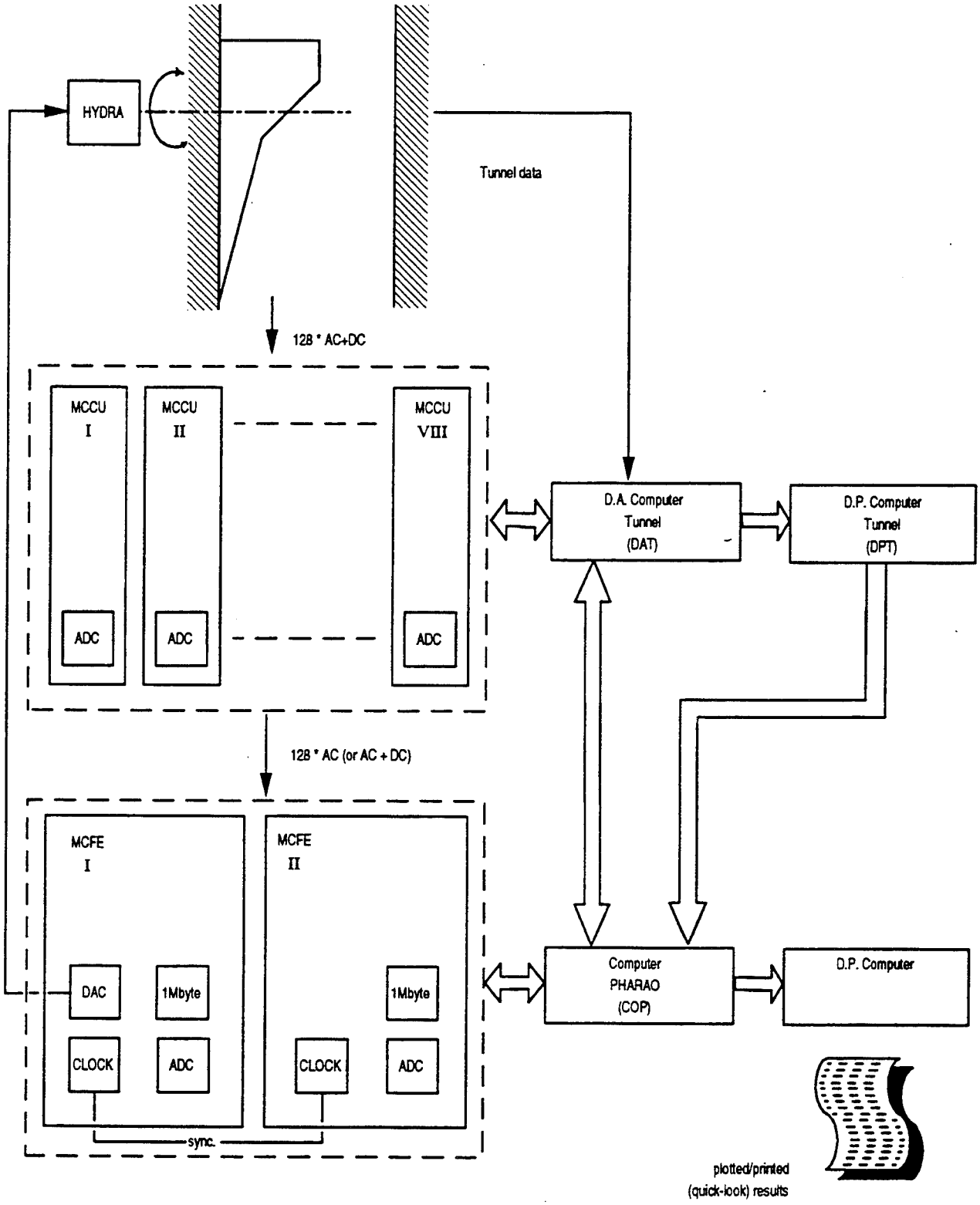

Fig. 9 Measurement system during test on SiS configuration

designed by NLR. For other features of the MCCU's the reader is referred to Reference 5.

Each Multichannel Front-End (MCFE) has a 750 kHz ADC and a crystal controlled clock. In every MCFE 64 modules are integrated. Each module has a computer-programmable (antialiasing) low-pass filter and a pre- and postfilter amplifier. The front-end modules are also provided with a sample/hold circuit to enable real simultaneous sampling of the different channels. Special synchronization between the two MCFE's was used to ensure simultaneous sampling of all signals. The highest possible sample rate of the PHARAO configuration depicted in Figure 9 was about 11 kHz. Especially at high frequencies, the data flow between MCFE's and computer would be too large. Therefore the MCFE's are equipped with 1 Mbyte local memory, which acts like a buffer between the measured samples and the memory of the host computer. In one of the MCFE's a quadruple DAC was embedded. This DAC was fully programmable, providing both the harmonic signals for model oscillation and the signals which represent maneuver inputs.

The MCFE's were operated remotely controlled according to the scheme in Figure 9. The measuring process was governed by the Computer of PHARAO (COP). It controlled directly the MCFE's. Control of MCCU's was exercised by the Data Acquisition computer of the wind Tunnel (DAT), but only on instruction of the PHARAO computer. In this way ranging, setting the MCCU mode, overload detection, and ADC scans for all MCCU's simultaneously, could be performed independently by the tunnel computer. On request by COP, the data acquired by DAT were sent to COP. At each data point the measured time traces and corresponding spectra as calculated by a microprogrammed FFT coprocessor card in the COP system, were stored on an optical disk. To this data were added the dc data and (amplifier-) settings obtained from DAT and the corrected tunnel data obtained from the data processing computer of the wind tunnel (DPT). Processing of the data to (quick-look) results was done by a separate computer which had direct access to the data on the optical disk of COP.

3 PREPARATORY TESTS

Before the tunnel entry of the model, the natural frequencies, corresponding vibration modes and generalized masses were determined by the impact method in a separate test. The model was mounted on its main balance beam. The balance beam was mounted on the shaft which was supported by bearings mounted at the turntable of the tunnel sidewall. The (very stiff) turntable was supported in a special frame which provided the possibility of doing these tests outside the wind tunnel.

With the results of these tests it was possible to choose oscillation frequencies for the wind tunnel test program in such a way that (higher harmonics of) the driving frequency were not very close to natural frequencies of the model. The results of the vibration analysis were also used as input for the flutter calculations which were done before the wind tunnel test.

As an example, Figure 10 shows the frequency response function of an impact and the response for the SiS configuration. The different peaks associated with the natural vibration modes can be distinguished clearly. These modes are shown in Figures 11b through 11d, while Figure 11a presents the undeformed grid.

Measuring with balances in unsteady wind tunnel tests requires the subtraction of the inertial loads from the total loads to obtain the aerodynamic loads. For harmonic excitation with frequencies below 8 Hz, the model was considered rigid and the (small) inertial loads were easily determined from known mass properties of the model and angular accelerations determined from the displacement transducer output. For the processing of data of runs with harmonic excitation at frequencies above 8 Hz or maneuver data the "mode fit" procedure (see Section 4.2.3.1) was used. For this procedure it was necessary to determine the relation between the output of all accelerometers and the main balance for all natural frequencies. These relations were measured during a preparatory test in which the model was oscillated harmonically at all natural frequencies below 250 Hz. Also these relations were measured (at 10 Hz) for a pure pitch motion of the rigid model.

Note that the deformations of the balance are presented for each data point (see e.g. Table 6). For this purpose the stiffness matrix of the balance was determined in a separate preparatory jig test, enabling the calculation of the deformations during the data reduction.

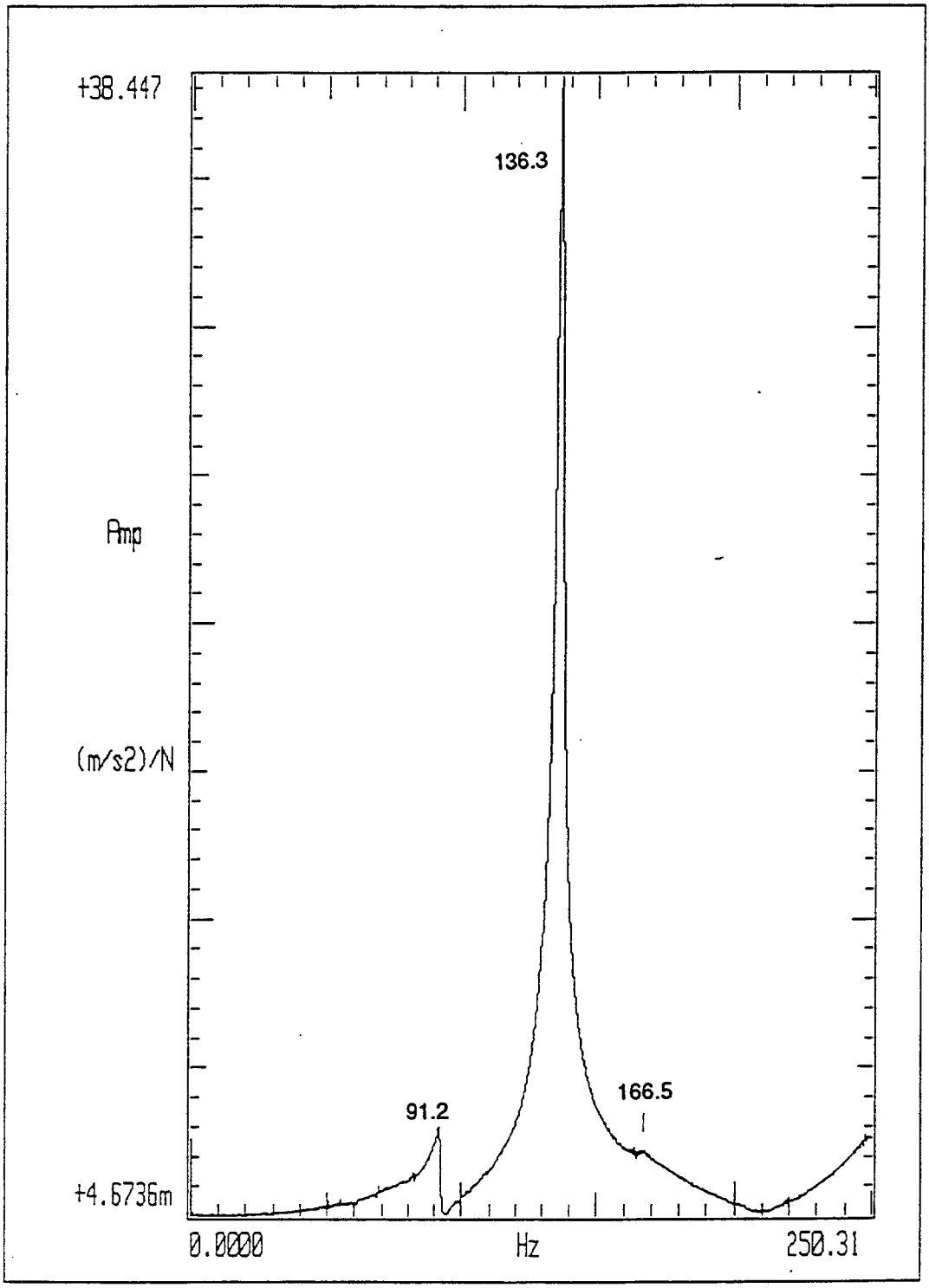

Fig. 10 Frequency response function of an impact at point 84 and the response at point 113 (see Fig. 11a)

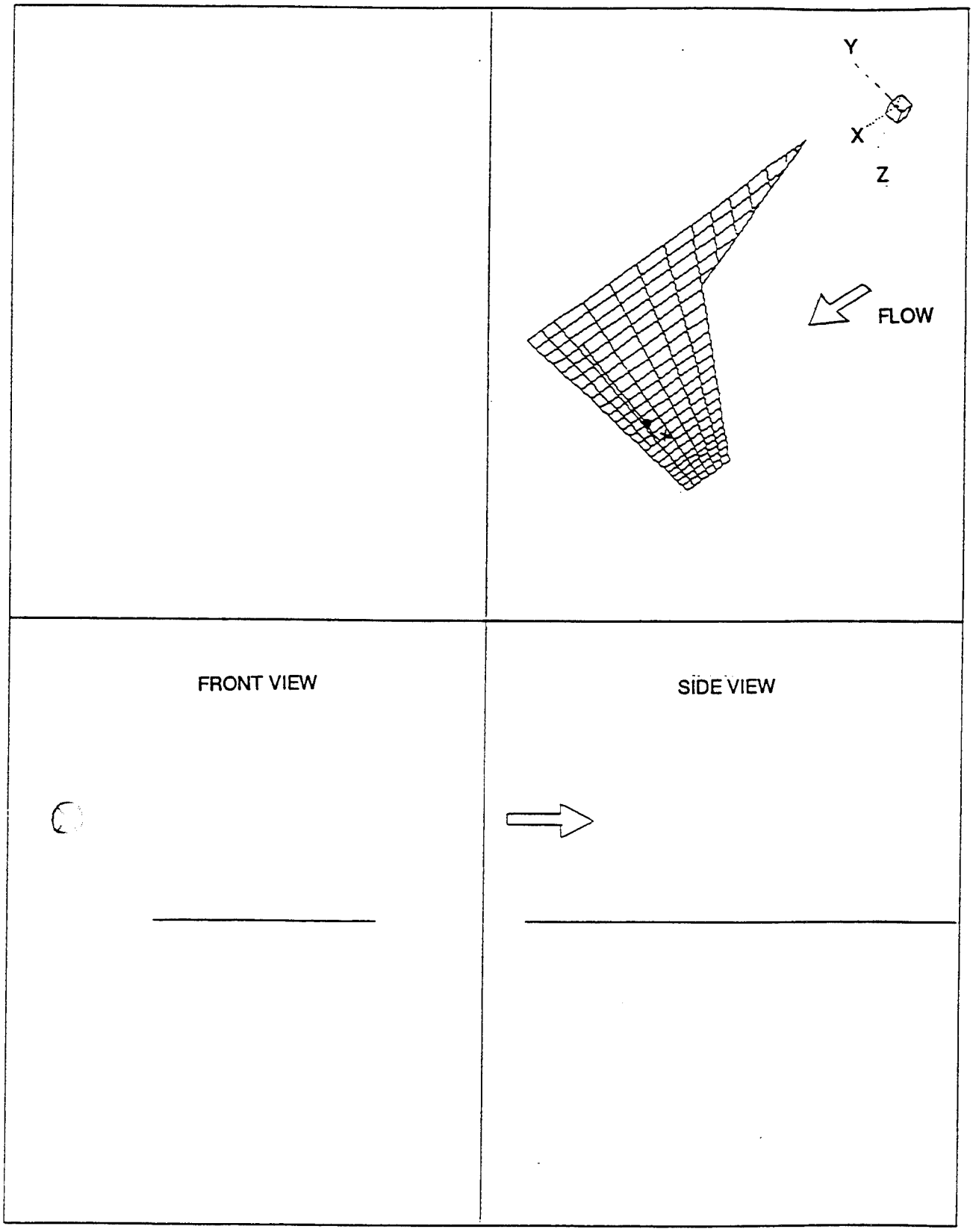

Fig. 11a Undeformed grid used for impact testing
• point 84, x point 113

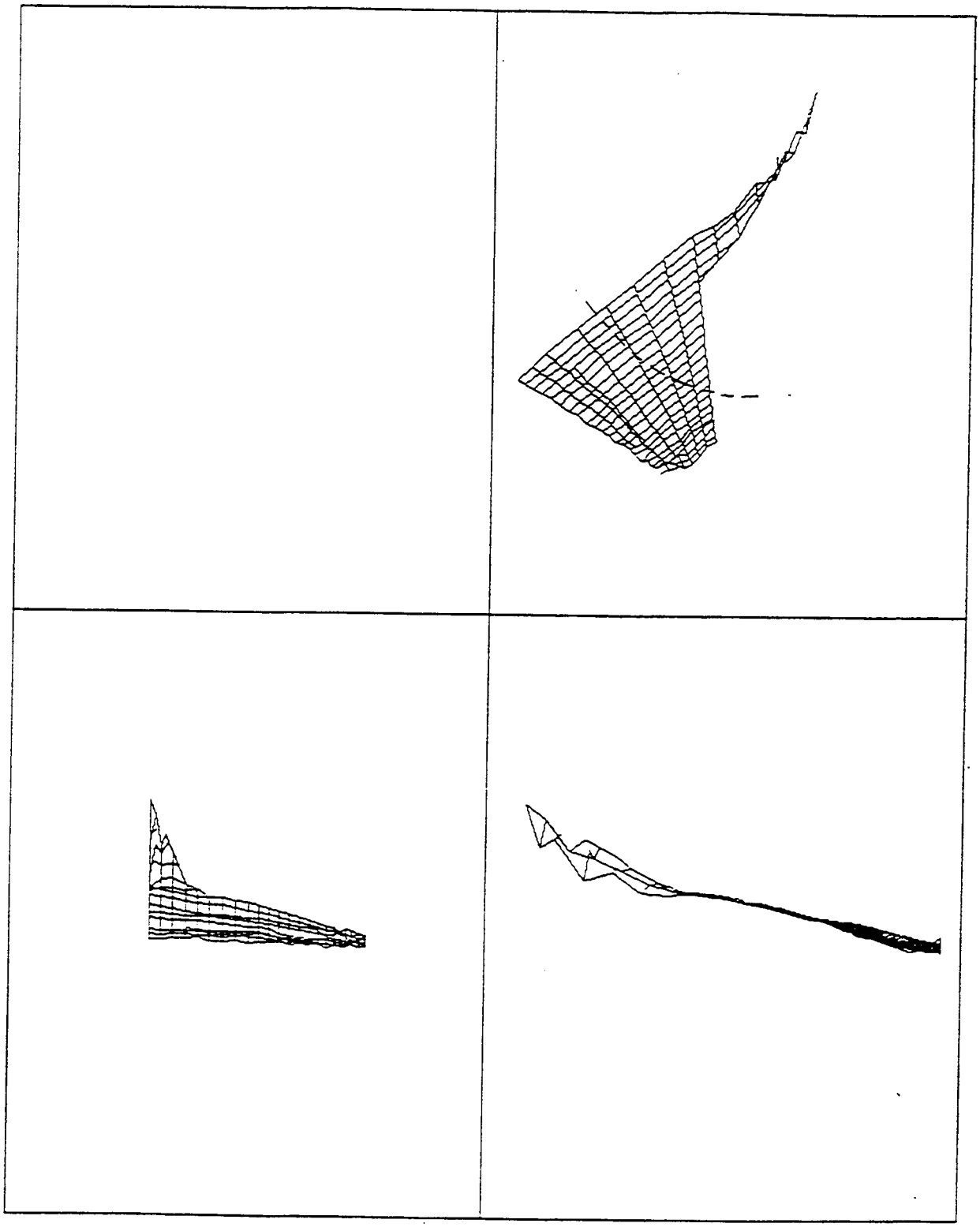

Fig. 11b Natural vibration mode at 91.2 Hz: torsion of the main balance and pitch rotation of the wing with (small) additional bending of wing tip and strake; (see indicated nodal line (- - -))

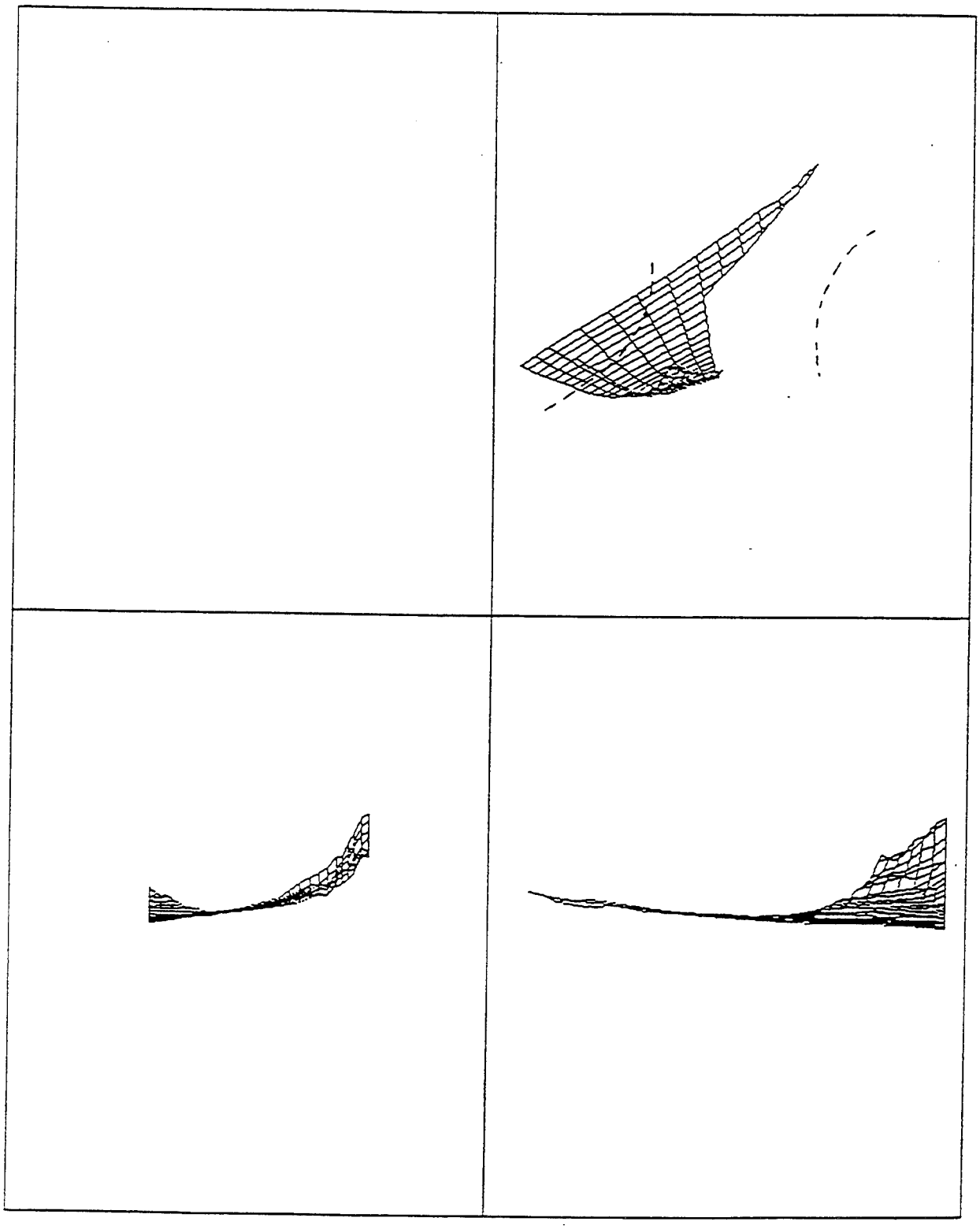

Fig. 11c Natural vibration mode at 136.3 Hz: bending combined with torsion, of the wing tip and a pitching motion of the root section with opposite phase as the tip rotation (see indicated nodal line (- - -))

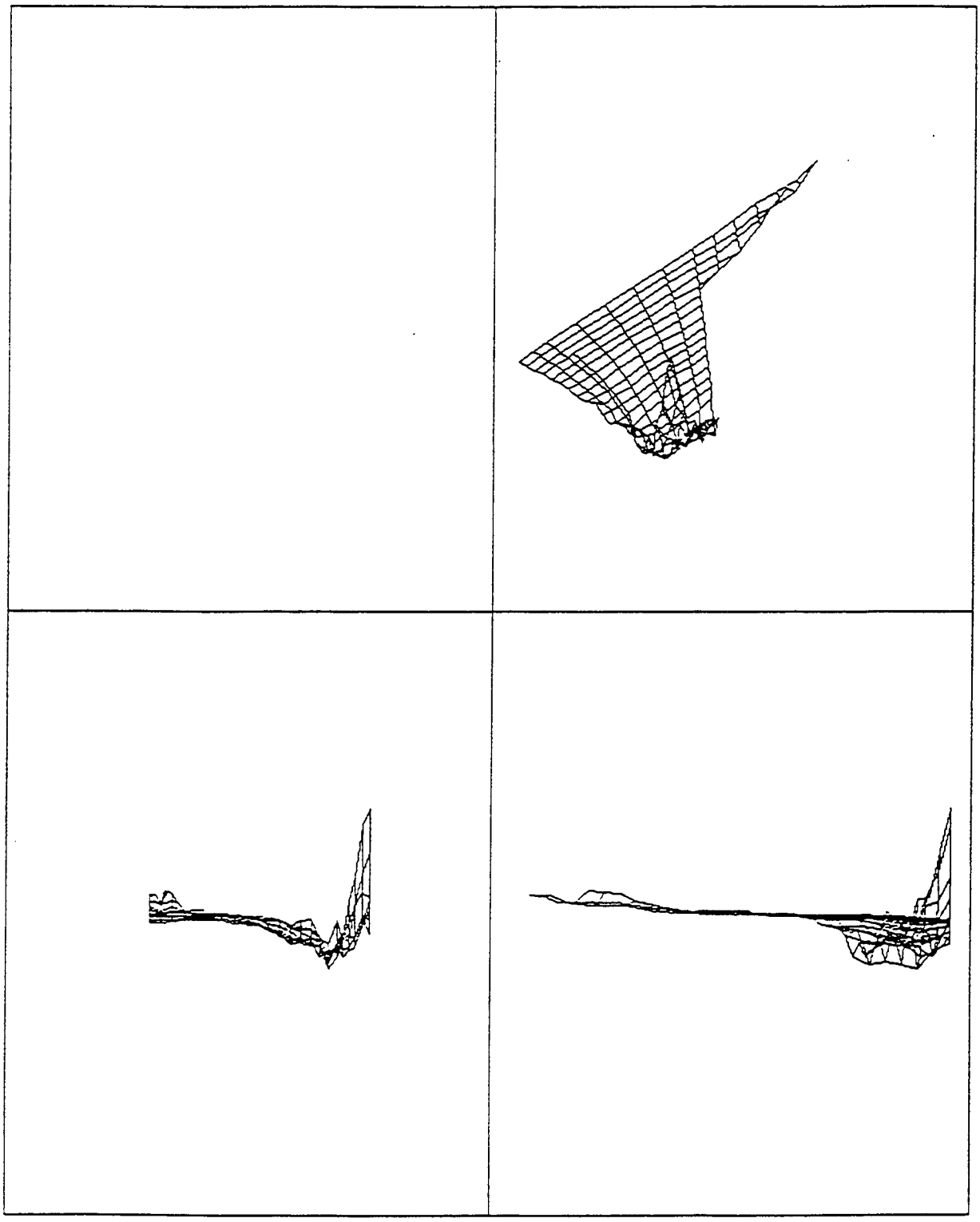

Fig. 11d Natural vibration mode at 166.5 Hz: second bending mode of the outboard wing panel

4 PROCEDURES

4.1 Data acquisition

During harmonic oscillation, signals were sampled with a frequency being a multiple of the model frequency. Both frequencies were perfectly synchronized as they were generated by the same clock (see Section 2.3).
The cut-off frequency of the first group of 64 antialiasing, equal time delay (ETD), 60 dB/octave filters which were programmable in steps of 1 Hz, was always 50 % of the bandwidth. The second group of 64 antialiasing, elliptic (ELL), 80dB/octave filters had steeper filter characteristics.
Therefore, the largest cut-off frequency below 80 % bandwidth was chosen. Due to the large increments (100 Hz) in the programmable cut-off frequency, this frequency was not always close to 80% bandwidth. Table 3 presents an overview of the different combinations of the model frequency, sample frequency, bandwidth and filter setting used for the data acquisition.

For all data points, including the maneuver simulations, always 4096 samples were stored in the measurement file for each measurement channel. Before and after each series of measurements the output of the sensors at zero-wind condition was stored in a so-called zero-measurement file.

4.2 Data processing

4.2.1 General

For the data points with harmonic oscillation of the model, the prime interest was in the different harmonic components (multiples of the model frequency). Therefore, Phase Locked Time Domain Averaging (PLTDA) was applied on the time traces stored in the measurement files. Further processing was done with the averaged time trace of one cycle of the model motion. After the correction for the characteristics of the antialiasing filters and the determination of the squared terms in the time domain, Fourier transformation to the frequency domain was applied. Application of sensor characteristics, corrections for zero measurements and determination of inertia loads on the balance were performed in the frequency domain. For data points with the model oscillating harmonically, the result was the mean value, the first harmonic and the second to the sixty-fourth harmonic component in the spectrum (realize that 128 samples per cycle were measured).

For the processing of the maneuvers, the procedure was in principle the same as above, except the fact that no averaging was done. So, one block of 4096

Table 3 Data acquisition parameters. For 5.7 to 15.2 Hz only harmonic oscillations were executed (see Tab. 4 (test program)); for 3.8 Hz only maneuvers were done (see Tab. 5 (test program)), for this case the "frequency" refers to 1/timescale of the full (1-cos) maneuver.

f_m	f_s $128*f_m$	BandWidth (BW) $0.5*f_s$ $64*f_m$	f_c ETD 50 % BW $0.25*f_s$ $32*f_m$	f_c ELL
3.8	486.4	243.2	121	100 (41% BW)
5.7	729.6	364.8	182	200 (55% BW)
7.6	972.8	486.4	243	300 (62% BW)
11.4	1459.2	729.6	364	500 (69% BW)
15.2	1945.6	972.8	486	700 (72% BW)

samples for each sensor was processed as a whole (realize that for the processing of the data points with oscillating model only 128 "averaged samples" representing one cycle of the model motion, were processed for each sensor).

For the data points with harmonic excitation only the first 16 out of 64 spectral lines of the results were considered to be relevant. Therefore only these values were stored in files to be printed and plotted for data presentation. For these spectral lines the correction due to the division by the antialiasing filter characteristic was small. For the maneuvers, in principle all spectral lines had to be processed to get the right time trace when, after corrections, the spectrum was Fourier transformed again. Because the magnitude of the filter characteristic was very small for the right hand side of the spectrum, resolution of the measurement became poor and dividing by the small number (of the filter characteristic) would yield a noisy result. Therefore the spectral lines above 1.5 times the cut-off frequency of the elliptic filters (1.5*100=150 Hz) were not used to reconstruct the corrected time traces. Also for the data, acquired with the use of the equal time delay filters, spectral lines above 150 Hz were neglected during the maneuver processing.

4.2.2 Pressures

Before the test the transducers were calibrated at three different temperatures within the range expected during the wind tunnel test. Although the transducers were so-called temperature compensated, the response on temperature steps was established in an 8-hours test, to enable correction for zero drift due to temperature effects. Zero drift in time was assumed to be linear between the two measurements at wind-off condition (zero-measurements), which were performed before and after each series of measurements. At each data point the temperature of the pressure transducers was measured and the corresponding calibration curves were used for processing. During the tests, some pressure transducers were not working properly (Table 2 gives an overview); their presence is ignored in the data processing. For details of the pressure integration to section coefficients, see Section 4.2.3.2.

4.2.3 Overall loads

4.2.3.1 Main balance

To obtain the (unsteady) aerodynamic loads, the inertia loads must be subtracted from the total loads measured by the balance. As the natural frequencies of the wind tunnel model were within the range of planned frequencies (including higher harmonics of those test frequencies) to be investigated, the model could not be considered rigid anymore. Therefore, inertia loads were determined with a procedure that accounts for the flexibility of the wing and main balance. This procedure was called the "mode fit procedure". It is based on the assumption that any motion of the harmonically excited wing model can be expressed as the weighted sum of the driven pitching mode and a limited number of natural vibration modes.

During preparatory tests the relation between balance loads and natural vibration modes as measured by the accelerometers in the model was established by exciting the model at all its natural modes with frequencies below 250 Hz (see Section 3). Also the balance loads at a low pitching frequency (10 Hz) were determined.

During the wind tunnel test the actual vibration mode was fitted as a linear combination of the natural vibration modes. As the balance loads for each natural mode were known (see Section 3), the total inertia loads correction was determined as a weighted linear summation of those loads.

Preparatory tests were performed to check the applicability of this method for the type of "beam balance" as used in this test. These tests were reported in References 6 and 7.

For harmonic excitation with frequencies below 8 Hz the model was considered as rigid and (small) inertia loads were easily determined from known mass properties of the model and angular accelerations determined from the displacement transducer output. Higher harmonics of those data points were processed in the same way. Above 8 Hz the excitation frequency or higher harmonics of the excitation frequency approached the natural frequencies of the model. Therefore all harmonics at tests with excitation frequencies higher than 8 Hz were processed with the "mode fit procedure".

Although the time scale of the maneuvers was fairly large (the length of a (1-cos) input corresponded to a frequency of 3.8 Hz), all spectral lines up to 150 Hz, which was well beyond the first natural frequency of the model, were

processed. To be consistent, for all spectral lines the inertia loads were determined with the "mode fit procedure".

4.2.3.2 Section coefficients

By integrating (trapezoidal rule) the measured steady and unsteady pressures, section coefficients were obtained. For the chordwise sections between the leading edge and the first pressure transducer a constant static and unsteady pressure was assumed. At the trailing edge the static pressure coefficient was assumed to be zero. Between the trailing edge and the last pressure transducer a constant unsteady pressure was assumed. In the same way spanwise sections were integrated from the plane of symmetry to the tip. Between the symmetry plane and the first pressure transducer a constant steady and unsteady pressure was assumed. At the tip the static pressure coefficient was assumed to be zero. Between the tip and the last pressure transducer a constant unsteady pressure was assumed. The result of the pressure integration was NOT multiplied by $1/\pi$ or $2/\pi$.

4.2.4 Tunnel corrections

For the test on the simple straked delta wing the maximum value of the blockage and upwash were estimated to be 3 % of the dynamic pressure and 0.5 deg. As tests on models like this simple straked delta wing at such extreme test conditions are rare, insufficient reference to define blockage and upwash as a function of other parameters like frontal area and Cd exists. Therefore, no blockage or upwash corrections were applied.

5 TEST PROGRAM

The SiS model was tested at only three Mach numbers:

- M = 0.225 To establish continuity with the low speed test of Reference 1.
- M = 0.600 As an intermediate Mach number to study the change in vortex flows with increasing compressibility effects.
- M = 0.900 To study the shock/vortex interactions.

All three Mach numbers were tested at a Reynolds number (based on the root chord) of $8.0*10^6$. Table 4 presents the program of the test with the oscillating model. At M= 0.225 also the tunnel was evacuated to obtain the Reynolds number (based on the root chord) of Reference 1, namely $3.8*10^6$. At M= 0.900 a series of incidences was also tested at a Reynolds number of $14*10^6$. The same (reduced-)frequency-amplitude combinations were used as in the test described in Reference 1.

The tests on the SiS configuration were started with two incidence sweeps at the Mach/Reynolds conditions of Reference 1, with and without the filler plate (see Section 2.2.3). The results with the filler plate installed showed the best agreement with the measurements on the full-span model with the same planform reported in Reference 1. It was decided therefore to perform all the other measurements (dpn's > 60) with the filler plate installed.

Also maneuver sequences were performed with time traces of the model incidence as presented in Figure 12. Table 5 presents an overview of the conditions for which maneuver simulations were done; in this table alpha does NOT indicate the starting angle of attack but the mean value of the adjusted minimum and maximum angle of attack during the sequence, while dalpha indicates half the difference between minimum and maximum.

In the test programs adjusted values have been collected. Measured values of α, $d\alpha$, etc. are included in the data presentation.

Table 4a Test program, Mach = 0.225, harmonic oscillations

Mach	0.225									
$Re*10^{-6}$	= 3.8		= 8.0							
freq	5.7		5.7			7.6			11.4	15.2
dalpha	0.5	0.5	0.5	4.0	8.0	2.0	4.0	8.0	2.0	2.0
alpha		#								
4.0										
5.0										
6.0	7	36	107	135	147	158	172	185	199	213
7.0										
8.0	8	37	108							
9.0										
10.0	9	38	109	136	148	159	173	186	200	214
10.5										
11.0										
11.5										
12.0	10	39	110							
12.5										
13.0										
14.0	11	40	111	137	149	160	174	187	201	215
15.0										
16.0	12	41	112							
17.0	13	42	113							
18.0	14	43	114	138	150	161	175	188	202	216
19.0	15	44	116							
20.0	16	45	117							
21.0	17	46	118							
22.0	6 18	35 47	106 119	139	151	162	176	189	203	217
23.0	19	48	120							
24.0	20	49	121							
25.0										
26.0	21	50	122	134 140	145 152	157 163	171 177	184 190	198 204	212
27.0										
28.0	22	51	123							
29.0										
30.0	23	52	124	141	146 153	164		191	205	218
32.0	24 25	53	125				178			
34.0	26	54	126	142	154	165		192		219
36.0	27	55	127				179			
38.0	28	56	128	143	155	166		193	207	220
40.0	29	57	129							
42.0	30	58	130	144	156	167	180	194	208	221
44.0		59	131			168	181	195	209	
46.0		60	132			169	182	196	210	
48.0			133			170	183	197		

without filler plate

Table 4b Test program, Mach = 0.600, harmonic oscillations

Mach	0.600							
Re*10^{-6}	= 8.0							
freq	5.7			7.6			11.4	15.2
dalpha	0.5	4.0	8.0	2.0	4.0	8.0	2.0	2.0
alpha								
4.0	325							
5.0								
6.0	326	357	371	382	394	406	420	438
7.0								
8.0	327							
9.0								
10.0	328	358	372	383	395	407	421	439
10.5								
11.0	329							
11.5								
12.0	330							
12.5								
13.0	331							
14.0	332	359	373	384	396	408	422	440
15.0	333							
16.0	334							
17.0	335							
18.0	336	360	374	385	397	409	423	441
19.0	337							
20.0	338							
21.0	339							
22.0	340	361	375	386	398	410	424	442
23.0	341							
24.0	342	363	370	381	393	405	419	437
25.0	343							
26.0	324 344	356 364	376	387	399	411	425	443
27.0								
28.0	345							
29.0								
30.0	346	365	377	388	400	414	426	444
32.0	347					412		
34.0	348	366	378	389	401	415	427	445
36.0	349					413		
38.0	350	367	379	390	402	416	428	446
40.0	351							
42.0	352	368	380	391	403	417	429	447
44.0	353							
46.0	354	369		392	404	418	430	448
48.0	355							

Table 4c Test program, Mach = 0.900, harmonic oscillations

Mach	0.900								
$Re*10^{-6}$	= 8.0								= 14.0
freq.	5.7			7.6			11.4	15.2	5.7
dalpha	0.5	4.0	8.0	2.0	4.0	8.0	2.0	2.0	0.5
alpha									
4.0	499								527
5.0	500								528
6.0	501	566	574	584	592	601	609	617	529
7.0	502								530
8.0	503								531
9.0	504								533
10.0	505	567	575	585	593	602	610	618	534
10.5									535
11.0	506								536
11.5									537
12.0	507								538
12.5									539
13.0	508								540
14.0	509	568	576	586	594 595	603	611	619	541
15.0	510								542
16.0	511								543
17.0	512								544
18.0	513	569	579	587	596	604	612	620	545
19.0	514								548
20.0	515								547
21.0	516								549
22.0	517	570	580	588	597	605	613	621	526 550
23.0	518								551
24.0	519	565		583	591	600	608	616	
25.0	520								553
26.0	521	571	581	589	598	606	614	622	554
27.0	522								555
28.0	523								556
29.0	524								557
30.0	525	572	582	590	599	607	615	623	558
32.0	559								
34.0	560								
36.0	561								
38.0	562								
40.0	563								
42.0	564								
44.0									
46.0									
48.0									

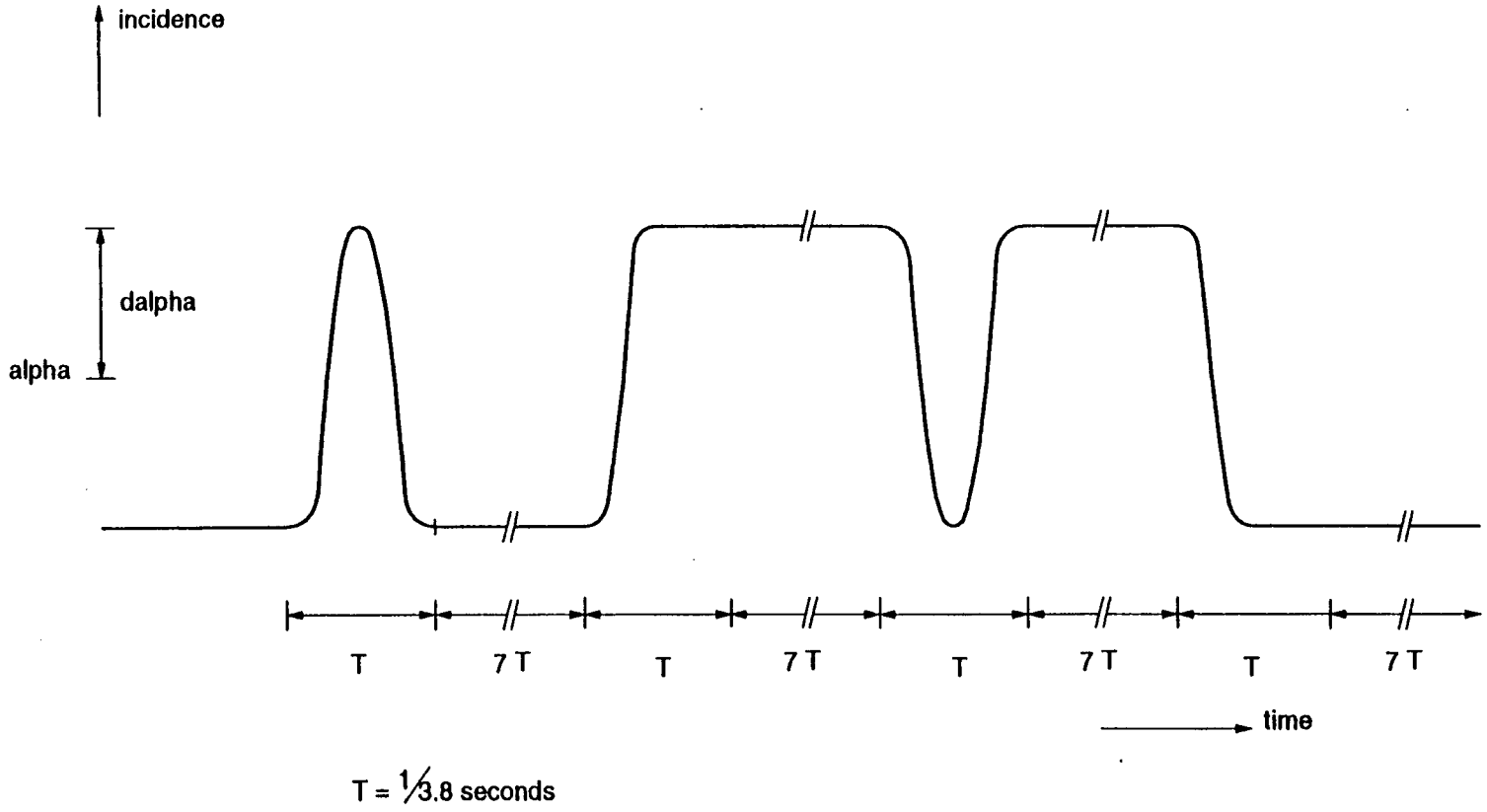

Fig. 12 Time trace of (I-COS) and "half" (I-COS) maneuver sequence

Table 5 Test program, maneuvers; "freq" = 3.8 Hz

Mach	0.225			0.600		0.900	
Re*10^{-6}	= 3.8	= 8.0		= 8.0		= 8.0	
dalpha	8.0	8.0	16.0	8.0	16.0	8.0	16.0
alpha							
6.0		235 236 237 238 239		454 455 456 457 458		625 639 640 641 642 643	
10.0		240 241 242 243 244					
14.0		245 246 247 248 249	296 297 298 299 300	459 460 461 462 463 464	487 488 489 490 491	644 645 646 647	662 663 664 665 666 667
18.0	64 65 67 75 76 77	250 251 252 253 254	301 302 303 304 305				
22.0		255 256 257 258	306 307 308 309 310	449 450 451 452 453	480 481 482 483 484	624 626 627 628 629 630 631 632 633 634 635 636 637 638	656 657 658 659 660 661
26.0	78 81 82 87 88	229 230 231 232 233 234 260 261 262 263 264 265	291 292 293 294 295				
30.0		266 267 268 269	311 312 313 314 315	465 466 467 468 469 470 471 472 473 474	492 493 494 495 496	648 649 650 651 652 653 654	
34.0	89 90 92 93 95	276 277 278 279 280	316 317 318 319 320				
38.0		281 282 283 284 285		475 476 477 478 479			
42.0		286 287 288 289 290					

6 PRESENTATION OF RESULTS

6.1 Wind tunnel test data

Part 2 presents five harmonics of five selected (see Section 7) data points of the test in plotted and tabulated form. Table 6 and Figure 13 show the format in which the data are presented.

Each table presents the test conditions (alpha,Mach,Re,Q,dalpha,frequency) and one harmonic (>0) component and the mean (0-th harmonic component) value of all measured quantities for one data point. Pressures and section loads are presented in nondimensionalized form. The inertia loads were subtracted from the balance loads, before overall aerodynamic loads were non- dimensionalized to aerodynamic coefficients. Also the ratio between the amplitude of the unsteady aerodynamic loads and the amplitude of the inertia loads is indicated (when **** are printed the ratio is larger than 10,000). The angular deflections, calculated from the total balance loads and the stiffness matrices, are presented to the right of the balance loads. To the right of the accelerations the vibration mode of each section equipped with accelerometers is expressed in heave at the pitching axis and rotation about this axis. Each plot presents one harmonic (>0) component of the pressure distribution; the mean (0-th harmonic component) pressure distribution is always included as a reference. The data of the five harmonics of the five selected data points are also available on a floppy disk.

Part 2 also presents plots of overall quantities like normal force and pitching moment coefficients versus incidence, in which the results of a large number of data points have been collected, including the five selected data points.

Part 3 presents the response on a maneuver sequence in plotted form for three selected (see Section 7) data points. All the quantities which were presented for the data points with harmonically oscillating model, together with inertia loads as separate quantities, are presented both as a time trace and as a cross-plot with the incidence signal. As an example, Figure 14 shows the response of the main balance in terms of overall load coefficients and angular deflections for the four parts of a maneuver sequence. The data presented in the plots are also made available as ASCII files on floppy disks.

When a sensor did not operate properly, no value is presented in the plots, prints and ASCII files. Readers who are interested to obtain part or all of the measured data should contact Lockheed Forth Worth Company or NLR.

Table 6 Example of (quick look-) printout of the mean and first harmonic component of the data measured at one data point (page 1/3)

Unsteady Transonic Delta Program DPN = 6

test conditions — Simple Strake configuration

alpha	= 21.914 deg	Q	= 3.138 kPa
Mach	= .225	Ptot	= 92.051 kPa
Re*10⁻⁶	= 3.804	Ttot	= 288.834 K
dalpha	= .546 deg		
freq	= 5.700 Hz		
k	= .193		
harm	= 1		

BALANCE LOADS		aerodynamic or <total> coefficients			aero inertia [%]	angular deflections [deg]		
position	comp.	Zero	Re 1	Im 1		Zero	Re 1	Im 1
main	CN	1.24332	2.30012	.70846	1197.71			
	Cm	.07572	.32252	-.03933	103.80	-.026	-.002	.000
	Cl	-.43299	-.52972	-.35483	327.90	-.034	.000	.000

ACCELERATIONS					vibration mode			
nr	x [mm]	y [mm]	Amplitude [m/s^2]	Phase angle rel. to LVDT [deg]	section	y/b [%]	heave at p.a [mm]	pitch [deg]
11	-425.6	-12.0	5.091	1.996				
12	-215.6	-12.0	2.619	2.024	1	2.878	.043	.530
13	167.4	-12.0	1.957	-176.855				
21	-138.6	-116.9	1.633	15.502				
22	-46.6	-116.9			2	28.034	.077	.558
23	121.4	-116.9	1.614	-165.610				
31	-74.6	-189.9	.731	18.711				
32	-10.6	-189.9			3	45.540	.112	.519
33	141.4	-189.9	1.779	-166.231				
41	29.4	-304.9	.252	-175.904				
42	89.4	-304.9	1.179	-178.644	4	73.118	.014	.570
43	152.4	-304.9	1.815	-178.404				
51	85.0	-374.9	.840	-172.336				
52	121.4	-374.9	1.496	-163.903	5	89.904	.360	.703
53	157.4	-374.9	1.970	-165.651				

Table 6 Example of (quick look-) printout of the mean and first harmonic component of the data measured at one data point (page 2/3)

Unsteady Transonic Delta Program DPN = 6

PRESSURES section 1 c = 300.65 mm y =-209.06 mm

nr. up	nr. low	x/c [%]	Cp 0	ReCp 1	ImCp 1
101		2.00	-1.873	-1.066	-1.857
102		5.00	-2.012	2.189	-2.245
103		10.00	-1.843	2.740	-2.808
104		15.00	-2.348	10.524	-5.204
105					
106		30.00	-1.683	-6.564	-1.022
107		40.00	-1.335	-8.354	-.397
108		50.00	-1.174	-7.972	-.256
109		60.00	-1.173	-8.303	-.164
110		70.00	-1.251	-9.758	.333
111		79.00	-1.380	-10.265	1.247
112		82.50	-1.379	-7.242	1.336
113		85.00	-1.305	-3.256	1.036
114		90.00	-1.051	5.989	-.494
115		95.00	-.661	10.634	-2.360
	151	10.00	.633	.971	.182
	152	20.00	.528	1.124	.258
	153	40.00	.343	1.064	.312
	154	60.00	.257	.940	.256
	155	80.00	.175	1.008	.097

PRESSURES section 2 c = 246.21 mm y =-273.97 mm

nr. up	nr. low	x/c [%]	Cp 0	ReCp 1	ImCp 1
201		2.00	-.988	4.605	-2.448
202		5.00	-.994	4.319	-2.436
203		10.00	-1.077	6.677	-3.993
204		15.00	-1.017	6.234	-3.485
205		18.00	-.958	.094	-2.972
206		30.00	-.830	2.805	-1.333
207		40.00	-.710	4.770	-2.808
208		50.00	-.672	8.206	-4.374
209		60.00	-.678	7.421	-4.313
210		70.00	-.689		
211		79.00	-.729	.910	-2.834
212		82.50	-.807	-.819	-2.311
213		85.00	-.815	-1.938	-1.740
214		90.00	-.918	-3.116	-.992
215		95.00	-1.006	-1.194	-1.050
	251	10.00	.617	.781	.283
	252	20.00	.513	.950	.312
	253	40.00	.335	.944	.302
	254	60.00	.222	.871	.239
	255	80.00	.067	.969	.050

PRESSURES section 3 c = 194.13 mm y =-336.06 mm

nr. up	x/c [%]	Cp 0	ReCp 1	ImCp 1
301	2.00	-.596	1.008	-1.084
302	5.00	-.601	1.041	-1.136
303	10.00	-.589	.957	-1.127
304	15.00	-.589	1.087	-1.160
305	18.00	-.572	-.167	-.698
306	30.00	-.541	.373	-.735
307	40.00	-.495	-.294	-.420
308	50.00	-.499	-.357	-.246
309	60.00	-.461	-.134	-.614
310	70.00	-.427	-.001	-.565
311	79.00	-.424	-1.383	.016
312	90.00	-.476	-5.161	1.564

PRESSURES section 4 c = 144.42 mm y =-395.32 mm

nr. up	x/c [%]	Cp 0	ReCp 1	ImCp 1
401	2.00	-.408	-1.393	1.020
402	5.00	-.406	-1.529	1.145
403	10.00	-.377	-1.719	1.291
404	15.00	-.411	-2.029	1.459
405	18.00	-.418	-2.110	1.494
406	30.00	-.385	-.951	.798
407	40.00	-.372	.438	-.020
408	50.00	-.336	.569	-.376
409	60.00	-.295	.022	-.707
410	70.00	-.292	-.444	-1.079
411	79.00	-.292	-1.297	-.978
412	90.00	-.322	-2.313	-.491

Table 6 Example of (quick look-) printout of the mean and first harmonic component of the data measured at one data point (page 3/3)

Unsteady Transonic Delta Program

DPN = 6

PRESSURES section 5 b = 82.70 mm x =-269.60 mm

nr. up	y/b [%]	Cp 0	ReCp 1	ImCp 1
501	6.62	-.466	-1.150	-.472
502	20.43	-.593	-2.373	-.237
503	34.05	-.864	-4.494	.193
504	47.67	-1.378	-6.485	.575
505	54.49	-1.610	-6.484	.441
506	61.29	-1.744	-5.743	.138
507	68.10	-1.667	-4.950	-.093
508	74.91	-1.423	-4.514	-.189
509	81.72	-1.153	-3.551	-.284
510	88.53	-1.146	-3.204	-.372

PRESSURES section 6 b = 233.73 mm x = -60.62 mm

nr. up	y/b [%]	Cp 0	ReCp 1	ImCp 1
601	38.90	-1.680	-4.728	.133
602	42.93	-1.906	-5.125	-.173
603	46.93	-1.900	-5.797	-.440
604	50.99	-1.734	-6.660	-.582
605	59.03	-1.329	-7.005	-.624
606	67.07	-1.407	-8.606	-.872
607	71.11	-1.809	-9.646	-1.360
608	75.56	-2.844	-5.587	-2.097
609	80.00	-3.437	4.132	-2.402
610	84.44	-2.323	2.003	-2.726
102	89.45	-2.012	2.189	-2.245

PRESSURES section 7 b = 417.90 mm x = 100.71 mm

nr. up	y/b [%]	Cp 0	ReCp 1	ImCp 1
701	22.71	-.014	-.061	-.145
702	28.21	-.308	.244	.313
703	33.72	-1.060	-.854	1.318
704	39.26	-1.518	-6.458	1.368
705	44.69	-1.412	-11.004	.904
109	50.03	-1.173	-8.303	-.164
706	55.28	-1.081	-1.670	-2.100
707	60.46	-.958	7.984	-5.050
208	65.56	-.672	8.206	-4.374
708	70.59	-.577	-.220	-.174
709	75.54	-.549	.450	-.530
307	80.42	-.495	-.294	-.420
710	85.22	-.466	-.682	.063
711	90.19	-.436	-1.864	1.188
405	94.60	-.418	-2.110	1.494

SECTION COEFFICIENTS

section	comp.	Zero	Re 1	Im 1
1	CN_u	1.433	2.855	1.038
	CN_l	.329	1.018	.209
	CN_t	1.762	3.872	1.247
	Cm_u	-.244	-.956	.034
	Cm_l	-.027	-.249	-.038
	Cm_t	-.271	-1.205	-.004
2	CN_u	.800	-3.366	2.817
	CN_l	.294	.914	.212
	CN_t	1.094	-2.453	3.029
	Cm_u	-.174	.382	-.625
	Cm_l	-.013	-.240	-.025
	Cm_t	-.187	.142	-.650
3	CN_u	.479	.820	.257
	Cm_u	-.094	-.664	.139
4	CN_u	.331	.967	-.018
	Cm_u	-.064	-.262	-.222
5	CN_u	1.025	3.951	.066
	Cl_u	-.569	-2.179	-.032
6	CN_u	1.759	3.954	.788
	Cl_u	-.891	-1.464	-.663
7	CN_u	.584	.981	.305
	Cl_u	-.323	-.430	-.171

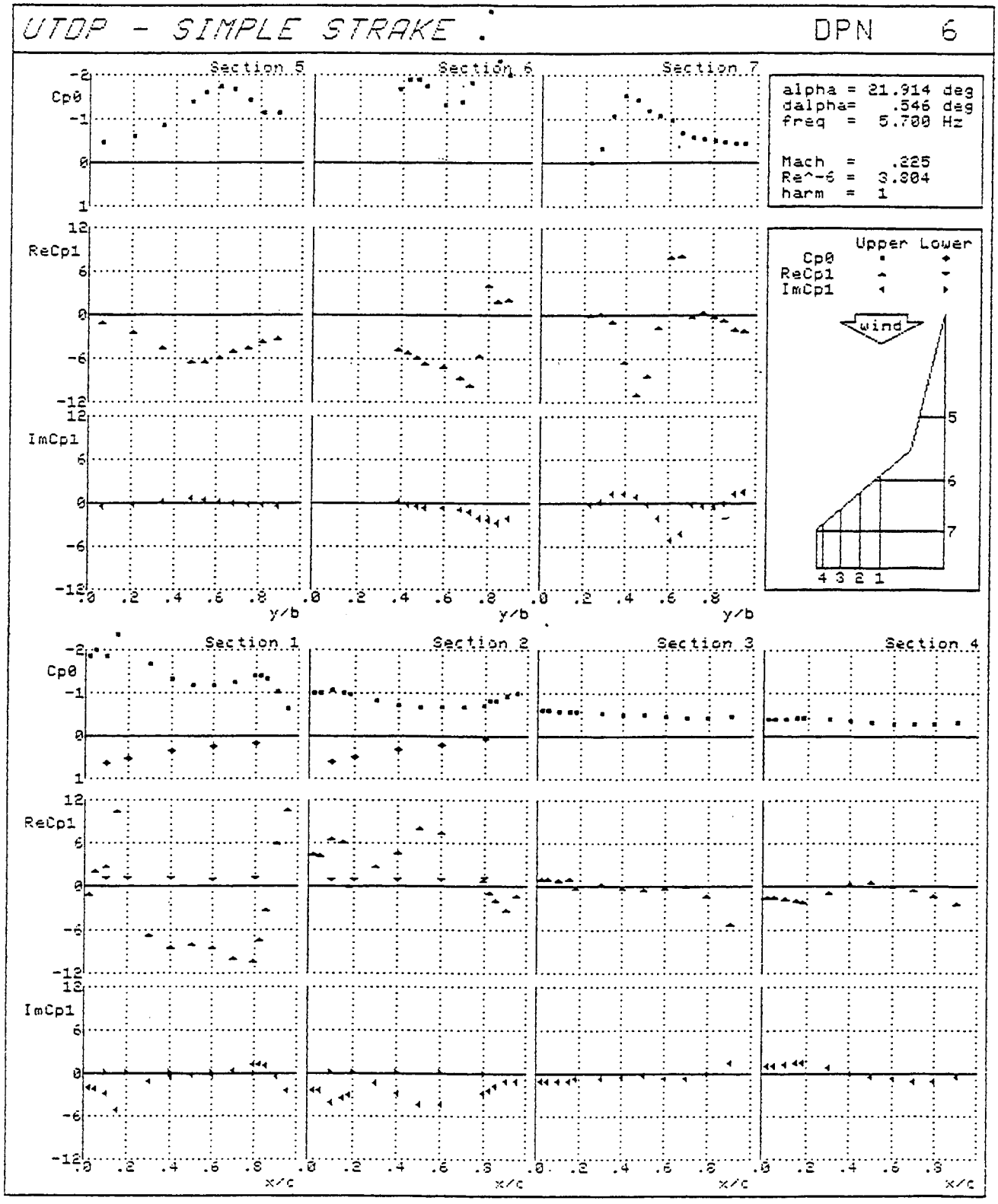

Fig. 13 Example of (quick look-) plot of the mean and first harmonic component of the data measured at one datapoint

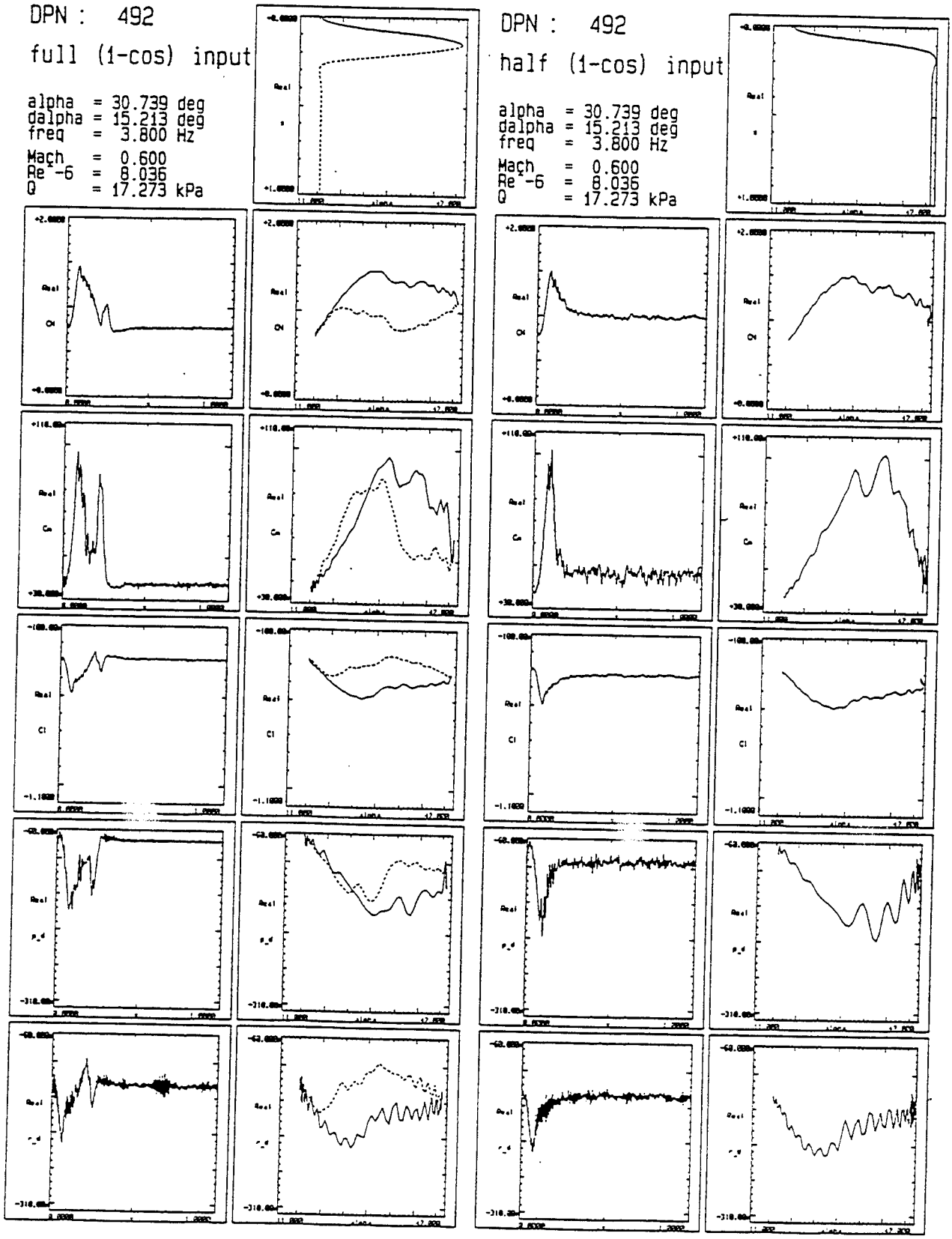

Fig. 14 Example of the response of the main balance on a manoeuver sequence (page 1/4)

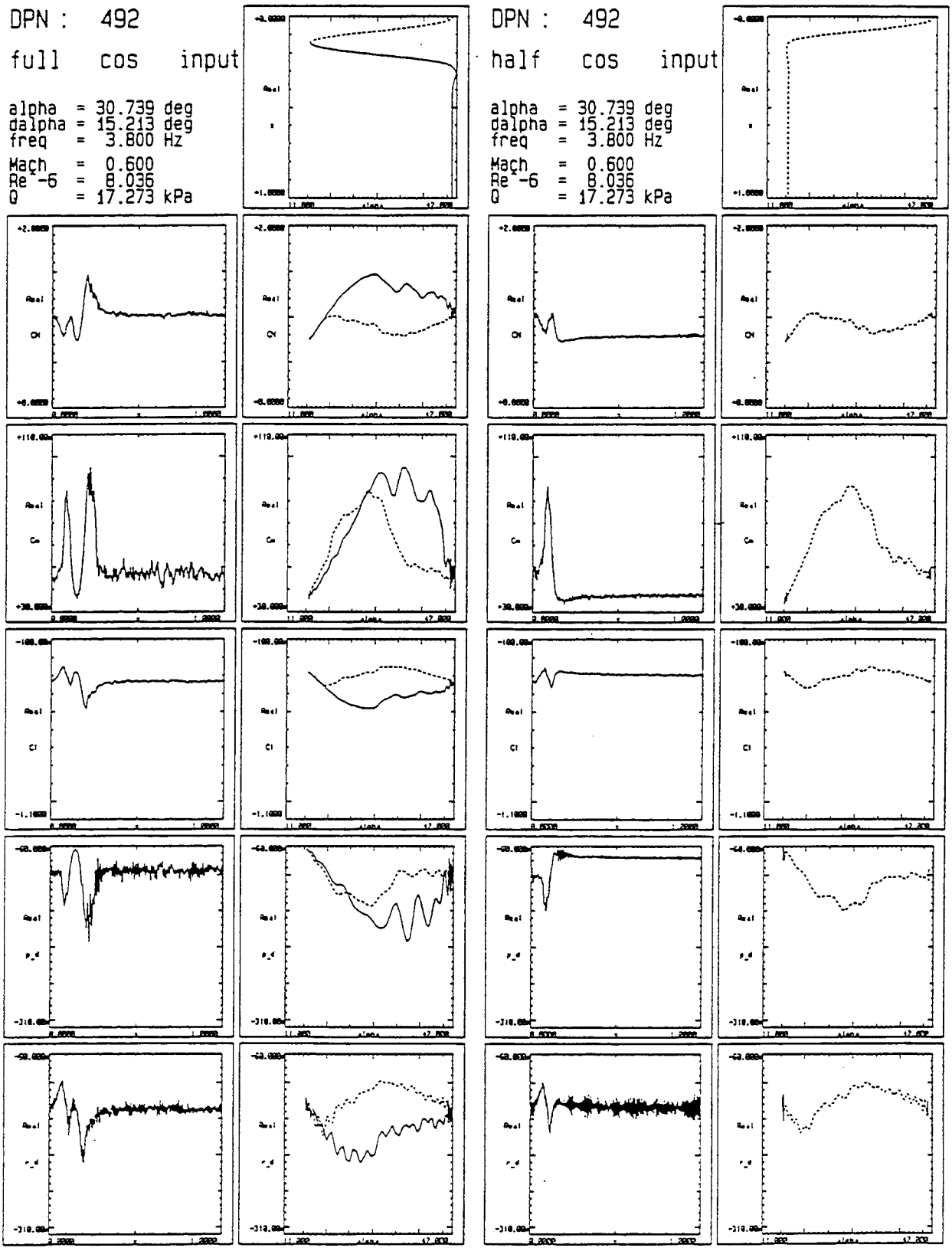

Fig. 14 Example of the response of the main balance on a manoeuver sequence (page 2/4)

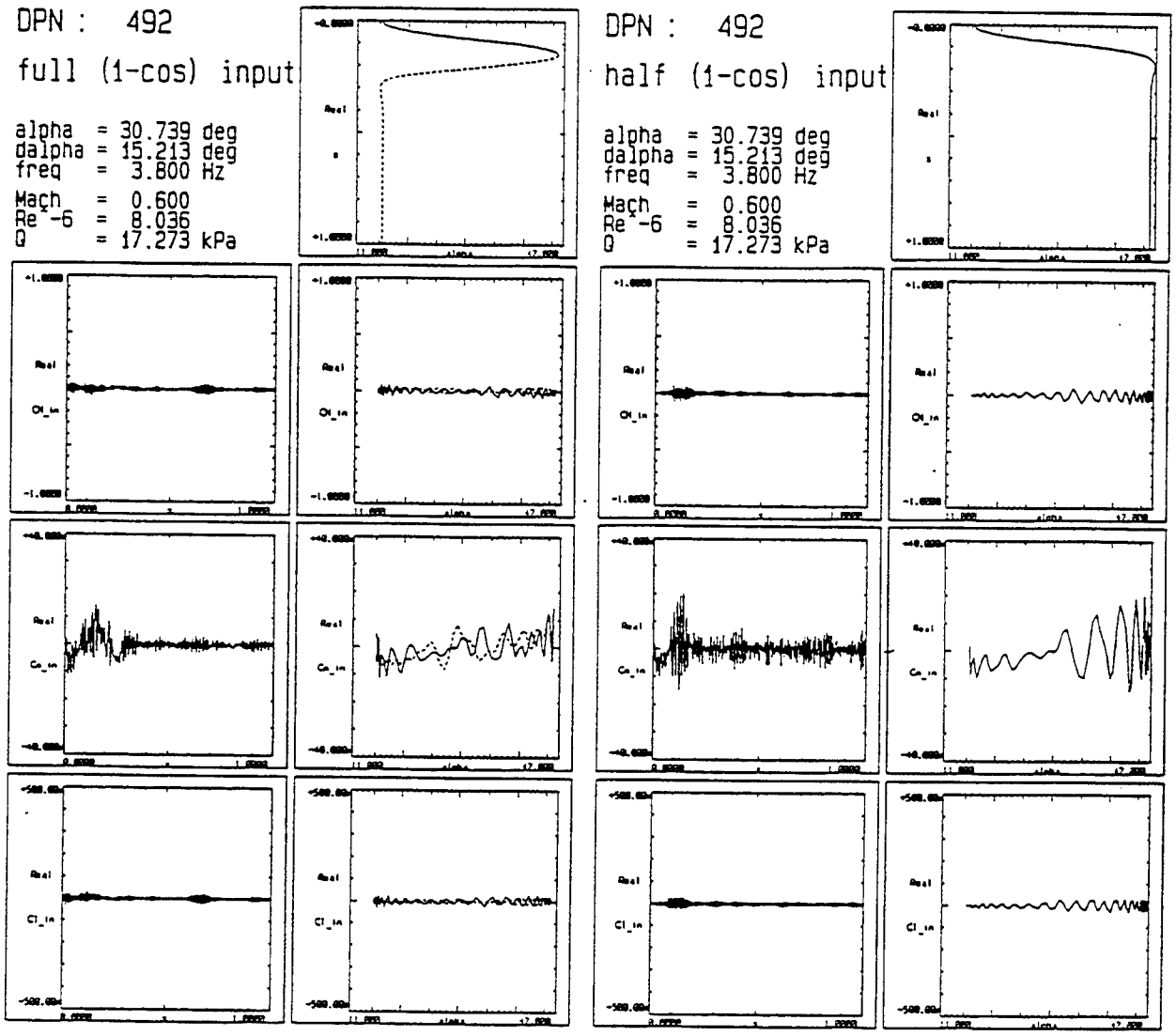

Fig. 14 Example of the response of the main balance on a manoeuver sequence (page 3/4)

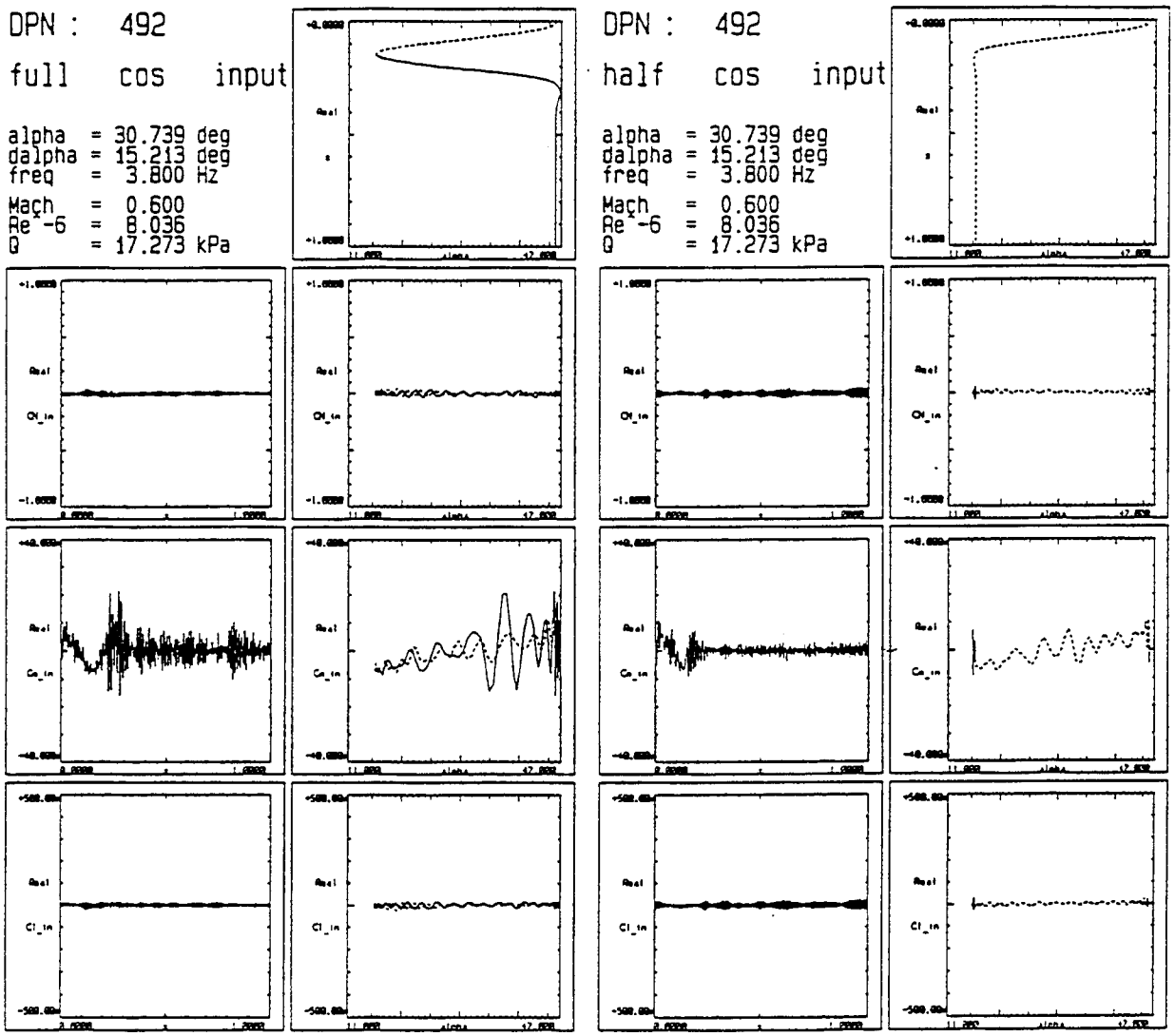

Fig. 14 Example of the response of the main balance on a manoeuver sequence (page 4/4)

6.2 Model geometry

Figures 1 to 7 and Appendices A and B provide the most important geometric data of the model. Readers who are interested to obtain the geometric data (e.g., in the CATIA or VDAFS format), should contact Lockheed Forth Worth Company or NLR.

7 BRIEF DISCUSSION OF SOME RESULTS; SELECTION OF PRESENTED DATA POINTS

The rationale for selecting the data points presented in Parts 2 and 3 is discussed in this section.

Part 2 data points were taken from the oscillatory testing of the model. The points selected for this part were chosen to highlight (1) vortex flow breakdown, and (2) onset of Shock Induced Trailing Edge Separation (SITES) and leading edge separation at transonic speeds. The effect of Mach number is the primary point of interest in selecting these data points.

At M=0.225, data point 151 shows the effect of the model oscillating between 14 deg incidence and 30 deg incidence at 5.7 Hz. With vortex bursting starting at about 22 deg, this oscillation provides maximum pitch rate at burst point. Similar data are given for M=0.60 in data point 375 where vortex breakdown apparently begins between 23 and 24 deg. The data point chosen for M=0.90 is 605 at the higher frequency of 7.6 Hz which provides an approximately constant reduced frequency when compared with data point 375 at Mach=0.60. In the case of data point 605, vortex bursting begins at about 18 deg incidence for M=0.90. As a reference, the mean and first harmonic component of the pressure distributions of data points 151,375 and 605 are included in this part of the report (Figures 15, 16 and 17).

The onset of SITES and leading edge separation occurs between 10 and 12 deg on the simple straked wing at Mach=0.90. In order to highlight these transitions data point 358 was chosen to show how aerodynamics responded to oscillations of 4 deg amplitude at 10 deg mean angle and M=0.60, where no such transitions occur. Data point 593 was then chosen to show SITES/leading edge separation transition at M=0.90 at the same conditions. Frequency for the M=0.60 case was 5.7 Hz and for the M=0.90 case was 7.6 Hz in order to maintain an approximately constant reduced frequency. Figures 18 and 19 show the mean and first harmonic component of the pressure distributions of data points 358 and 593.

Part 3 data points are taken from the large amplitude maneuvering part of the simple straked wing test. The large amplitude motions of 15 deg amplitude centered on a mean angle of 22 deg provide a dynamic variation of flow fields covering attached, vortex, burst vortex and developing separated flows for incidences from 7 to 37 deg. The three Mach numbers are represented by data point 306 (M=0.225), 480 (M=0.60), and 656 (M=0.90). In all cases the frequency was held constant at 3.8 Hz in order to simulate the same maneuver at different speeds. Since these data points are for transient and not for

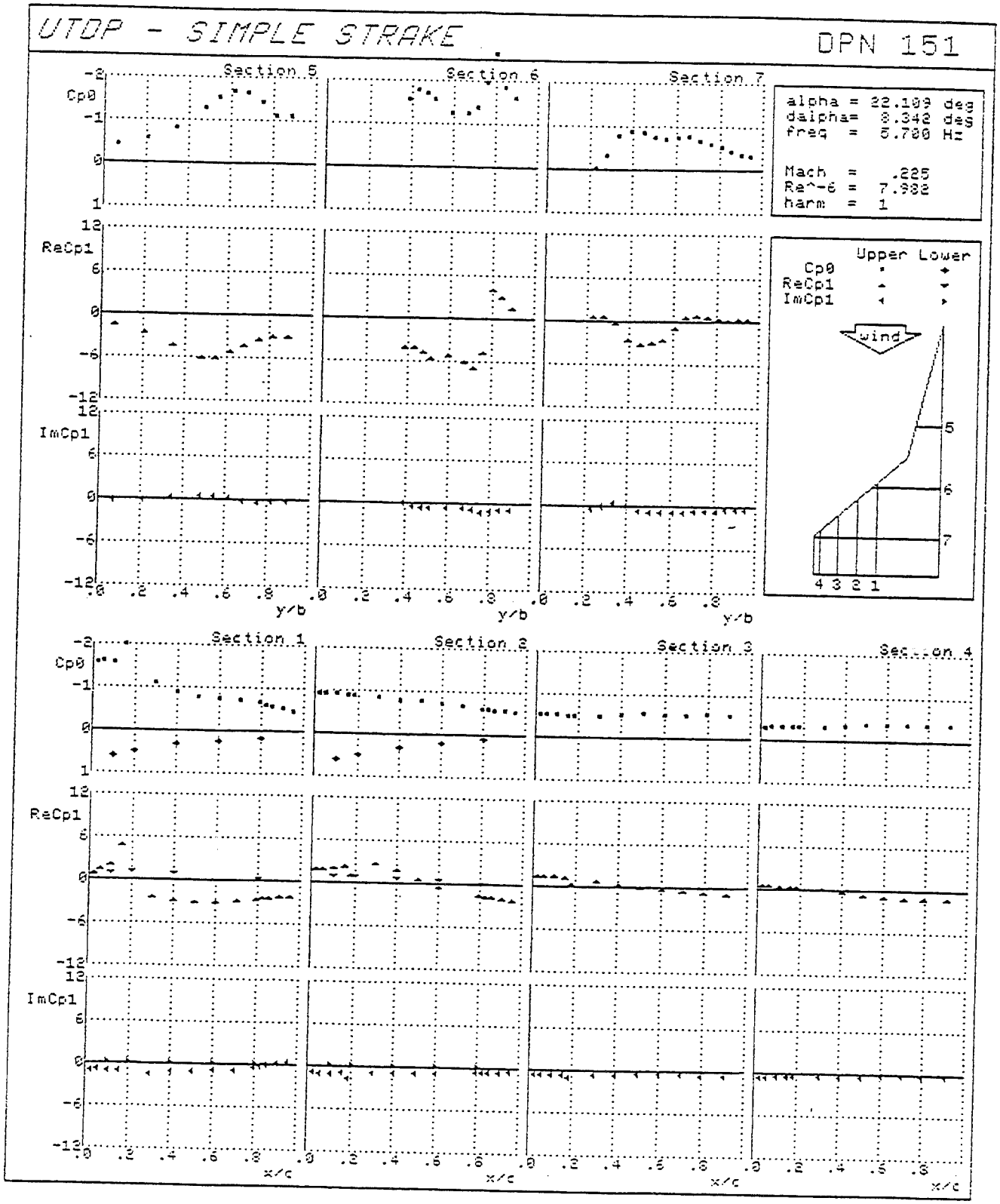

Fig. 15 Mean and first harmonic component of the pressure distribution measured at datapoint 151 (first datapoint selected for extensive presentation in part II)

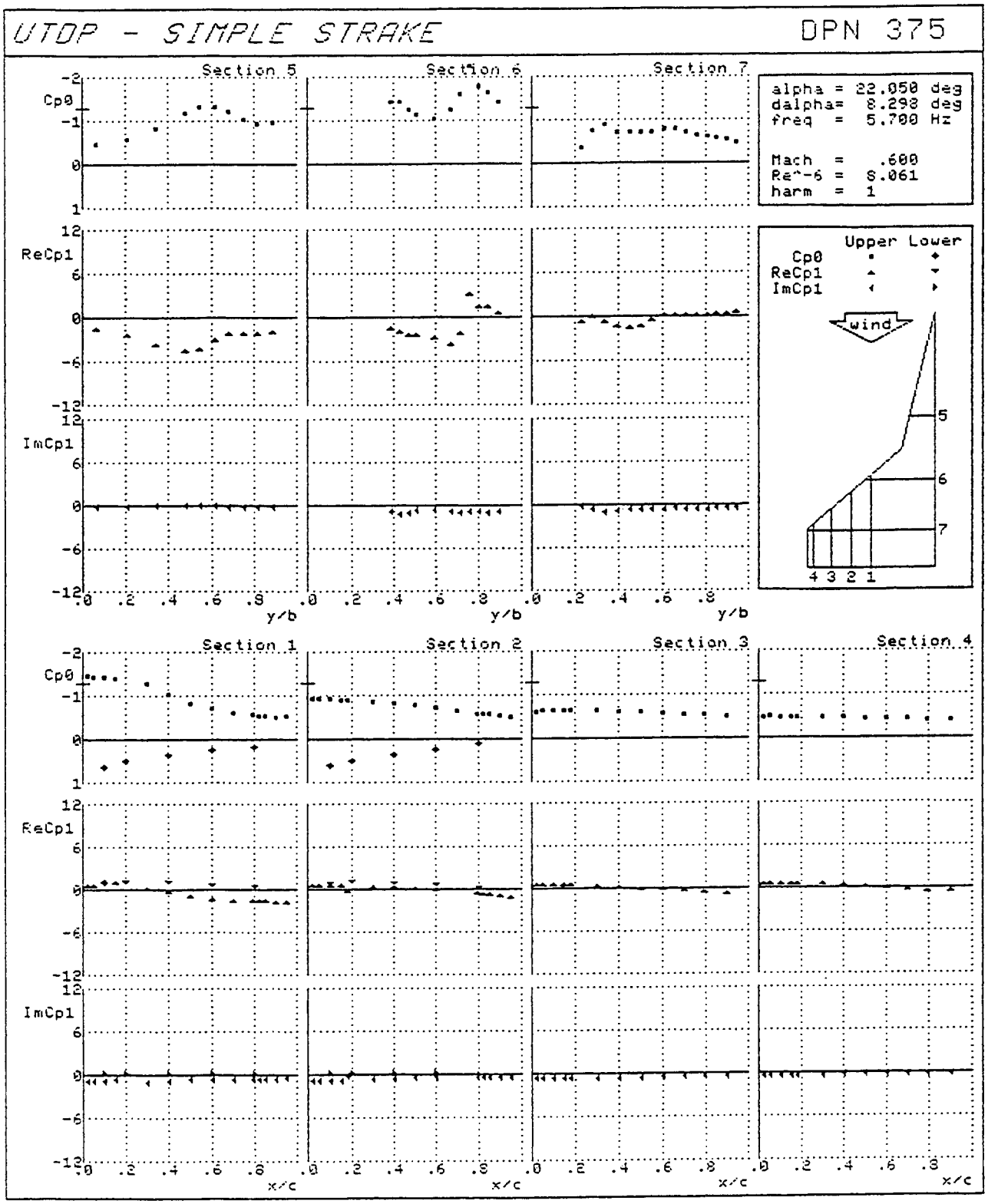

Fig. 16 Mean and first harmonic component of the pressure distribution measured at datapoint 375 (second datapoint selected for extensive presentation in part II)

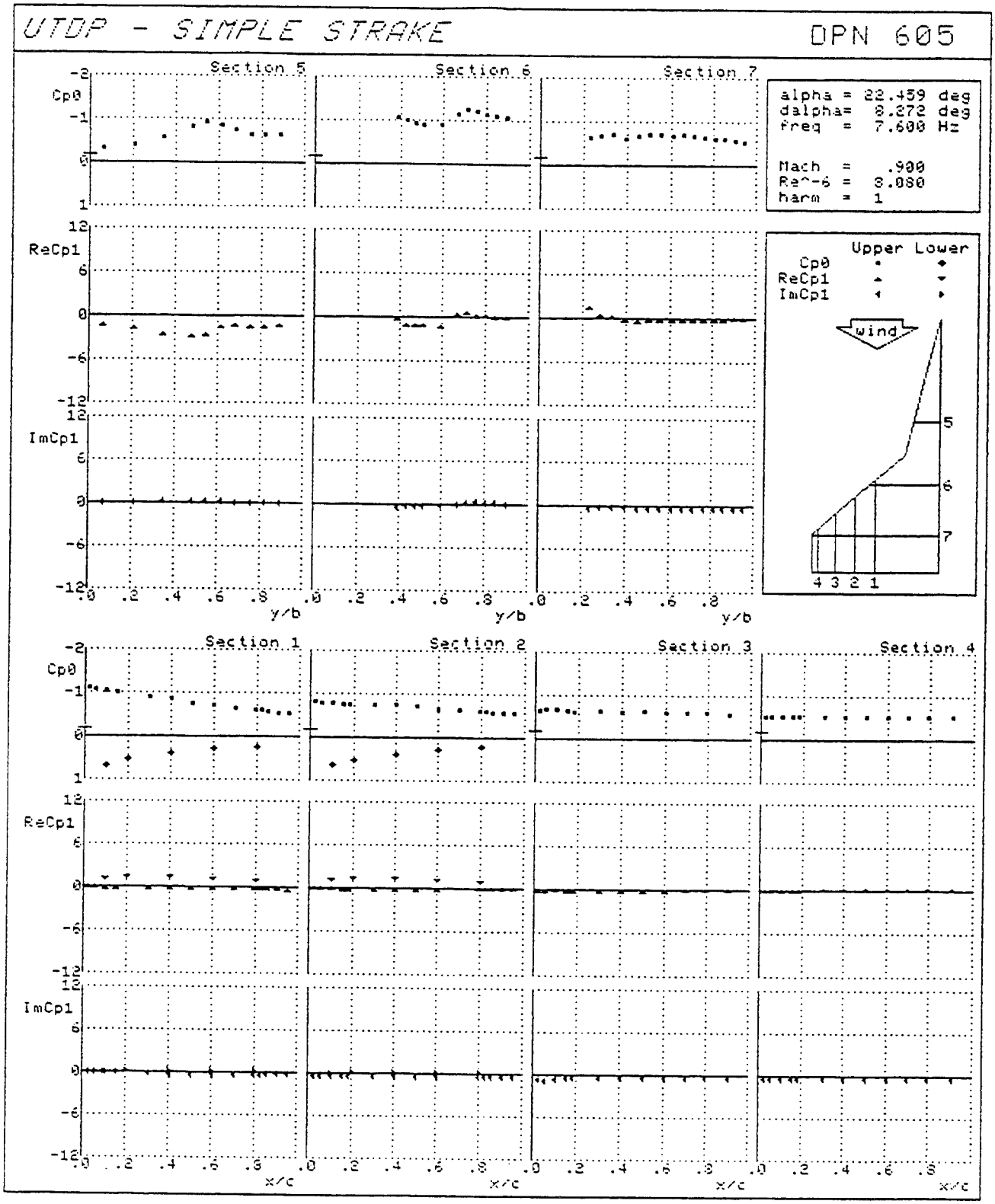

Fig. 17 Mean and first harmonic component of the pressure distribution measured at datapoint 605 (third datapoint selected for extensive presentation in part II)

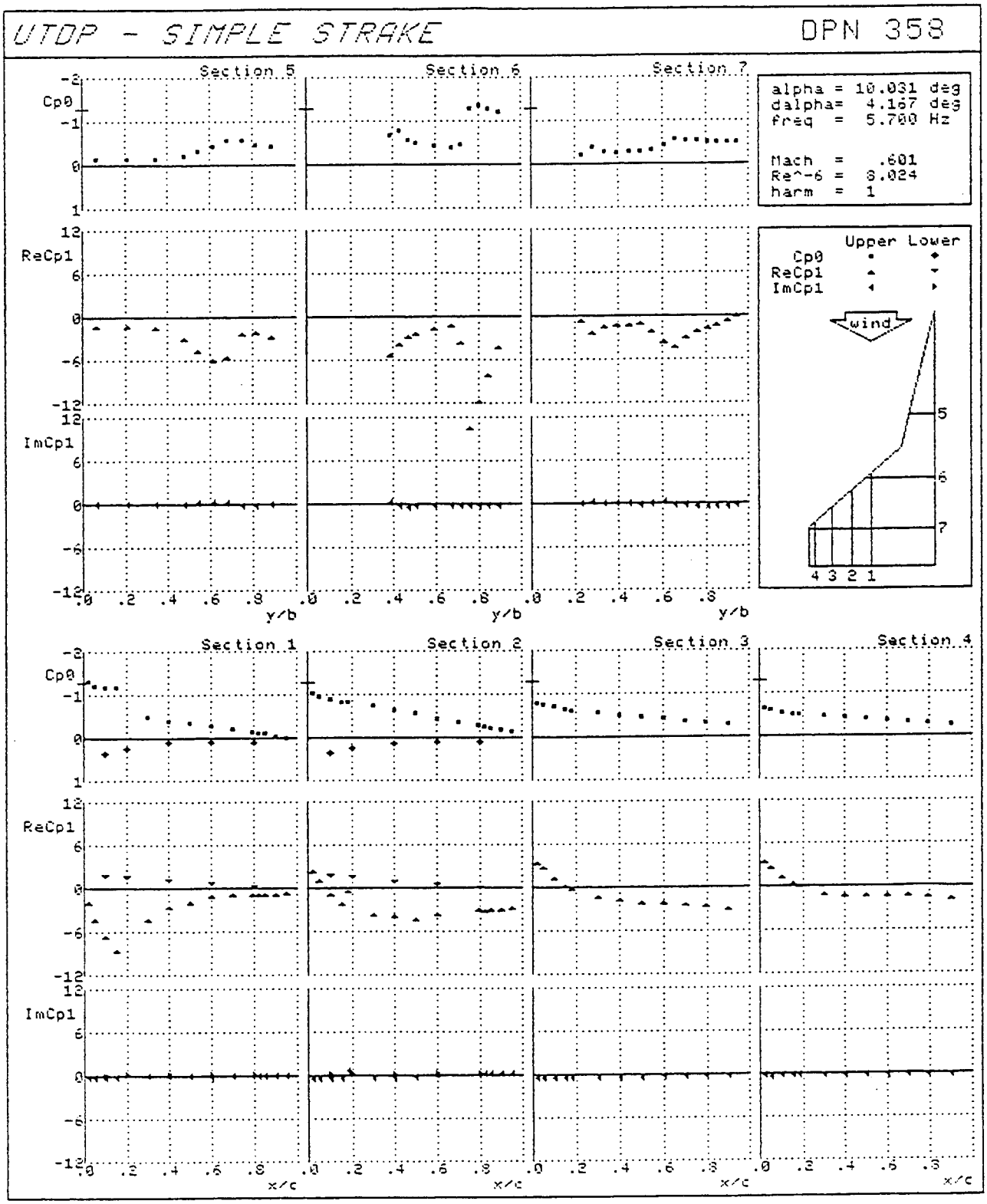

Fig. 18 Mean and first harmonic component of the pressure distribution measured at datapoint 358 (fourth datapoint selected for extensive presentation in part II)

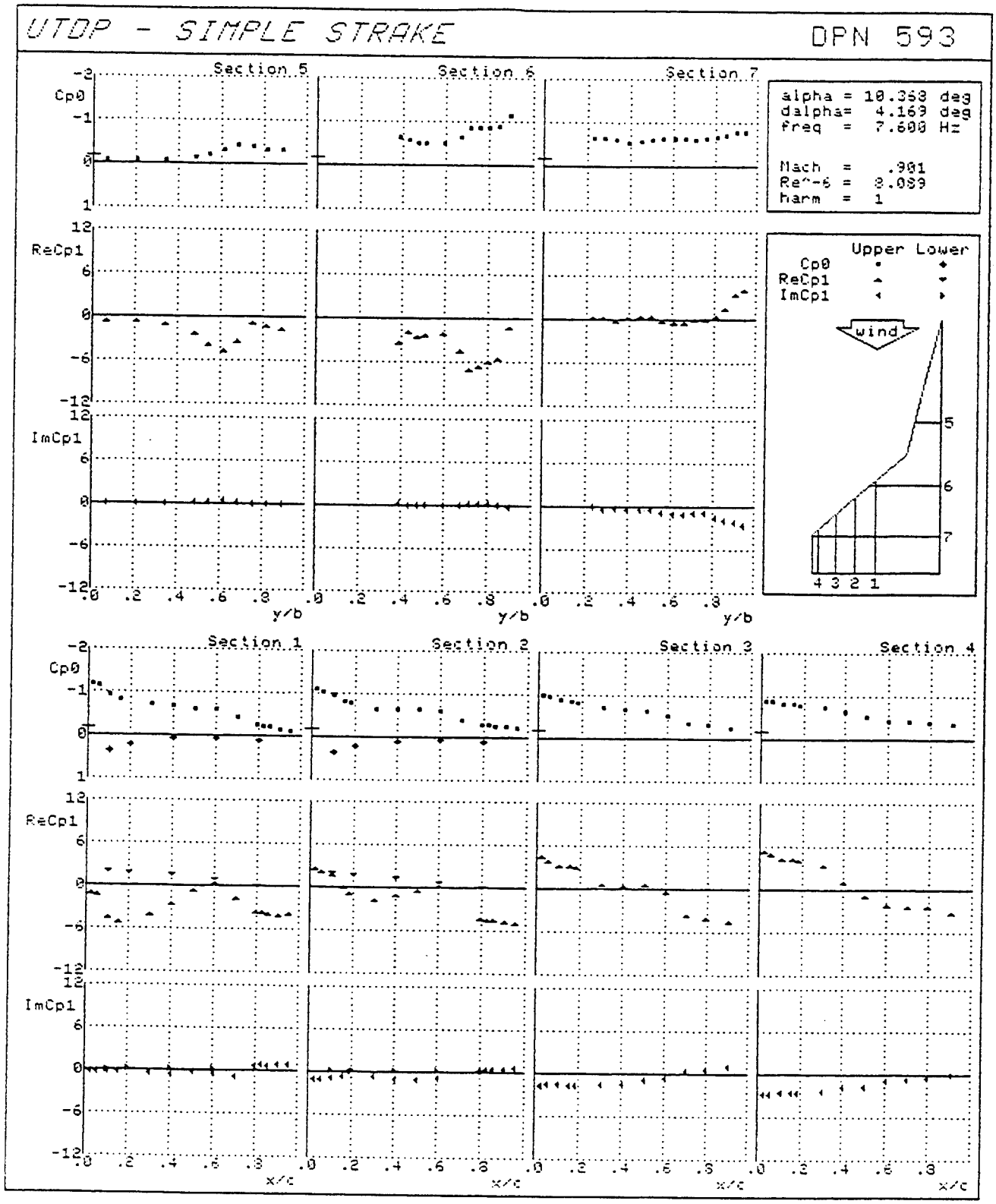

Fig. 19 Mean and first harmonic component of the pressure distribution measured at datapoint 593 (fifth datapoint selected for extensive presentation in part II)

oscillatory motions, they are represented in a time history format and thus do not have the harmonic form that is used in Part 2. Because of the large quantity of data within these data points, only three were chosen for Part 3. In this part, as a reference, only the time histories of the balance quantities are presented for the three data points in Figures 20, 21 and 22.

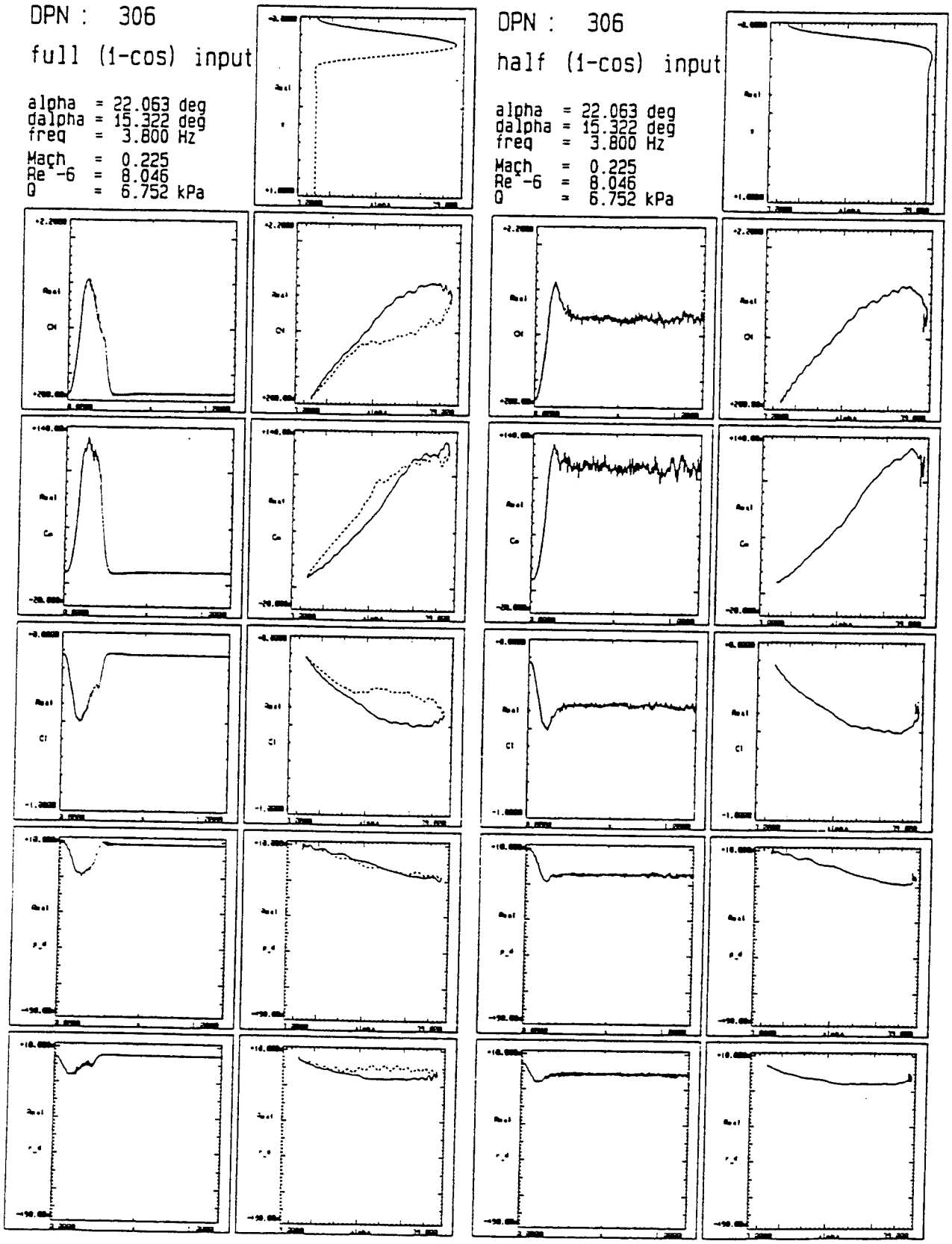

Fig. 20 Time histories of the balance quantities measured at datapoint 306 (first datapoint selected for extensive presentation in part III) page 1/4

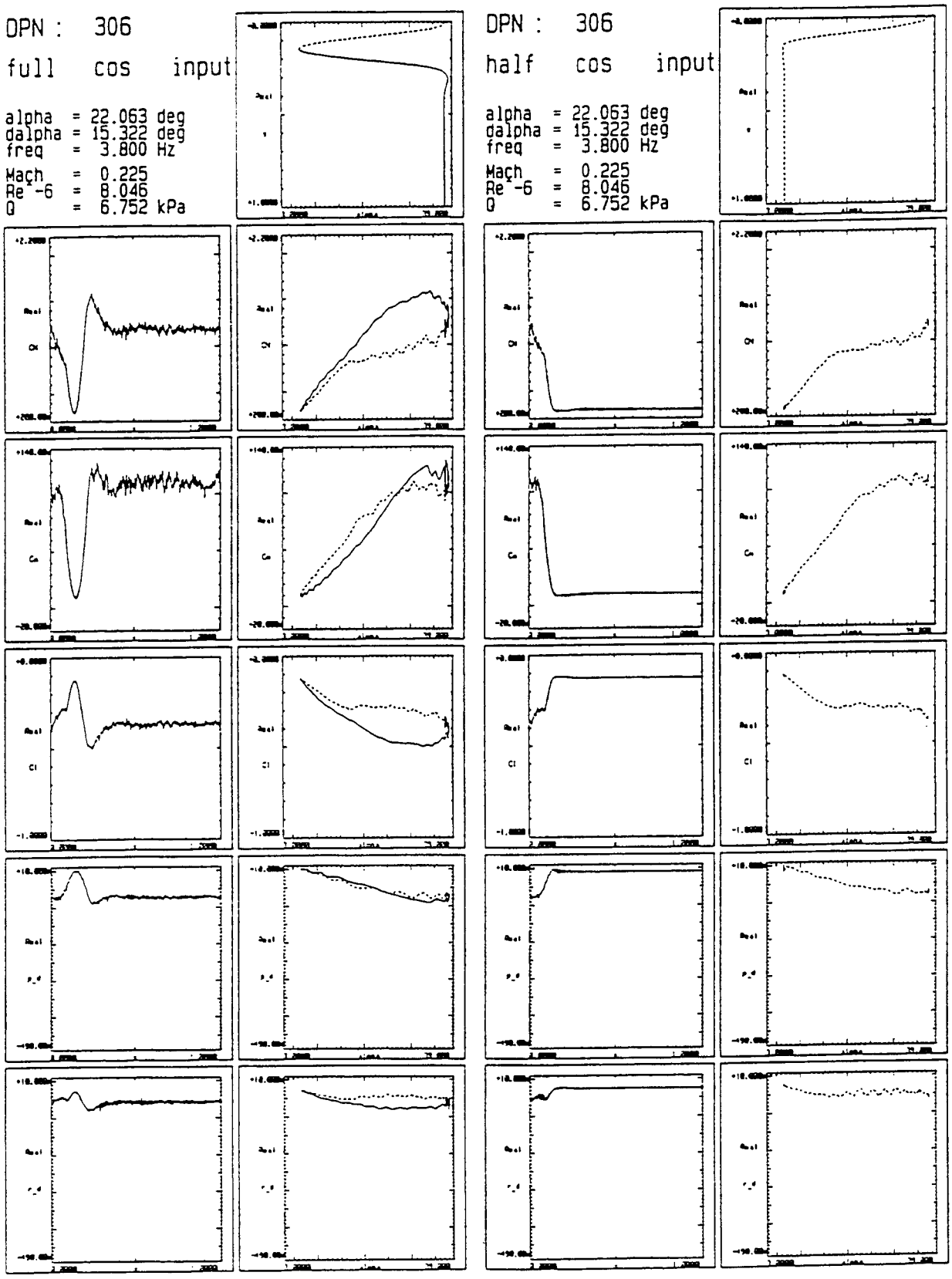

Fig. 20 Time histories of the balance quantities measured at datapoint 306 (first datapoint selected for extensive presentation in part III) page 2/4

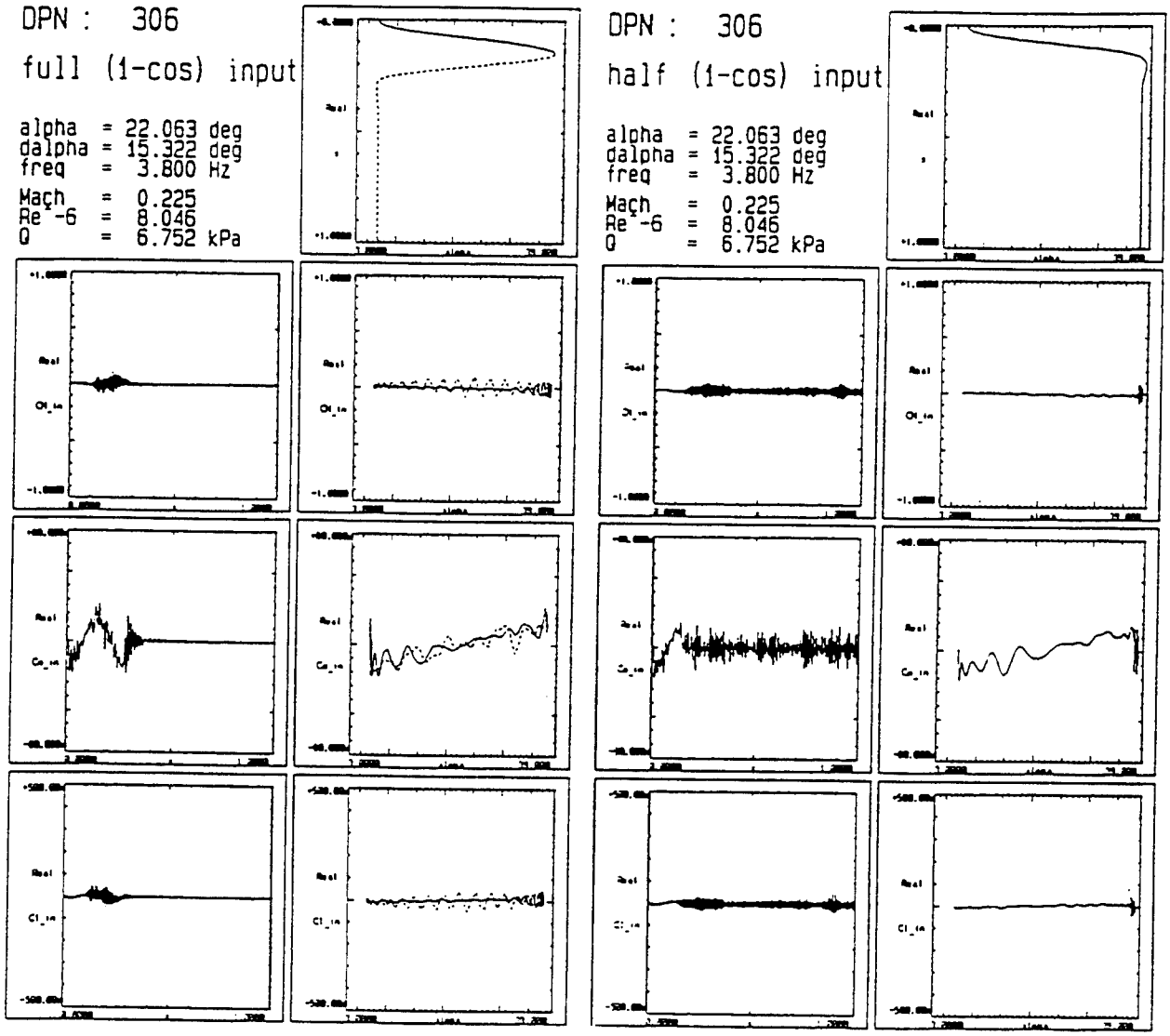

Fig. 20 Time histories of the balance quantities measured at datapoint 306 (first datapoint selected for extensive presentation in part III) page 3/4

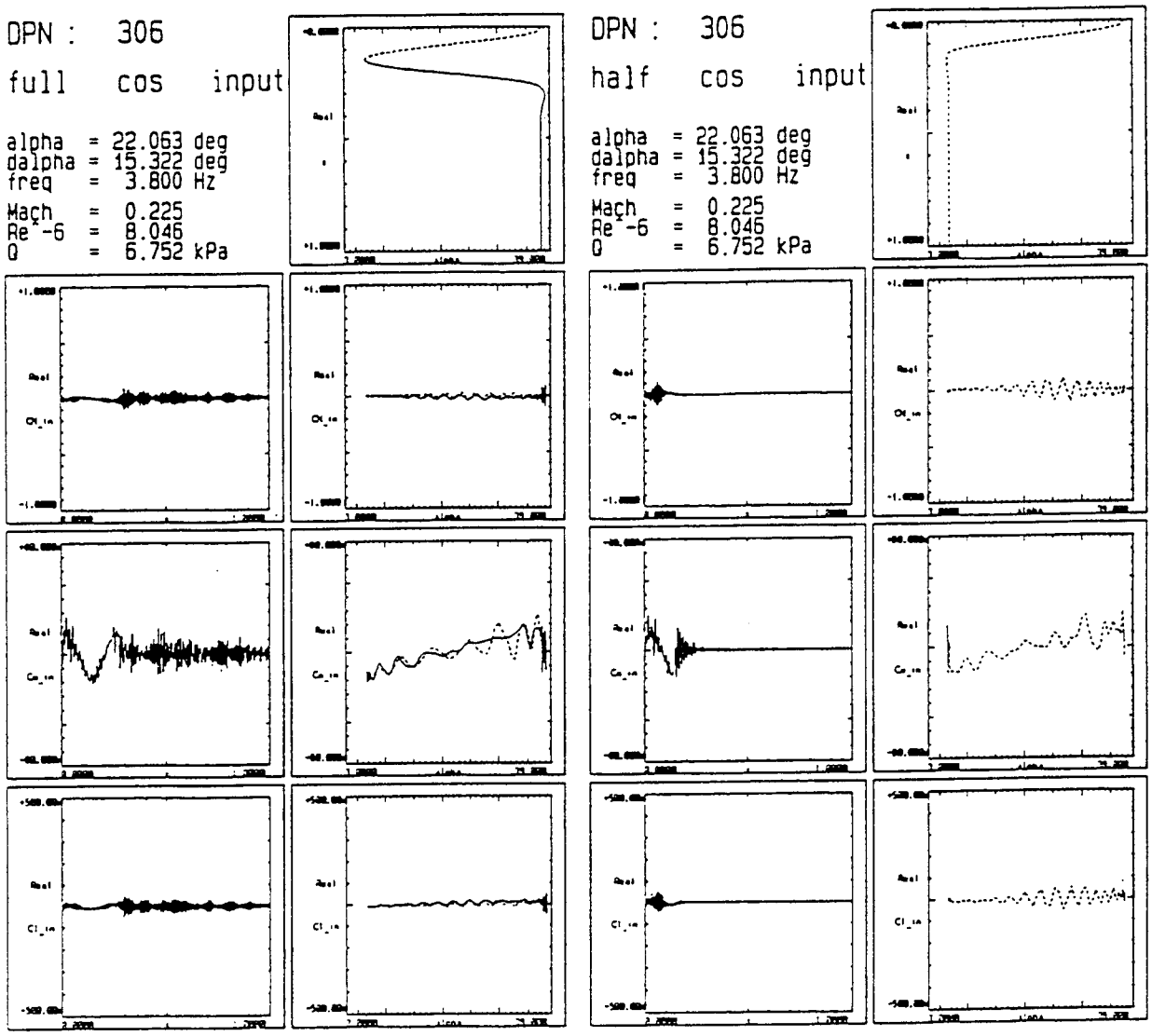

Fig. 20 Time histories of the balance quantities measured at datapoint 306 (first datapoint selected for extensive presentation in part III) page 4/4

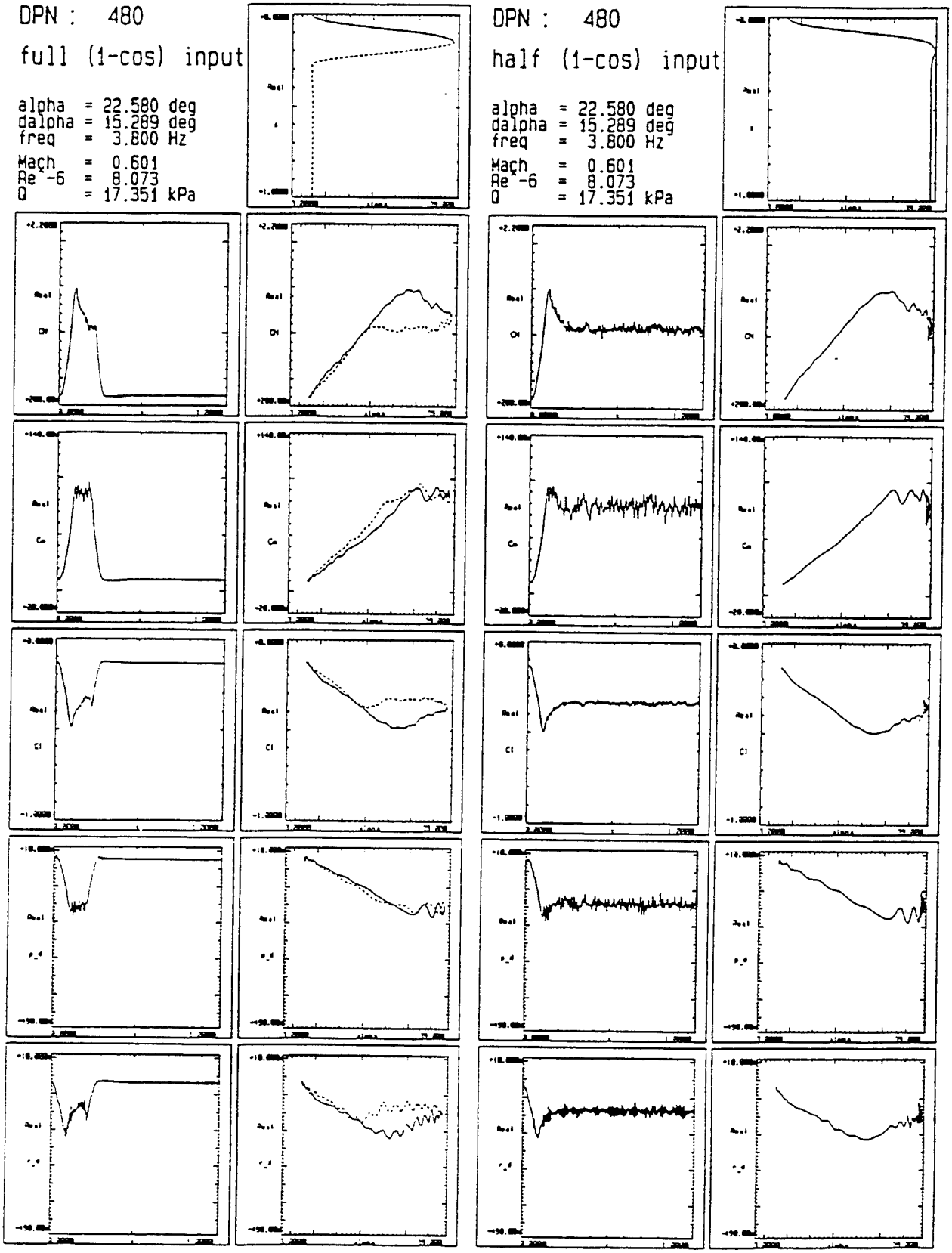

Fig. 21 Time histories of the balance quantities measured at datapoint 480 (second datapoint selected for extensive presentation in part III) page 1/4

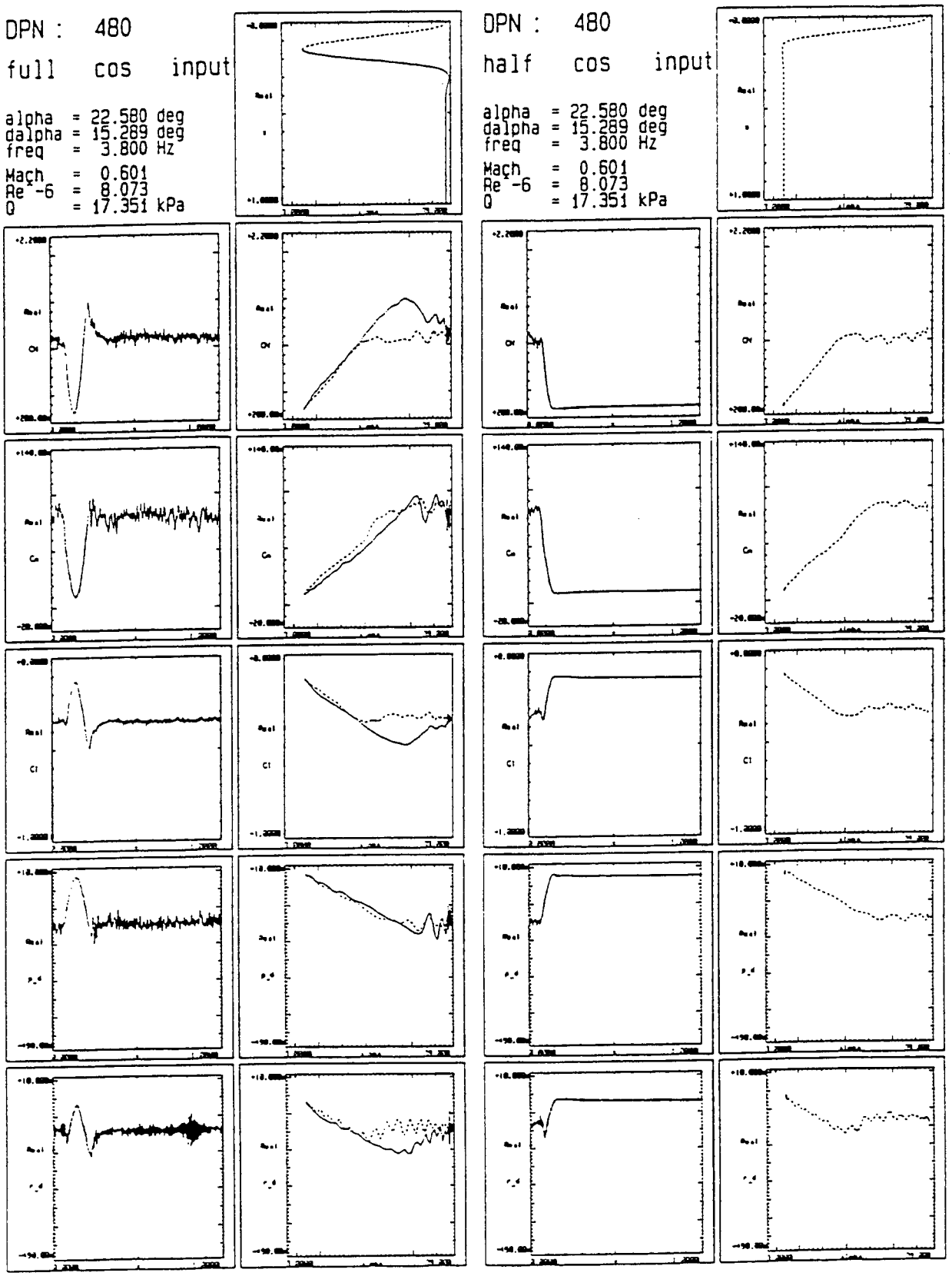

Fig. 21 Time histories of the balance quantities measured at datapoint 480 (second datapoint selected for extensive presentation in part III) page 2/4

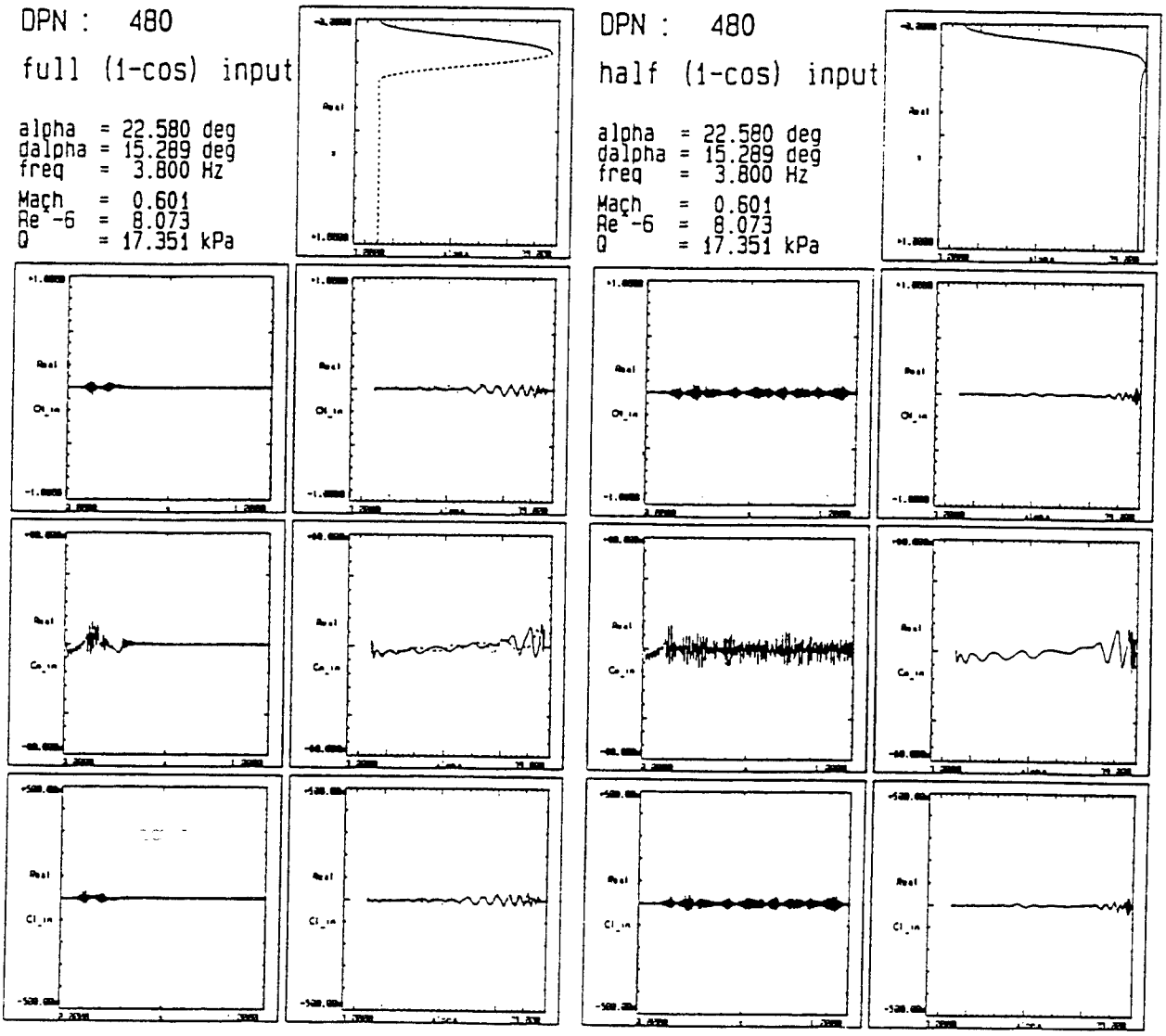

Fig. 21 Time histories of the balance quantities measured at datapoint 480 (second datapoint selected for extensive presentation in part III) page 3/4

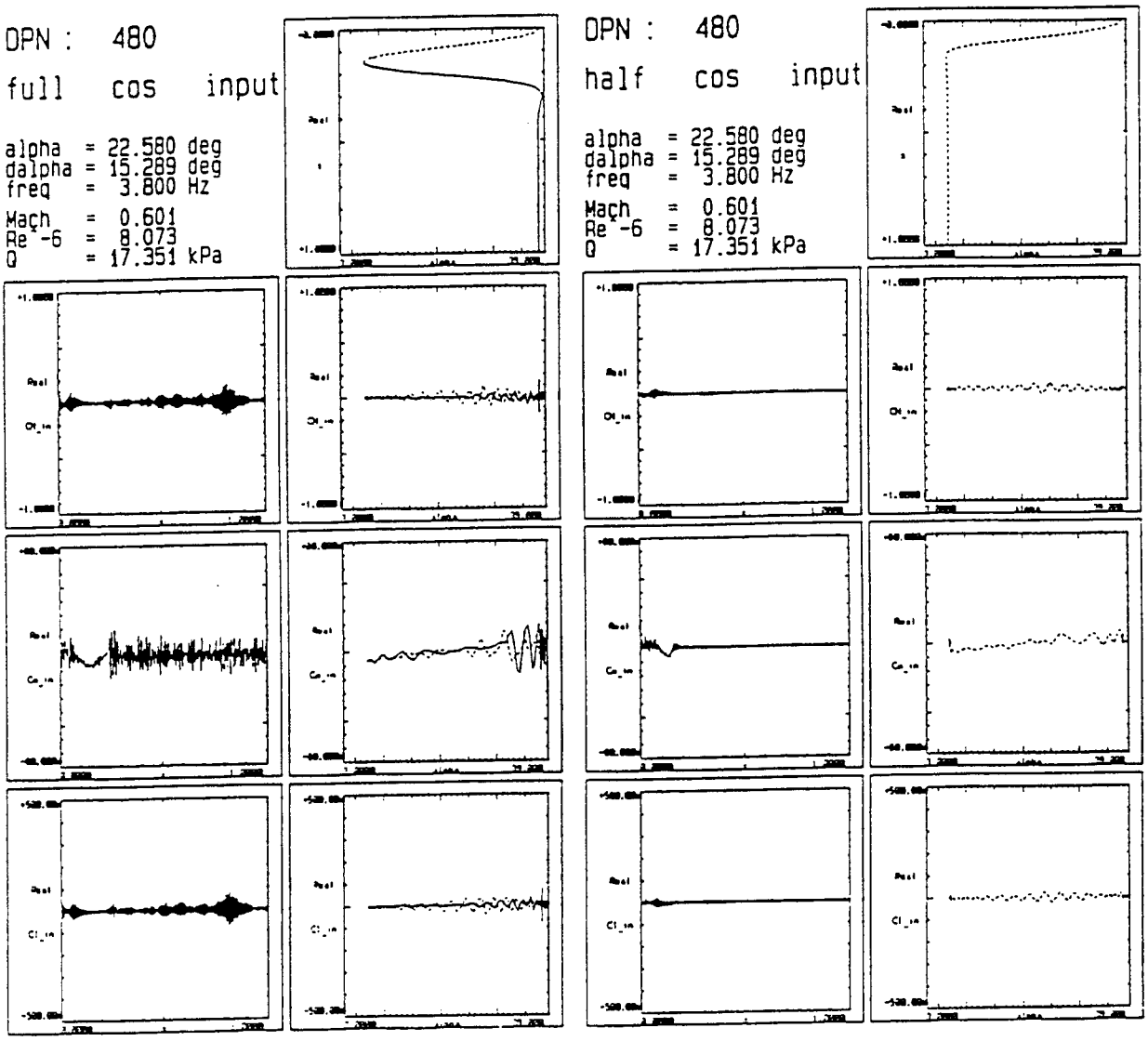

Fig. 21 Time histories of the balance quantities measured at datapoint 480 (second datapoint selected for extensive presentation in part III) page 4/4

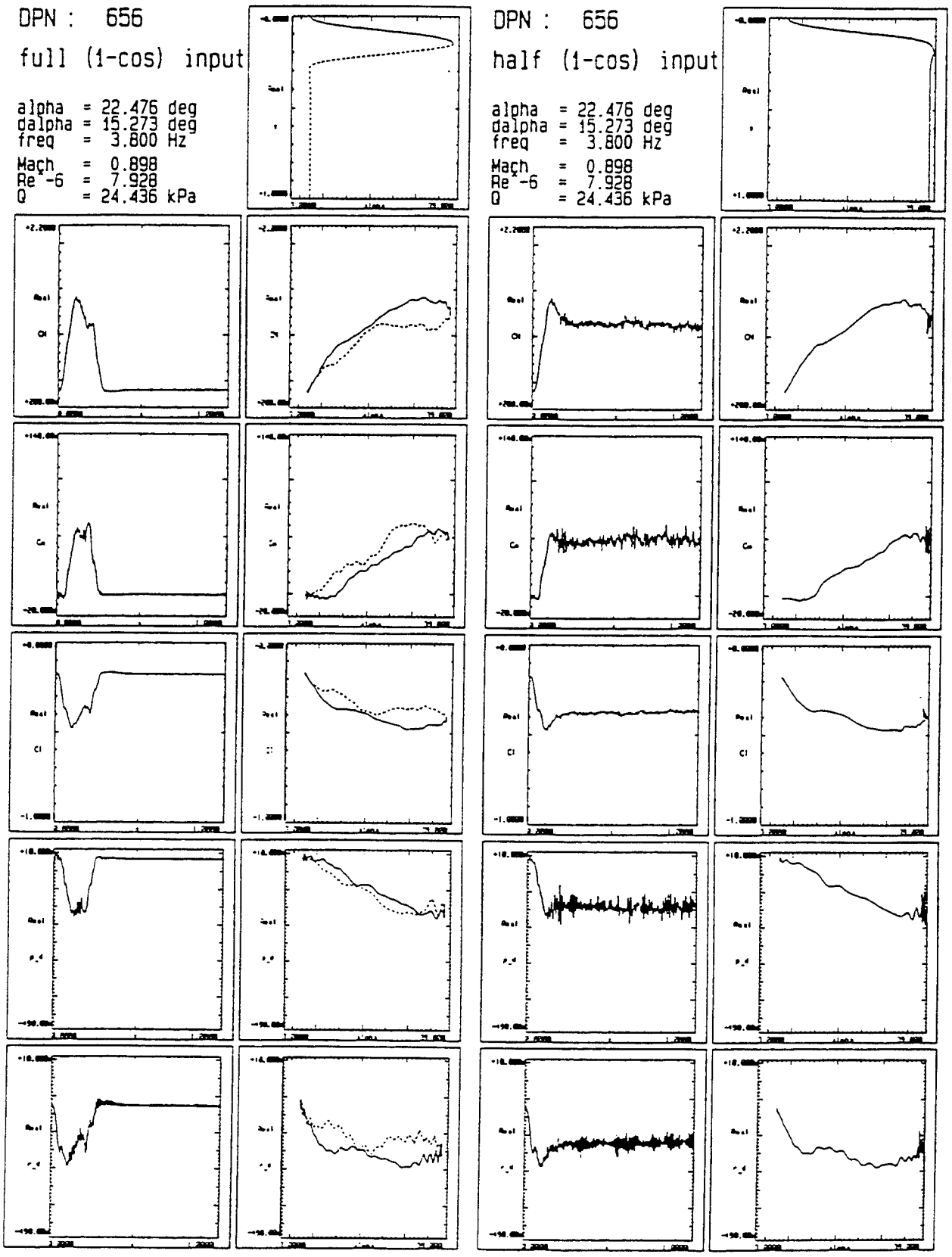

Fig. 22 Time histories of the balance quantities measured at datapoint 656 (third datapoint selected for extensive presentation in part III) page 1/4

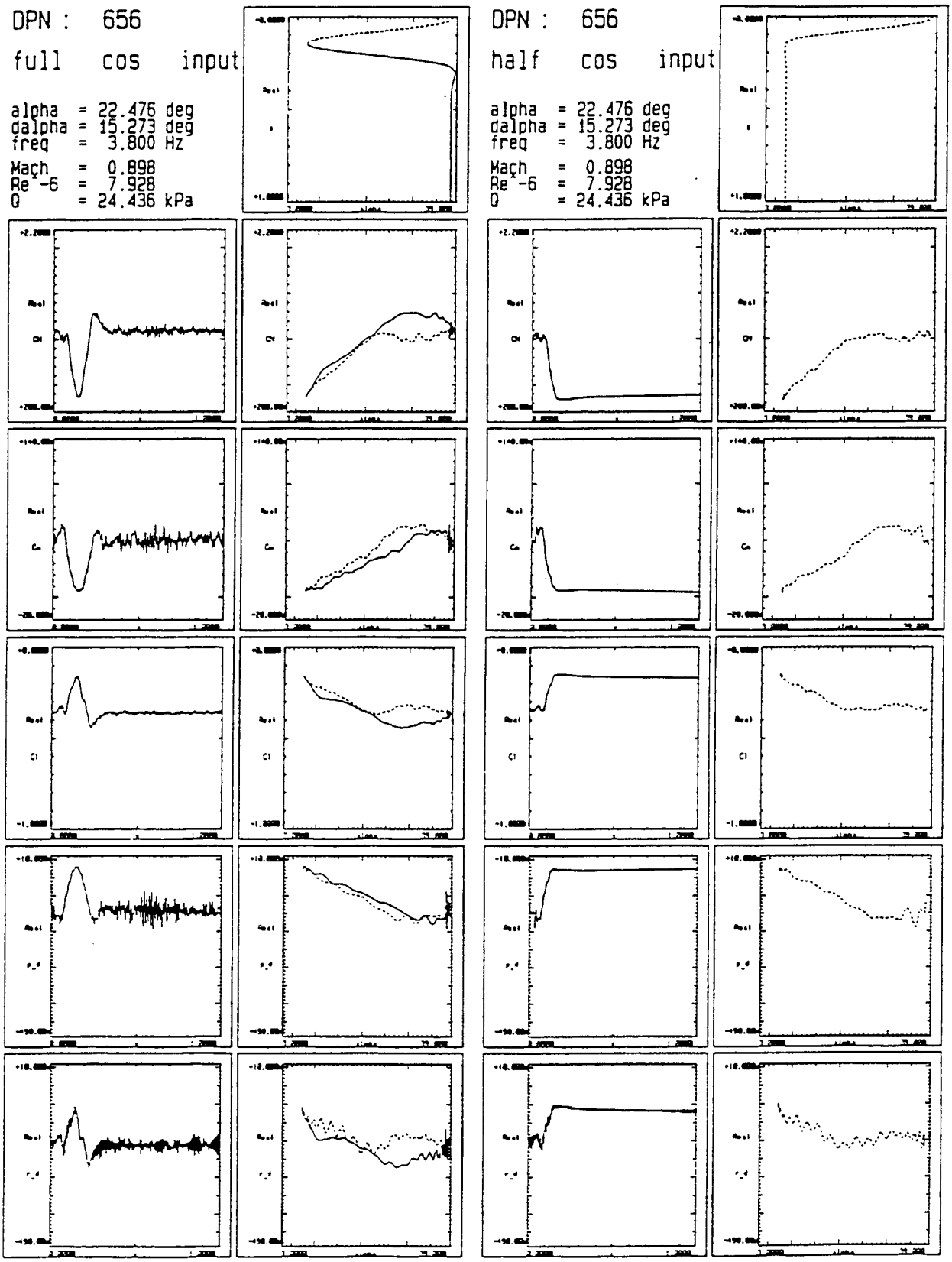

Fig. 22 Time histories of the balance quantities measured at datapoint 656 (third datapoint selected for extensive presentation in part III) page 2/4

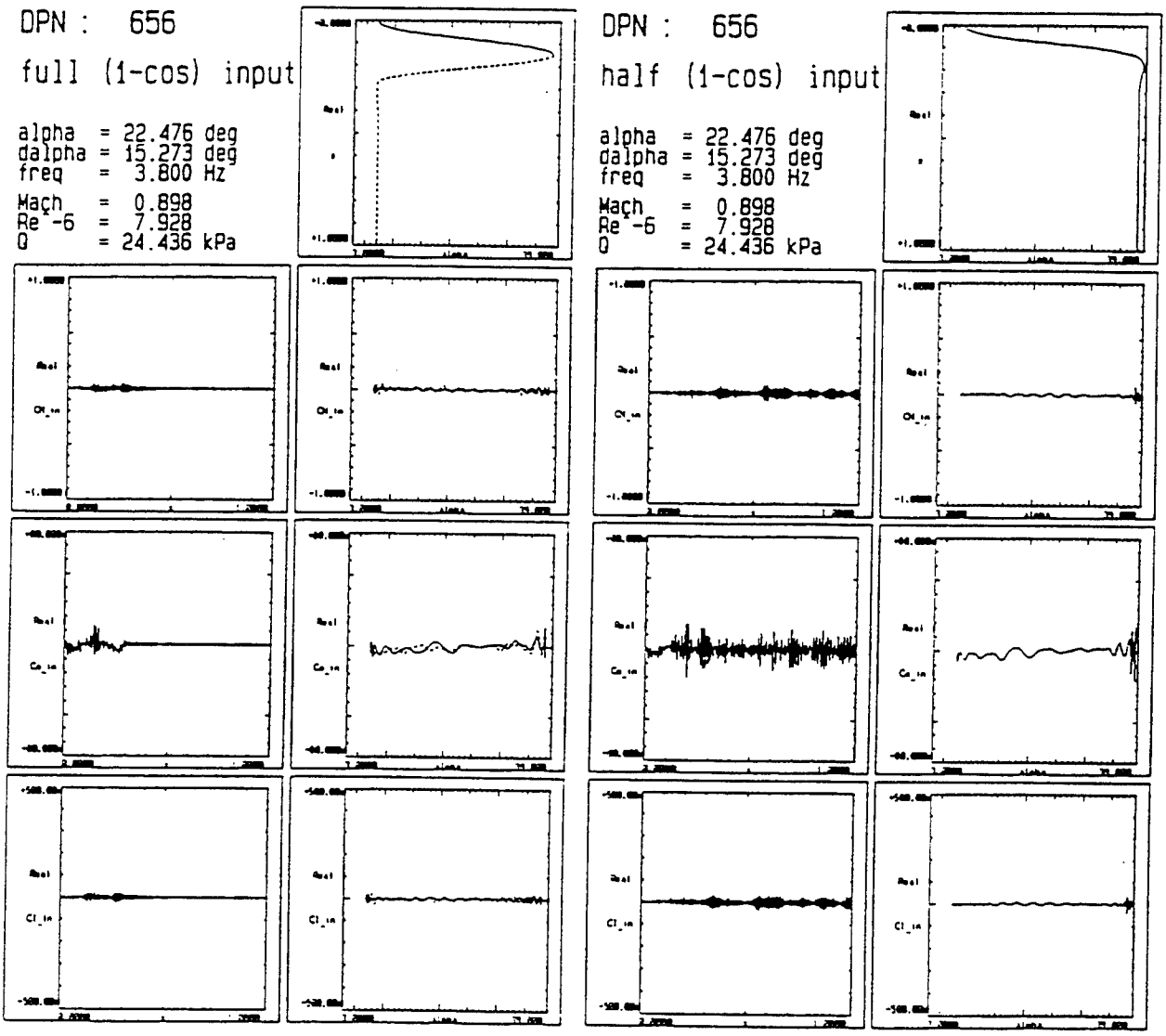

Fig. 22 Time histories of the balance quantities measured at datapoint 656 (third datapoint selected for extensive presentation in part III) page 3/4

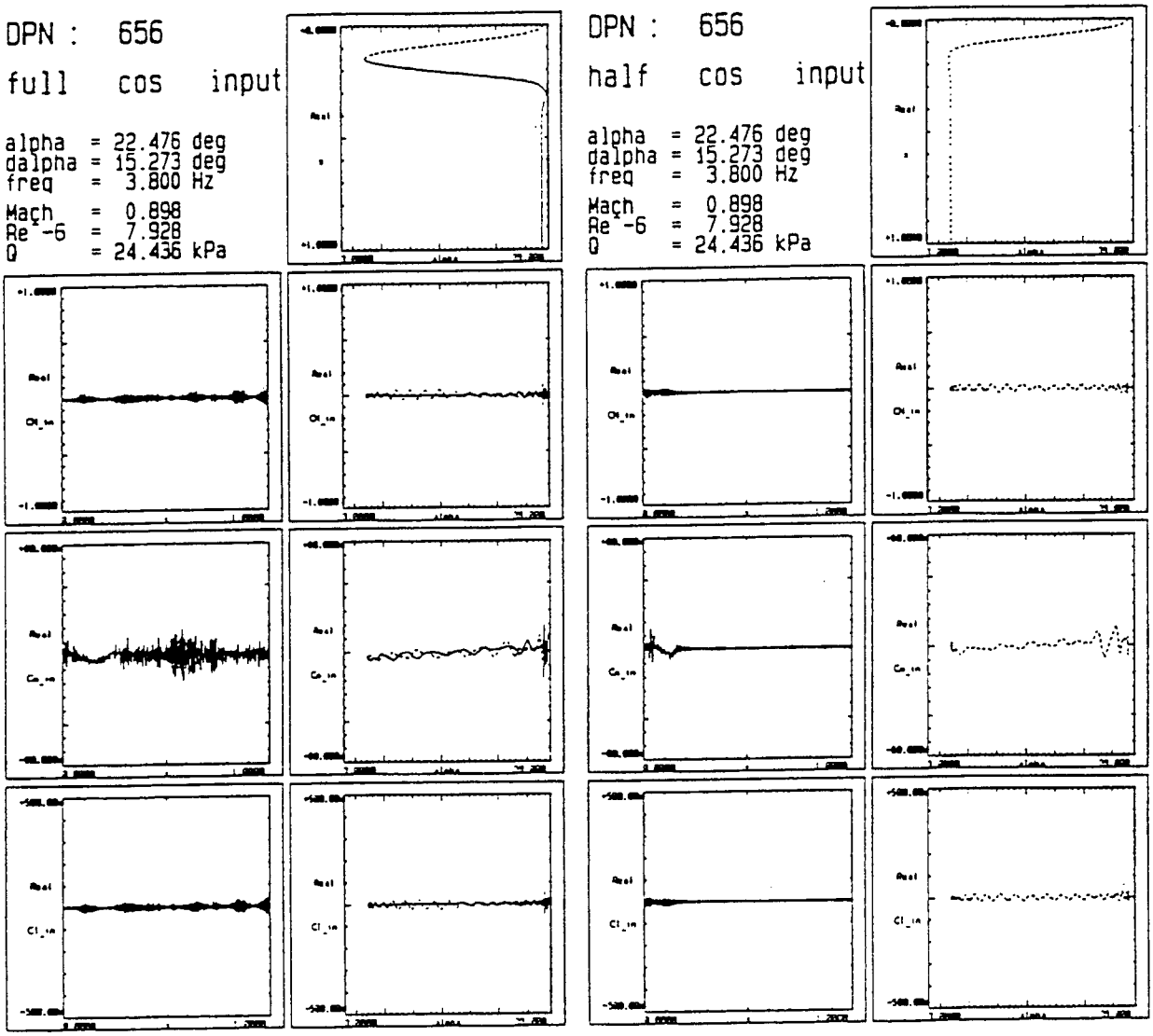

Fig. 22 Time histories of the balance quantities measured at datapoint 656 (third datapoint selected for extensive presentation in part III) page 4/4

8 FINAL COMMENTS

8.1 Test time per data point

Data acquisition time was generally in the order of seconds. Directly after data acquisition the wind tunnel turntable was rotated to the next mean incidence, while the model was kept oscillating at a fixed frequency-amplitude combination. Data processing was done when no acquisition was needed. For each data point quick-look prints and plots with the mean and first harmonic component of all sensors were presented about 1 MINUTE after data acquisition when no interference with data acquisition of the next data point occurred. The quick-look format was the same as the format used for the final data presentation.

8.2 Quasi-steady results

Also measurements were performed at very low frequencies. No really steady measurements were performed; as a consequence, no derivatives could be calculated.

8.3 Accuracy

Concerning the accuracy of measured aerodynamic data, it is generally recognized that it is extremely difficult to quantify the accuracies in a justified way. Based on the accuracies of the instrumentation, hardware components and the methods used in the software, together with the results of repeatability runs and experience from previous wind tunnel tests, the accuracies for the test were estimated. The estimates for the accuracy of the mean flow, model motion, pressure coefficients, and the total (aerodynamic + inertia) loads on the balance are collected in Table 7. The accuracy of sectional coefficients is determined by the accuracy of the pressure coefficients (as indicated in Table 7), the number and location of the pressure transducers and the gradients in the (unsteady) pressure distribution. Therefore no single value, applicable to all data points, could be included in Table 7. The accuracy of the unsteady aerodynamic loads as measured by the balance is determined by the accuracy of the balance , the ratio between aerodynamic and inertia loads (which is always presented in the printed tables, see also Section 6.1) and the accuracy of the inertia loads. The accuracy of the inertia loads on the balance as determined by the "mode fit procedure" (see Section 4.2.3.1) is determined by both the accuracy of the

Table 7 Estimated accuracies

1.	Mean test conditions		
	Mach number	+/- 0.001	
	Reynolds number	+/- 0.1	per cent
	Dynamic pressure	+/- 0.2	per cent
2.	Model position/motion		
	Turntable position	+/- 0.002 + 0.0004*alpha(in deg)	deg
	Steady incidence of shaft relative to turntable	+/- 0.005	deg
	Pitch amplitude shaft	+/- 0.005	deg
	Pitch deflection of main balance beam	+/- 0.001	deg
	Reduced frequency	+/- 0.0005	
	Amplitude of accelerometers	+/- (0.01*|ampl.| + 0.15)	m/s^2
3.	Balance loads	+/- 1.0	per cent
4.	Pressure coefficients		
	Steady (mean)	+/- 0.3	per cent
	Unsteady	+/- 0.5	per cent

measured accelerations and the accuracy of the procedure which fits the measured vibration mode with a weighted, linear combination of natural vibration modes. For all data points, processed with the "mode fit procedure", the measured accelerations were fitted with a mean accuracy better than 1 per cent.

8.4 Oscillation amplitude

The dalpha, as determined from the signal of the LVDT connected to the shaft of the excitation mechanism, is presented in the test conditions of each data point (see e.g., Table 6, first page). All the unsteady signals were nondimensionalized with this value. When the small amplitude of the torsional deformation of the balance beam (see e.g., Table 6, first page) is added to this value, the amplitude of the wing pitch motion at the attachment of the wing to the balance beam is obtained. When no torsional deformation of the wing is assumed, this value should be the same as the pitch amplitudes as obtained from the accelerometers in the wing (see e.g., Table 6, lower part first page).

The maximum pitch rate during the LCO test (see Section 2.2.1 and Figure 1) was much higher than at the SiS test. Because the outboard wing panel was used in both tests, the range of the accelerometers (1000 m/s^2) had to be high enough for the LCO test. As a result for many data points, especially at the SiS test, the accelerometers operated in a very small part of their range. Consequently, the pitch amplitude deduced from the output of the accelerometers is not very accurate (see e.g., Table 6, lower part first page) for these data points.

9 CONCLUDING REMARKS

The aims mentioned in Section 1.2 have been achieved:

A very large data base with steady and unsteady aerodynamic loads on a semispan model of a straked delta wing, performing both harmonic pitch oscillations as well as maneuvers, was generated. The data can be used directly for flow analysis and evaluation of computer codes.

Out of about 400 data points with the model oscillating harmonically in pitch, only 5 data points are presented extensively in this report (see Part 2). The results of these 5 data points are provided in printed and plotted form as well as in ASCII files on floppy disk. Out of about 200 data points with maneuver simulation, only 3 are presented completely (see Part 3) in plotted form as well as in ASCII files on floppy disks.

10 REFERENCES

1. Cunningham, A.M., Jr.; den Boer, R.G., Unsteady Low-Speed Wind Tunnel Test of a Straked Delta Wing, Oscillating in Pitch, NLR TR 87146 L, (Parts I through VI), 1987, also: AFWAL-TR-87-3098 (Parts I through VI), 1988.
2. Users' guide to the 1.60*2.00 m2 High Speed Wind Tunnel of the Nationaal Lucht-en Ruimtevaartlaboratorium (National Aerospace Laboratory) NLR, 1977.
3. Boer, R.G. den, Report of the design of two semispan wind tunnel models with corresponding support system, to be used for unsteady tests in the high speed tunnel (HST) of the National Aerospace Laboratory (NLR) in the Netherlands, NLR CR 89057 L, 1989.
4. Poestkoke, R., Hydraulic test rig for oscillating wind tunnel models, NLR MP 76020 U, 1976.
5. Meer, T.A. ter, User Manual for the Multi-Channel Conditioning Unit, NLR-AW-90-002, 1990.
6. Geurts, E.G.M., Experiments with a trial strain gage balance Memorandum AE-88-005U, National Aerospace Laboratory (NLR), Amsterdam, The Netherlands, 1988.
7. Geurts, E.G.M., Continued dynamic experiments with a trial strain gage balance. NLR-TR-89052 L, National Aerospace Laboratory (NLR), Amsterdam, The Netherlands, 1989.

APPENDIX A Axis system and sign conventions

Figure A.1 presents the body fixed axis system for the SiS model:

x-axis. In the wing reference plane (WRP), parallel to the root chordline of the basic wing panel at a distance of 62.3 mm. The WRP is the plane defined by the root chordline of the basic wing panel and the line which connects the 0 % chord points of the basic wing panel.

y-axis. In the wing reference plane, perpendicular with the x-axis, going through 48.24 per cent of the root chordline of the basic wing panel.

z-axis. Perpendicular to x-axis and y-axis.

The y-axis coincides with the rotation axis of the excitation mechanism. The z=0 plane is the wing reference plane (WRP). Both the root chordline of the basic wing panel, the rotation axis (= y-axis) and the line connecting the 0 % chord points are in this plane.

The trailing edge is one straight line. Due to the twist, this line is crossing the WRP at the root chord of the basic wing panel. Although the apex of the strake is in the WRP, the chordline of the y=0 section is not precisely in the WRP; it has a 0.0803 deg more positive angle of attack than the root chordline of the basic wing panel.

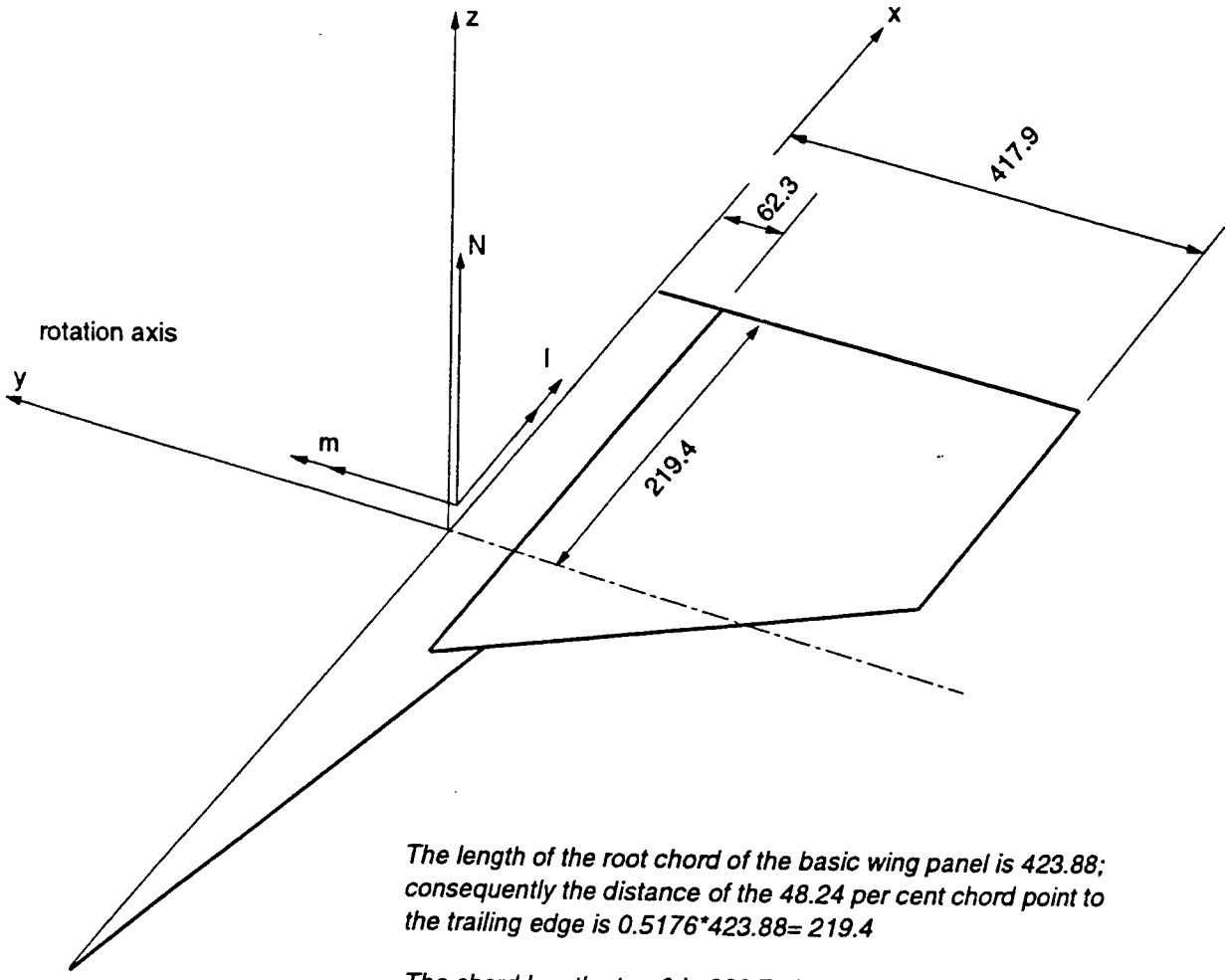

*The length of the root chord of the basic wing panel is 423.88; consequently the distance of the 48.24 per cent chord point to the trailing edge is 0.5176*423.88= 219.4*

The chord length at y=0 is 820.7; the point at a distance of 219.4 from the trailing edge corresponds to 73.27% local chord.

Figure A.1 The body fixed axis system (dimensions in mm)

APPENDIX B Basic wing panel geometry

This appendix gives only an overview of the geometry of the wing panel.

The main dimensions of the wing panel are indicated in Figure B.1. The wing reference plane (WRP) is defined by the root chordline and the line connecting the 0 % chord points. The rotation axis of the experiment was located in this plane. Some characteristics of the wing panel are listed below.

sweep angle of leading edge : 40 deg

airfoil section: NACA 64A204 (mod.) (all sections); lower side of the sections of the inboard part of the wing is thickened.

twist : -3.0 deg; the y = -62.3 section has 0.0 deg incidence with respect to the wing reference plane (WRP), the y = -417.9 section has -3.0 deg incidence; the panel is linearly lofted between root and tip.

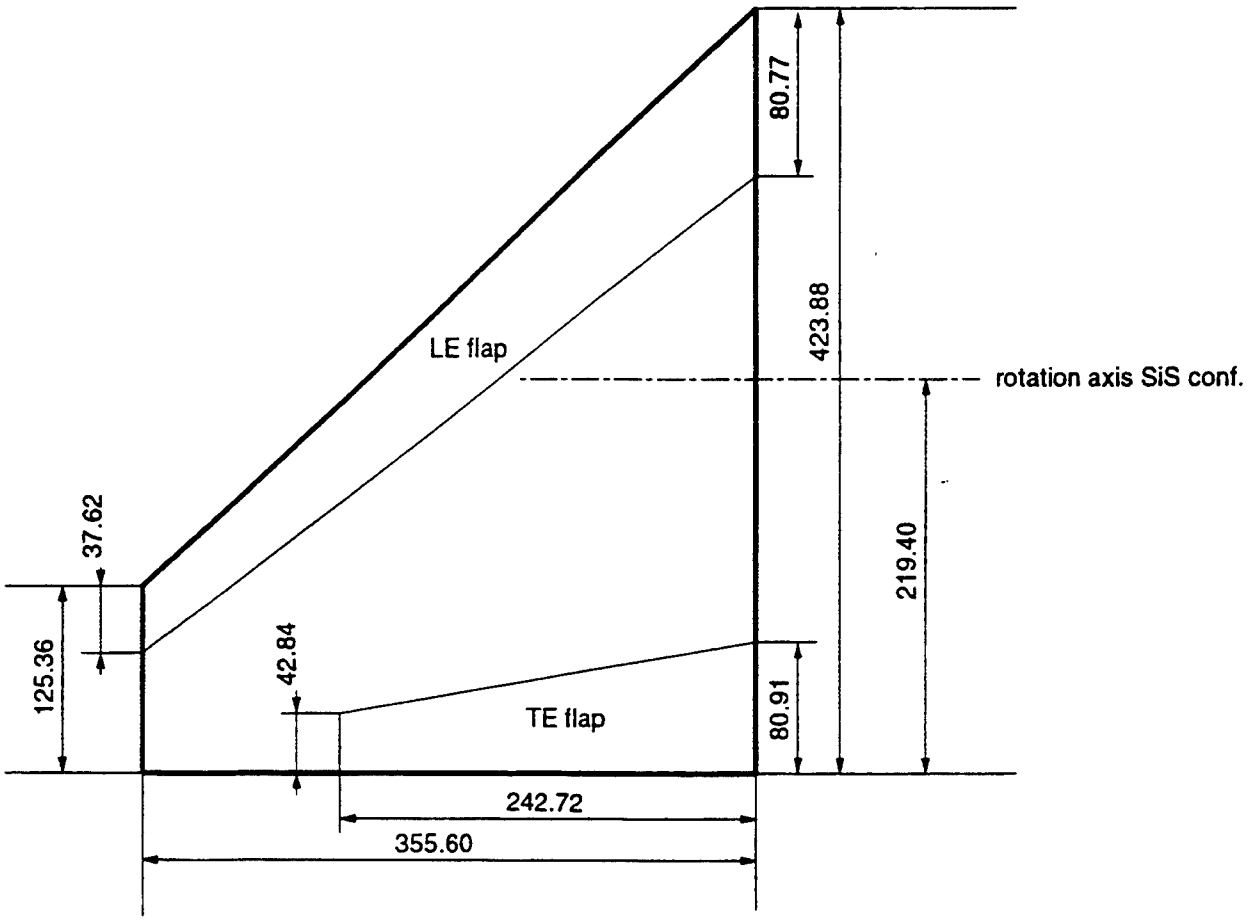

Figure B.1 Dimensions of the outboard wing panel